2011

Theoretical Study Of Beam Transformations By Volume Diffraction

Sergiy V. Mokhov
University of Central Florida

THEORETICAL STUDY OF BEAM TRANSFORMATIONS BY VOLUME DIFFRACTION

by

SERGIY V. MOKHOV
M.S. Taras Shevchenko National University of Kyiv, 1996
M.S. University of Central Florida, 2008

A dissertation submitted in partial fulfillment of the requirements
for the degree of Doctor of Philosophy
in CREOL, the College of Optics and Photonics
at the University of Central Florida
Orlando, Florida

Summer Term
2011

Major Professor: Boris Ya. Zeldovich

ABSTRACT

Laser beams can be manipulated by volume diffractive elements in addition to conventional optical elements like mirrors, lenses, and beam splitters. Conventional optical elements can be described by applying the basic laws of reflection and refraction at the surfaces of the elements. Even diffraction by surface gratings utilizes relatively simple mathematics. This is to be contrasted with the volume diffraction, which requires coupled wave theory in the slowly varying envelope approximation (SVEA) to obtain accurate results. Efficient spatially distributed diffraction of laser beams is possible due to the high coherence of laser light, and it occurs at specific resonant Bragg conditions.

This research work is inspired and driven by the successful development of recording technology for robust, high-efficiency volume Bragg gratings (VBGs) in photo-thermo-refractive (PTR) glass. Mostly VBGs of the reflective type are discussed in this dissertation. Starting with an analysis of electro-magnetic wave propagation in layered media, we have reformulated Fresnel and volume reflection phenomena in terms of a convenient parameter – strength of reflection. The influence that the different non-uniformities inside a VBG have on its spectral properties has been examined. One important result of this work is the proposal of moiré VBG and the derivation of an analytical expression for its bandwidth. A multiplexed VBG used as a coherent combiner is discussed as well. Beam distortion via transmission through and/or reflection by a heated VBG due to residual absorption is analyzed.

To my mother Valentyna, my father Valeriy and my sister Ludmyla.

TABLE OF CONTENTS

LIST OF FIGURES vii

CHAPTER ONE: INTRODUCTION 1

CHAPTER TWO: STRENGTH OF REFLECTION 11

Parameterization of the transfer matrix by strength of reflection 11

Decomposition of Fresnel reflection in terms of strength of reflection 15

Propagation of electro-magnetic waves in layered media 16

Formalism of strength of reflection in other branches of physics 20

CHAPTER THREE: PROPERTIES OF UNIFORM VBG AND FRESNEL CORRECTIONS 25

SVEA equations for reflection by VBG 25

Kogelnik's analytical solution for a uniform VBG 27

Influence of Fresnel reflections 30

CHAPTER FOUR: NON-UNIFORM VBGS 35

Propagation of EM waves in a non-uniform VBG 35

Theory of light reflection from a chirped VBG 37

CHAPTER FIVE: RESONANT CAVITIES IN VBGS 40

Fabry-Perot resonator based on uniform VBGs 40

Resonant cavity in moiré VBG 44

Bandwidth of resonant cavities in terms of strength of reflection 49

Bandwidth of a tunable moiré filter 57

CHAPTER SIX: MULTIPLEXED VBGS IN PTR GLASS 65

Properties of PTR glass 65

Probabilistic amplitude masks for phase plates in PTR glass 67
Slanted reflective and transmissive VBGs 70
Multiplexed reflective VBG for coherent beam combining 78
CHAPTER SEVEN: HIGH-POWER SPECTRAL BEAM COMBINING WITH VBGS UNDER THERMAL DISTORTIONS 82
Beam quality parameter based on second moments 82
Hermite-Gaussian and Laguerre-Gaussian modes 86
Variation of losses with detuning in reflective VBG 89
Heat transfer in a VBG plate under laser beam exposure 94
Non-uniform heat transfer problem for a VBG plate with thermally stabilized edges 99
Deterioration of beam quality under operation by heated VBG 102
Spectral beam combining with thermally distorted VBGs 105
Higher tolerance of Super-Gaussian beams to thermal distortions 109
CHAPTER EIGHT: CONCLUSION AND SUMMARY OF CONTRIBUTIONS 112
LIST OF REFERENCES 114

LIST OF FIGURES

Figure 1. Notations for the incident $A(z)$ and reflected $B(z)$ waves in the approximation of infinitely wide plane beams with account of the reflections from both boundaries, $z = 0$ and $z = L$, as well as the reflection by the VBG. 18

Figure 2. Solid lines: potential well $k_0^2 - k^2(z) = -2/\cosh^2 z$ yielding non-reflection and incident beam energy $k_0^2 = 0.09$. Dashed lines: fluxes $|A(z)|^2$ and $|B(z)|^2$ of counter-propagating wave function components. 24

Figure 3. Reflectivity R of a VBG with account of the interference of reflection from the VBG alone with two extra contributions: from the two boundaries of the specimen, for all possible phase combinations. Values of R are between the dashed curves for Fresnel 4% reflections from bare boundaries, and are between dotted curves for anti-reflection coatings (ARC) at 0.3% each. 33

Figure 4. Asymmetry in transmission spectra. Solid line, our experiment; dotted line, our model. 36

Figure 5. Reflection spectra of a uniformly chirped Bragg grating. 38

Figure 6. Intensity profiles $|A|^2$ and $|B|^2$ inside a chirped VBG for the central resonant wavelength. 39

Figure 7. Experimental setup for the coherent combination of two VBGs in PTR glass. 41

Figure 8. Experimental transmission of two π-shifted VBGs. 42

Figure 9. Spectral shift of resonant transmission due to phase shift $\Delta\gamma$ between two grating modulations. 43

Figure 10. Sketch of the envelope and simulated transmittance of a moiré filter. 46

Figure 11. Experimental spectral selectivity of a moiré VBG filter. 47

Figure 12. Transmission spectra of a tunable moiré VBG filter at different illumination points. 48

Figure 13. Photosensitivity curve of PTR glass depending on the exposure dosage. 66

Figure 14. The central area of a probabilistic amplitude mask for recording vortex phase plate (left) and the local area with a filling factor 0.25 (right). 68

Figure 15. 4*f* optical system for spatial filtering. 69

Figure 16. Beam geometries of slanted reflective and transmissive VBGs. 72

Figure 17. Diffraction efficiency of transmissive VBG depending on detuning for different coupling strengths. 76

Figure 18. Spectral properties of a double MVBG with three-wave coherent coupling: a) notation of waves; b) incident wave F; c) incident wave A.....81

Figure 19. Experimental spectral reflection profile of a VBG compared with simulation (thin line).....92

Figure 20. Experimental variation of the absorption ratio versus the detuning and the analytical expression (thin line).....93

Figure 21. Normalized temperature profiles $T(r)$ inside a VBG across aperture for two different values of heat removal coefficient: the upper line corresponds to h = 100 W/(m^{2}K), the curve below corresponds to h = 800 W/(m^{2}K) and it is closer to the normalized profile intensity, which is depicted by the thin black line. 97

Figure 22. Temperature profiles $\langle T(y=0)\rangle_z$ of a VBG with edges fixed at T_{edge} = 55°C: a) no beam; b) reflection of 160 W Gaussian beam; c) transmission of 160 W Gaussian beam. 101

Figure 23. Scheme for spectral combining of N beams with the use of $N-1$ VBGs. 106

Figure 24. Intensity profiles of Gaussian and super-Gaussian beams with the same power and widths corresponding to the criterion of 0.01 of the residual power outside the circle with the same radius. 110

Figure 25. M_x^2 of Gaussian and super-Gaussian beams propagated through a heated glass plate as a function of the absorbed power $C\cdot\alpha_{10}\cdot P_{tot}$. 110

CHAPTER ONE: INTRODUCTION

Optics is one of the oldest parts of physics and its establishment was strongly connected with the development of methods of transformation of light beams and the theoretical analysis of these methods. Starting from the basic reflection and refraction laws of geometrical optics, people came to create lenses first, and then to create telescopes, which has lead to the creation of modern physics. The methods of geometrical optics faithfully described the propagation of light at that time and the usefulness of these methods only grew with time; now, they are fundamental tools for any optical engineer around the world.

Recognition of the wave nature of light has lead to the analysis of interference and diffraction phenomena in optics. Scalar wave theory is usually sufficient for the description of such phenomena. However, in some cases, like refraction of light at relatively large incidence angles, the methods of full-vectorial electromagnetic theory are required. The spectral properties of light waves usually become apparent through the material dispersion of optical elements or the angular dispersion of surface diffractive gratings. Modern branches of optics, such as quantum information, require new quantum theoretical methods which will not be discussed in this dissertation.

During the last fifty years new light sources and lasers of different types were proposed and built. Light beams produced by lasers are characterized by high coherence and directionality and, thanks to these properties, lasers find many applications in science and industry. These properties of laser beams allow one to manipulate them by a new method – volume diffraction. One of the most impressive realizations of volume diffraction is volume holography.

This dissertation is devoted mostly to the general theoretical problems of the coherent propagation and interaction of light with optical media and analytical and numerical calculations of some particular applications with strong emphasis on the calculation of diffraction efficiencies of different VBGs by coupled wave theory methods. The recording material used for VBGs in this dissertation is photo-thermo-refractive (PTR) glass. It has advantages in comparison with other materials; those advantages being high uniformity, low losses and high thermal stability. The topics covered in this dissertation are actually wider than just the calculation of the reflection properties of particular holograms made in PTR glass. The dissertation is based on up-to-date published papers [1-5] and conference presentation abstracts [6-27] done by author in co-authorship with his advisor Prof. B. Zeldovich and members of Prof. L. Glebov's research group.

Before starting an overview of the approaches and results in volume diffraction theory, we consider first a broader class of problems. One of the most fundamental topics in electrodynamics is the propagation of electromagnetic (EM) waves in layered media. The term "layered" means that all properties of the media depend on one Cartesian coordinate only; for definiteness, on *z*. Almost any textbook on electrodynamics devotes considerable space to this problem, see e.g. [28-Born 99, 29-Landau 84, 30-Haus 84]. The natural starting point in the study of this subject is the consideration of reflection and refraction of an EM wave (of TE or TM polarization) at a sharp plane boundary between two homogeneous media. These phenomena are quantitatively described by well-known Fresnel formulae. The phenomena of propagation in layered media are discussed in specialized books [31-Brekhovskikh 80, 32-Yeh 88]. The matrix approach was used, for example, in [28-Born 99, 30-Haus 84, 32-Yeh 88]. Detailed consideration of boundary refraction and reflection of EM wave suffers from the absence of

generalization and often leads to recursive computational schemes for even simple layered systems. For example, the reflectance of a plate is calculated in [31-Brekhovskikh 80, 33-Hecht 01] through the summation of a geometrical progression of powers of the reflection coefficient with a phase factor accounting for the thickness of the plate.

The importance of fundamental research in EM wave propagation has increased in recent years, due to active research in fabrication and analysis of metamaterials, which have a negative refractive index [34-Veselago 68, 35-Pendry 03]. There are no known natural materials with such an unusual property. However, negative refraction was observed in a special artificially created materials in the radio frequency range first [36-Shelby 01, 37-Parazzoli 03, 38-Houck 03], and then in the optical spectrum [39-Shalaev 05, 40-Sarychev 07, 41-Dolling 07].

Another wide class of layered media with propagation parameters dependent upon one coordinate consists of distributed feedback systems. Kogelnik and Shank first proposed them for integrated optics applications [42-Kogelnik 72]. Distributed feedback structures couple counter-propagating waves with opposite phase velocities in the body of the medium. This is to be contrasted with the feedback due to reflection at the boundaries. Modulation of distributed parameters leads to specific transmission and reflection properties of such systems. As a result, they can be used as mirrors and filters, and the most important of their characteristics is the narrow spectral band width of their action [43-Schmidt 74]. One fundamental realization of a system with distributed parameters is a Bragg mirror, which has a small sinusoidal modulation of the material parameters; usually this is a sinusoidal modulation of the real dielectric permittivity. When the propagation wavelength of incident wave in this media is equal to the round-trip distance along one period of modulation, the weak reflected waves from all periods interfere

constructively, and strong reflection occurs at that wavelength. If the input wavelength is tuned away from this resonant Bragg condition, the reflection rapidly drops. The reflection coefficient of more than 99% at the resonance frequency can be (and actually has been) achieved for a large enough thickness of such a filter. The functional dependence of this resonance reflection in the reflection band is mostly flat. The full spectral width of reflection of such a strong filter may be kept to less than 200 picometers for optical wavelengths. For example, such filters, being recorded in fibers [44-Othonos 97], may be used for the separation of wavelength channels in communications. In practice the signal filtering is usually realized with the use of thin, multilayer dielectric films [45-Kazovsky 96, 46-Madsen 99], similar to antireflection coatings. The properties of such a commonly used periodic, multilayer stack may be obtained from the consideration of this stack as a consecutive set of uniform layers. Such a stack is equivalent also to a Bragg grating with the relevant Fourier component of the refractive index modulation corresponding to the actual step-index modulation of the multilayer filter.

In the case of two combined distributed feedback systems, the interference of their reflection processes may be constructive or destructive, depending on the relative phase factor between their complex reflection coefficients. If two identical successive reflective VBGs are separated by small distance, which corresponds to a π-shift between their sinusoidal modulations of refractive index, then the narrow transmission peak will be observed at the mutual resonance frequency. This fundamental fact was experimentally observed for different types of distributed feedback systems. In particular, early experiments were done for planar slab dielectric gratings [47-Norton 97]; a few years ago this transmission peak was observed for coupled chiral fibers [48-Kopp 03]. Finally, a Fabry-Perot spectral filter was implemented with use of two compound

VBG mirrors. The author of this dissertation participated in the theoretical study of this implementation of a VBG filter [2-Glebov 08]. The narrow transmission peak of such a filter can be linearly tunable, if a mechanism for the linear change of the phase gap in the vicinity of π is implemented.

Recent achievements in the fabrication of high quality VBGs in PTR glass [49-Efimov 04] promise to make a strong influence on laser design. Their stability with respect to high power radiation makes VBG-PTR devices especially attractive. The high spectral selectivity of these gratings was mentioned above. They also have strong angular selectivity; as a result they can select one of several transversal modes in cavity, so that their natural application is for narrowing emission spectra of different types of semiconductor [50-Volodin 04] and solid-state [51-Chung 06] lasers. If a VBG is longitudinally chirped or, in other words, if it has a gradually changing period, then this grating will reflect different wavelengths from different parts inside its volume. It was shown [52-Liao 07] that femtosecond pulses can be stretched and then compressed by such a grating with an efficiency of about 95%. VBG has very good tolerance to high power laser beams. Real fabricated surface diffractive gratings may contain small defects, which are sources of potential damage. Due to its narrow reflection bandwidth, a given VBG may serve as an almost totally reflective mirror for a laser beam with the resonant wavelength and, at the same time, may serve as a transparent element for another beam; the resonant wavelength must be separated from second by a mere few hundred picometers [53-Andrusyak 07]. As a result, these two high power beams can be combined while preserving the diffraction divergence. The power of a combined beam is increased without an increase in the product of (Area)×(Solid Angle). Remarkably, this fact does not contradict the theorem of

brightness conservation, compare to [54-Leger 93], because the final beam consists of two of several close, but different, wavelengths. Other schemes for beam combining are discussed in [55-Fan 05].

Historically, the optical coupled-wave theory of volume gratings had its predecessors in the research on the diffraction of X-rays in crystals. The theoretical approach of the so-called "kinematic theory" was equivalent to the 1st-order Born approximation in scattering theory, which can be applied for relatively weak scattering processes. Subsequent theoretical formulation included the interaction between propagating waves; it was called the "dynamical theory" [56-Pinsker 78, 57-Cowley 95] and it gives correct the "pendulum solution" for the transmission problem. Namely, energy is first transferred from incident wave *A* into scattered wave *B*, however the wave *B* may, in its turn, transfer its energy back into the wave *A*. Finally, Kogelnik formulated a general coupled-wave theory for a thick volume hologram with sinusoidal modulation of the refractive index [42-Kogelnik 69]. The consideration by Kogelnik allowed for accounting for the so-called "slanted" gratings, i.e. those in which the Bragg planes were neither parallel, nor perpendicular to the input plane of the specimen.

Rigorous vectorial computational algorithms for the investigation of light propagation in arbitrary layered media were developed with good success many years ago; see e.g. the work of Prof. Moharam [58-Moharam 82] and also [59-Sharlandjiev 85]. Prohibitively long computational time and potentially poor convergence may be considered as disadvantages of these methods. Usually people work with homogeneous distributed feedback systems, and the analytical results are known for them. The numerical approach is sometimes necessary for the analysis of chirped systems, for example, such chirping may arise due to temperature [60-

Lauzon 94] or strain [61-Hill 94EL] gradients. The properties of the system can also be changed by external high power laser illumination through nonlinear processes. As a result, a guided-mode resonance filter was demonstrated to be optically tunable in [62-Dobbs 06]. Artificially implemented controlled chirp, in particular in fibers, can be used for the compensation of dispersion [63-Komukai 98, 64-Hill 94OL]. Usually the chirp of the grating is considered to be in the form of a quadratic spatial dependence of phase. Then, the spectral behavior of the reflectance is still symmetric around the resonant frequency; however, zeros of the reflectance between the lobes are “washed out”. In some cases, it is also important to consider another type of the chirp, the cubic term in spatial dependence of the phase. That leads to an asymmetry in the sizes of the secondary lobes of the reflectance; this asymmetry was observed in fibers [65-Mizrahi 93]. The simplest way of numerically analyzing an arbitrary nonuniform distributed feedback system is the so-called “staircase” approximation; the validity of such a numerical approach is discussed in [66-Popov 02].

The media for the propagation of light discussed above were characterized by a scalar permittivity ε and a scalar permeability μ with a dependence on one spatial coordinate z. In the case of uniaxial or biaxial media the electric permittivity ε is a tensor. The propagation of light in anisotropic crystals and in complex-structured periodic media is discussed in [67-Belyakov 92]. Many optical applications are based on liquid crystals, which also exhibit optical anisotropy. Reflection of light by cholesteric liquid crystals is very strong and spectrally selective. This quality may be used in the liquid-crystal display industry, see the monographs [68-Khoo 93, 69-de Gennes 93]. The planar nematic liquid-crystal structure with the director twisted in the light

propagation direction was studied in the research group of Prof. Zeldovich [70-Sarkissian 06]. In the present work, we will consider beam propagation only in isotropic media.

The classical phenomena of light propagation are formulated mathematically by the equations of mathematical physics. Generally, these equations are partial differential equations of the second order [71-Morse 53]. In the monochromatic case the problems for layered media are described in a one-dimensional way with boundary conditions at the planes $z = z_1$ and $z = z_2$, defined for values of one spatial variable z only. Many fundamental analytical results and conclusions based on numerical calculations are obtained for one-dimensional problems; that is why we paid so much attention to them. Generalization of layered media problems is necessary in order to investigate a slab of media with varying parameters along one direction when that direction is not normal to the boundary planes. Another important type of such objects are slanted VBGs, which have fringes that are not parallel to boundary planes. Widely used examples of such gratings are transmission holograms with fringes perpendicular to the boundaries. The diffraction of light by a slanted VBG is formulated as a one-dimensional problem and it has been solved analytically [42-Kogelnik 69] using the correct phase-matching of two propagating wave vectors with the grating wave vector at the boundaries. If the thickness is small enough, then the slanted grating becomes a planar grating, so that the inclusion of higher orders of diffraction becomes necessary for accurate results [72-Moharam 81].

Beside the ordinary practical purposes of manipulating light propagation in applied optics like steering or reflecting of beams by VBGs, some new specific applications could be found by recording more than one grating in the sample. The early work [73-Alferness 75] explored the angular selectivity of a transmission hologram made with two crossed holographic gratings

recorded in one volume specimen. If the coupling strength of the two gratings is not uniform, but adiabatically changed between two gratings from one side to other, then this grating coupling three waves demonstrates large efficiency. What is remarkable is that this high efficiency of transmission VBG may be achieved with almost no dependence on the grating strength and on the polarization [74-Tsai 06OL]. A reflecting hologram with two recorded gratings crossed at a right angle offers high angular and spectral selectivity [75-Tsai 06OE]. Some results for beam propagation inside the transmission hologram of a doubly recorded grating are presented in [76-Zhao 00]; that work has also a good list of references.

Despite the continuous growth of the storage capacity of standard electronic memory, there is still a strong interest in realizing holographic optical storage, which promises fast data access [77-Hong 96]. Unfortunately, no materials for fast writing and reading have been found at the present. Almost all volume holographic elements are operated in a scheme in which the incident and diffracted waves contact the specimen through parallel boundary planes in transmission or reflection. Analytical solutions are significantly more difficult for holograms with a 90-degree geometry, where two coupled waves enter and exit the specimen on crossed boundary planes. This corner geometry allows one to potentially design compact architectures for holographic memory modules [78-Psaltis 97]. A comparison of transmission and the 90-degree holographic recording geometry is performed in [79-Psaltis 03]. The importance of mathematical methods for the analysis of holographic data was shown in experiments with holographic recording of ultrafast fs-laser pulses [80-Centurion 06]. Standard system of coupled equations for propagating waves in volume diffractive element was first formulated in X-ray crystallography [81-Takagi 69].

The present research work is devoted mostly to volume diffraction theory, but PTR glass technology used in related experiments is applicable also for fabricating ordinary phase plates by creating of permanent refractive index change across the aperture of a PTR glass plate. The author has participated in this research connected to phase plates. Several optical applications are to be mentioned, based on phase plates and done by different groups around the world. A non-exhaustive list is: the correction of the wave front distortions of propagating optical beams [82-Baker 09], shaping the wavefront for laser material processing [83-Sueda 04], creating optical vortices for enhanced astronomical observations [84-Swartzlander 08], for optical testing of random media [85-Popoff 10], dynamic optical trapping [86-Curtis 02], quantum cryptography [87-Merolla 99], quantum entanglement [88-Oemrawsingh 06], generation of Airy beams [89-Siviloglou 07,90-Polynkin 09], focusing of light for nonlinear optics applications [91-Sola 08], and pulse shaping by phase modulation of spatially resolved spectral components [92-Meshulach 98].

CHAPTER TWO: STRENGTH OF REFLECTION

Parameterization of the transfer matrix by strength of reflection

Reflection of light by a layered media is the subject of an enormous number of works, including numerous monographs [28-Born 99, 29-Landau 84, 30-Haus 84, 31-Brekhovskikh 80, 32-Yeh 88, 93-Azzam 87]. In particular, the reflection of light by Volume Bragg Gratings (VBGs) is usually studied in the Slowly Varying Envelope Approximation (SVEA) [42-Kogelnik 69, 93-Collier 71, 94-Zeldovich 92]. This chapter is devoted to the theoretical study of the general properties of reflecting elements. We allow for the modulation of both the dielectric permittivity, $\varepsilon(z)$, and the magnetic permeability, $\mu(z)$. The latter is especially important in connection with the new types of materials, including the ones with $\varepsilon < 0$, $\mu < 0$; see the review [35-Pendry 03].

For a better perspective, let us first consider the transmission VBG which couples two plane waves, A and B, both having positive z-components of the Poynting vector: $P_z = |A|^2 + |B|^2$. Here, the z-axis is normal to the boundaries of the VBG. The absence of absorption results in the conservation law: P_z =const. Writing the matrix relationship for wave coupling in linear media, $A(z) = N_{AA} \cdot A(0) + N_{AB} \cdot B(0)$, $B(z) = N_{BA} \cdot A(0) + N_{BB} \cdot B(0)$, one comes to the conclusion that the matrix $\hat{N}(z)$ must be unitary; i.e. it belongs to the elements of the unitary group U(2).

Consider now a reflecting device, where the waves A and B propagate in opposite directions with respect to z-axis, so that $P_z = |A|^2 - |B|^2$. The absence of absorption results in the conservation law: $|A|^2 - |B|^2 = \text{const}$. Writing the matrix relationship for wave coupling in linear media,

$$A(z) = M_{AA} \cdot A(0) + M_{AB} \cdot B(0), \quad B(z) = M_{BA} \cdot A(0) + M_{BB} \cdot B(0), \qquad (2.1)$$

one can deduce from the assumption of energy conservation that the matrix $\hat{M}(z)$ satisfies the conditions:

$$\hat{M} = \begin{pmatrix} \alpha & \beta \\ \gamma & \delta \end{pmatrix}, \quad |\alpha|^2 - |\gamma|^2 = 1, \quad |\delta|^2 - |\beta|^2 = 1, \quad \alpha\beta^* = \gamma\delta^*. \qquad (2.2)$$

The most general form of such a matrix $\hat{M}$ depends on four real parameters: the strength *S*, an inessential phase ψ and two phases ζ and η:

$$\hat{M} = e^{i\psi} \begin{pmatrix} e^{i\varsigma} & 0 \\ 0 & e^{-i\varsigma} \end{pmatrix} \begin{pmatrix} \cosh S & \sinh S \\ \sinh S & \cosh S \end{pmatrix} \begin{pmatrix} e^{-i\eta} & 0 \\ 0 & e^{i\eta} \end{pmatrix}. \qquad (2.3)$$

The determinant of such a matrix equals $\exp(2i\psi)$, so the modulus of that determinant is equal to one. Such matrices constitute a U(1,1) group: their multiplication and inversion leaves them within the same set. One can see an analogy between our transformation of the wave amplitudes (2.1)−(2.3) and the Lorentz transformation if $|A|^2$ plays the role of c^2t^2, $|B|^2$ the role of x^2 and the quantity tanh *S* corresponds to the velocity parameter $\beta = V/c$, where *V* is the relative velocity of the two coordinate frames.

The physical addition of two sequential elements with the parameters S_1, ψ_1, ζ_1, η_1 and S_2, ψ_2, ζ_2, η_2, respectively, yields the element described by the matrix $\hat{M}_3 = \hat{M}_2\hat{M}_1$, i.e. the matrix of the same type (2.3). Here is the expression for the resultant strength parameter S_3:

$$S_3 = \operatorname{arcsinh} \sqrt{\sinh^2(S_1 + S_2)\cos^2\tau + \sinh^2(S_1 - S_2)\sin^2\tau}, \quad \tau = \varsigma_1 - \eta_2, \qquad (2.4)$$

which can vary due to mutual phase difference between the reflective elements. Equation (2.4) is probably known to mathematicians who have worked with the group U(1,1). However, in the physical context of reflection it was first derived in our work [1-Mokhov 08].

Knowing of the matrix $\hat{M}(z)$ allows one to find the amplitudes of the reflection and transmission coefficients. For example, to solve the problem with the wave *A* incident on the layer at the front surface , $z = 0$, and with no wave *B* incident on the back surface, $z = L$, one substitutes the boundary conditions $A(0) = 1$, $B(L) = 0$ into (2.1), to get

$$\begin{aligned} 0 = M_{BA}(L) + M_{BB}(L)\cdot r \quad \Rightarrow \quad r = r(B \leftarrow A) = -\frac{M_{BA}(L)}{M_{BB}(L)} = -e^{-2i\eta}\tanh S, \\ R = \left|r(B \leftarrow A)\right|^2 = \tanh^2 S. \end{aligned}, \qquad (2.5)$$

With the same boundary conditions we can also calculate the amplitude transmission coefficient and the intensity transmittance

$$\begin{aligned} t(A \leftarrow A) = A(L) = M_{AA} + M_{AB}\cdot r = \frac{M_{AA}M_{BB} - M_{AB}M_{BA}}{M_{BB}} = \left|\det \hat{M} = 1\right| = \frac{1}{M_{BB}(L)}, \\ T = \left|t(A \leftarrow A)\right|^2 = \frac{1}{\left|M_{BB}(L)\right|^2} = \frac{1}{\cosh^2 S} = 1 - R. \end{aligned} \quad .(2.6)$$

We have used the property that $\det \hat{M} = 1$ for lossless media.

The presence of the hyperbolic tangent function in the reflection coefficient is very satisfying: when the strength *S* goes to infinity, the reflection goes to 1 asymptotically. Kogelnik's theory of reflection by VBGs predicts the following value of the resultant strength [42-Kogelnik 69]:

$$R_{\mathrm{VBG}} = \tanh^2 S,\ \ S = \operatorname{arcsinh}\left(S_0 \frac{\sinh\sqrt{S_0^2 - X^2}}{\sqrt{S_0^2 - X^2}} \right),\ \ S_0 = |\kappa| L,\ \ X = \left(\frac{\omega n}{c}\cos\theta_{\mathrm{inside}} - \frac{Q}{2} \right) L \ . \ (2.7)$$

Here, S_0 is the strength of the VBG at the perfect Bragg matching condition when detuning parameter is $X = 0$, the coupling parameter $|\kappa| = \frac{1}{2}(n_1\omega/c)/\cos\theta_{\text{inside}}\cdot|\cos(\mathbf{E}_A,\mathbf{E}_B)|$ corresponds to a modulation of the refractive index $\delta n(z) = n_1\cos(Qz)$. The angle θ_{inside} is the propagation angle of the waves *A* and *B* inside the material of the VBG. Note that our formula (2.7) is mathematically identical to the result found by [42-Kogelnik 69], but it is written in a somewhat different form.

If a reflective VBG slab has certain residual reflection from the boundaries, $R_1 = |r_1|^2$ and $R_2 = |r_2|^2$, then one must consider the possibility of coherent interference between the main VBG refection from (2.7) and these two extra contributions. Consideration of the result in (2.4) allows one to predict that at any particular wavelength and/or angle of the incident wave, the strength S_{tot} of the total element will be within the limits

$$S_{\text{VBG}} - |S_1| - |S_2| \le S_{\text{tot}} \le S_{\text{VBG}} + |S_1| + |S_2|, \quad S_{1,2} = -\operatorname{arctanh} r_{1,2}\,. \qquad (2.8)$$

Consider a particular example of the grating strength $S_{\text{VBG}} = 3.0$ at resonance, so that $R_{\text{VBG}} = 0.99$. Even if one has to deal with Fresnel reflections, $R_1 = R_2 = 0.04$ for $n_0 = 1.5$, the modified reflection at the exact Bragg condition is within the bounds $0.978 \le R_{\text{tot}} \le 0.996$. On the contrary, in the spectral points of exactly zero R_{VBG}, the residual reflection varies within the interval

$$\tanh^2(S_1 - S_2) \le R \le \tanh^2(S_1 + S_2). \qquad (2.9)$$

In particular, if $R_1 = R_2 = 0.04$, then $0 \le R \le 0.148$. Another example is if $R_1 = R_2 = 0.003$, then $0 \le R \le 0.012$. Formula (2.9) allows one also to estimate the maximum and minimum reflection of a Fabry-Perot interferometer with lossless mirrors of un-equal reflectivities R_1 and R_2.

Decomposition of Fresnel reflection in terms of strength of reflection

Consider now a fundamental problem of electrodynamics: the reflection of light by the sharp boundary between two media at the incidence angle θ_1, so that the refraction angle is θ_2. We denote by ε_1, μ_1, ε_2, μ_2 the values of the dielectric permittivity and the magnetic permeability in these two media, so that the phase propagation speeds $v_{1,2}$ and impedances $Z_{1,2}$ are

$$v_j = \frac{c}{n_j} \quad c = \frac{1}{\sqrt{\varepsilon_{\text{vac}}\mu_{\text{vac}}}}, \quad n_j = \sqrt{\frac{\varepsilon_j \mu_j}{\varepsilon_{\text{vac}}\mu_{\text{vac}}}}, \quad Z_j = \sqrt{\frac{\mu_j}{\varepsilon_j}}, \quad j = 1,2\,. \tag{2.10}$$

The angles θ_1 and θ_2 are related by the Snell's law, which is governed by the propagation speed ratio, i.e. by the ratio of refractive indices n_1 and n_2, namely $n_1\sin\theta_1 = n_2\sin\theta_2$. Cases of total internal reflection (TIR) and/or an absorbing second medium require definition

$$\cos\theta_2 = \sqrt{1-\left(n_1/n_2\right)^2 \sin^2\theta_1} = C_2' + iC_2'', \quad C_2'' > 0\,. \tag{2.11}$$

The condition $C_2'' > 0$ guarantees that exponential decrease of the transmitted wave into the depth of the second medium. The amplitudes of reflection for TE and TM polarizations are well known:

$$r_{\text{TE}} \equiv r(E_y \leftarrow E_y) = \frac{\cos\theta_1/Z_1 - \cos\theta_2/Z_2}{\cos\theta_1/Z_1 + \cos\theta_2/Z_2}, \quad r_{\text{TM}} \equiv r(E_x \leftarrow E_x) = -\frac{Z_1\cos\theta_1 - Z_2\cos\theta_2}{Z_1\cos\theta_1 + Z_2\cos\theta_2}\,. \tag{2.12}$$

These expressions have two very instructive limiting cases. The first one is the case of two media, which have the same phase speeds $v_1 = v_2$ (and thus refractive indices), so that $\theta_1 = \theta_2$. In a surprising manner, the reflection coefficients for such a problem do not depend on the angle and are equal to each other:

$$r_{\mathrm{TE}} = r_{\mathrm{TM}} \equiv r_{\Delta Z} = \frac{Z_2 - Z_1}{Z_2 + Z_1}. \tag{2.13}$$

The other case corresponds to media 1 and 2 having exactly the same impedances, $Z_1 = Z_2$, but different propagation speeds, $n_1 \neq n_2$. In that case, the reflection coefficients are equal (up to the sign):

$$r_{\mathrm{TE}} = -r_{\mathrm{TM}} \equiv r_{\Delta \mathrm{v}}(\theta_1) = \frac{\cos\theta_1 - \cos\theta_2}{\cos\theta_1 + \cos\theta_2}. \tag{2.14}$$

In particular there is no reflection at normal incidence for the pair of impedance-matched media (stealth technology). Reflection strength values $S = -\mathrm{arctanh}\, r$ for these two limiting cases are

$$S_{\Delta Z} = \frac{1}{2}\ln\left(\frac{Z_1}{Z_2}\right), \quad S_{\Delta \mathrm{v}}(\theta_1) = \frac{1}{2}\ln\left(\frac{\cos\theta_2}{\cos\theta_1}\right). \tag{2.15}$$

Here is truly remarkable relationship, which we have found. One can produce the reflection strengths $S_{\mathrm{TE}}(\theta_1)$ and $S_{\mathrm{TM}}(\theta_1)$ by simple addition (for TE) or subtraction (for TM) of the speed-governed and impedance-governed contributions from (2.15):

$$S_{\mathrm{TE}}(\theta_1) = S_{\Delta Z} + S_{\Delta \mathrm{v}}(\theta_1), \quad S_{\mathrm{TM}}(\theta_1) = S_{\Delta Z} - S_{\Delta \mathrm{v}}(\theta_1), \tag{2.16}$$

and according to (2.6), $r = -\tanh S$. One can easily verify that the expressions (2.15) and (2.16) reproduce the standard formulae (2.12) identically.

Propagation of electro-magnetic waves in layered media

We have actually found (2.16) for ourselves not empirically but have derived the result of additivity for reflection strength S directly from Maxwell's equations. Starting from here, we proceed with the tedious work of deriving the relevant formulae. The idea is to formulate the

exact Maxwell equations for the layered medium in terms of two coupled amplitudes A and B propagating with $P_z > 0$ and $P_z < 0$ respectively. We consider the incidence plane to be the xz plane, for a monochromatic wave $\propto \exp(-i\omega t)$ incident upon a layered medium with the properties being z-dependent only. By θ_{air} we denote the incidence angle of the wave in air, so that

$$\mathbf{k}_{\text{air}} = \hat{\mathbf{x}} k_x + \hat{\mathbf{z}} k_{\text{air},z}, \quad k_x = \frac{\omega}{c} n_{\text{air}} \sin\theta_{\text{air}}, \quad k_{\text{air},z} = \frac{\omega}{c} n_{\text{air}} \cos\theta_{\text{air}}. \tag{2.17}$$

The waves in a layered medium are naturally separated into transverse electric (TE) and transverse magnetic (TM) parts. We will write the electric and magnetic vectors of the two polarizations using the appropriately normalized components u_x, u_y, u_z and w_x, w_y, w_z, respectively:

$$\text{TE}: \quad \mathbf{E}(\mathbf{r},t) = -\hat{\mathbf{y}} u_y(z) e^{ik_x x - i\omega t} \sqrt{Z(z)}, \ \mathbf{H}(\mathbf{r},t) = \left[\hat{\mathbf{x}} w_x(z) + \hat{\mathbf{z}} w_z(z)\right] e^{ik_x x - i\omega t} / \sqrt{Z(z)}, \tag{2.18}$$

$$\text{TM}: \quad \mathbf{E}(\mathbf{r},t) = \left[\hat{\mathbf{x}} u_x(z) + \hat{\mathbf{z}} u_z(z)\right] e^{ik_x x - i\omega t} \sqrt{Z(z)}, \ \mathbf{H}(\mathbf{r},t) = \hat{\mathbf{y}} w_y(z) e^{ik_x x - i\omega t} / \sqrt{Z(z)}. \tag{2.19}$$

Here and below we use the quantities $k(z)$, $p(z)$, $g(z)$, $f(z)$ defined by

$$k(z) = \frac{\omega n(z)}{c}, \quad p(z) = \sqrt{k^2(z) - k_x^2} = k(z)\cos\theta(z), \tag{2.20}$$

$$g(z) = \frac{1}{2}\frac{d}{dz}\ln\frac{1}{Z(z)}, \quad f(z) = \frac{1}{2}\frac{d}{dz}\ln\frac{p(z)}{k(z)} \equiv \frac{1}{2}\frac{d}{dz}\ln\cos\theta(z). \tag{2.21}$$

Maxwell's equations for the amplitudes of the TE polarization are

$$iku_y = \partial_z w_x - ik_x w_z + g w_x, \quad -ikw_x = -\partial_z u_y + g u_y, \quad -ikw_z = ik_x u_y, \tag{2.22}$$

they may be rewritten as

$$\partial_z u_y = g u_y + ikw_x, \quad \partial_z w_x = i\,p^2 \big/ k\, u_y - g w_x. \tag{2.23}$$

It is convenient to introduce the amplitudes $A(z)$ and $B(z)$ for TE polarization by the definitions, see Figure 1:

$$A_{\mathrm{TE}}(z)e^{ik_{\mathrm{air},z}z} = \frac{1}{\sqrt{8}}\left(\sqrt{\frac{p}{k}}u_y(z) + \sqrt{\frac{k}{p}}w_x(z)\right),$$
$$B_{\mathrm{TE}}(z)e^{-ik_{\mathrm{air},z}z} = \frac{1}{\sqrt{8}}\left(\sqrt{\frac{p}{k}}u_y(z) - \sqrt{\frac{k}{p}}w_x(z)\right). \qquad (2.24)$$

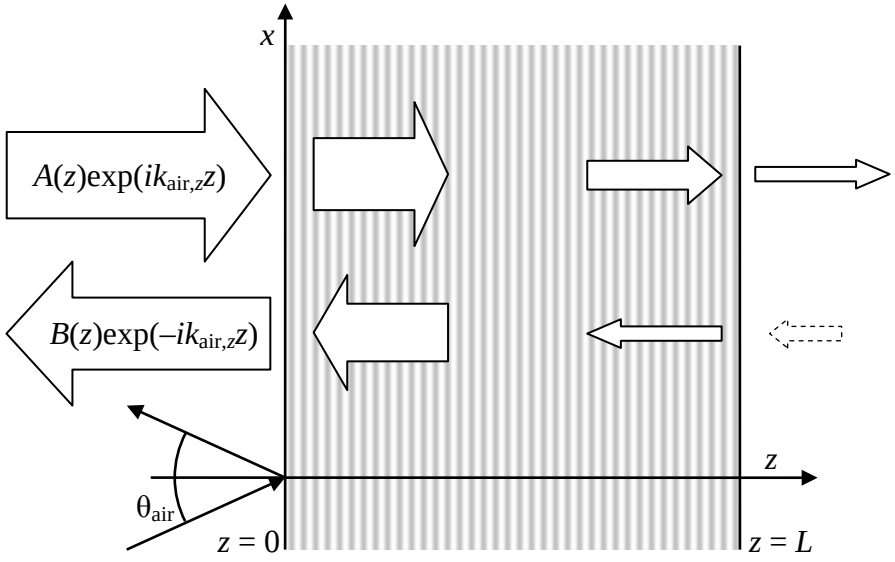

Figure 1. Notations for the incident $A(z)$ and reflected $B(z)$ waves in the approximation of infinitely wide plane beams with account of the reflections from both boundaries, $z = 0$ and $z = L$, as well as the reflection by the VBG.

The value of the z-component of the Poynting vector for any incidence angle at any point z is

$$P_z(z) = \frac{1}{4}\left(E_x H_y^* - E_y H_x^* + c.c.\right) = \left|A(z)\right|^2 - \left|B(z)\right|^2. \qquad (2.25)$$

It should be emphasized that we have deliberately chosen to normalize the amplitudes $A(z)$ and $B(z)$ such that the relationship (2.25) is valid at any point z. One may further consider the transformation (2.24) as a transition to "Slowly Varying Envelopes" (SVE) $A(z)$ and $B(z)$. It is important to emphasize, however, that no approximations were made up to this point. Indeed, the exact Maxwell equations for TE polarization are reduced by the coupled pair:

$$\frac{d}{dz}\begin{pmatrix} A_{\mathrm{TE}}(z) \\ B_{\mathrm{TE}}(z) \end{pmatrix} = \hat{V}_{\mathrm{TE}}\begin{pmatrix} A_{\mathrm{TE}}(z) \\ B_{\mathrm{TE}}(z) \end{pmatrix}, \quad \hat{V}_{\mathrm{TE}} = \begin{pmatrix} i\left(p(z) - k_{\mathrm{air},z}\right) & \left(g(z) + f(z)\right)e^{-2ik_{\mathrm{air},z}z} \\ \left(g(z) + f(z)\right)e^{2ik_{\mathrm{air},z}z} & -i\left(p(z) - k_{\mathrm{air},z}\right) \end{pmatrix}. \quad (2.26)$$

A similar set of transformations may be done for TM polarization:

$$\begin{gathered} -iku_x = -\partial_z w_y - g w_y, \quad -iku_z = ik_x w_y, \quad -ikw_y = ik_x u_z - \partial_z u_x + g u_x \quad \Leftrightarrow \\ \Leftrightarrow \quad \partial_z u_x = g u_x + i\,p^2/k, \quad \partial_z w_y = iku_x - g w_y, \end{gathered} \quad (2.27)$$

with the same parameters $k(z)$, $g(z)$, $p(z)$. The amplitudes of coupled TM waves are

$$\begin{aligned} A_{\mathrm{TM}}(z)e^{ik_{\mathrm{air},z}z} &= \frac{1}{\sqrt{8}}\left(\sqrt{\frac{k}{p}}u_x(z) + \sqrt{\frac{p}{k}}w_y(z)\right), \\ B_{\mathrm{TM}}(z)e^{-ik_{\mathrm{air},z}z} &= \frac{1}{\sqrt{8}}\left(\sqrt{\frac{k}{p}}u_x(z) - \sqrt{\frac{p}{k}}w_y(z)\right). \end{aligned} \quad (2.28)$$

Finally, the exact Maxwell equations for TM polarization are

$$\frac{d}{dz}\begin{pmatrix} A_{\mathrm{TM}}(z) \\ B_{\mathrm{TM}}(z) \end{pmatrix} = \hat{V}_{\mathrm{TM}}\begin{pmatrix} A_{\mathrm{TM}}(z) \\ B_{\mathrm{TM}}(z) \end{pmatrix}, \quad \hat{V}_{\mathrm{TM}} = \begin{pmatrix} i\left(p(z) - k_{\mathrm{air},z}\right) & \left(g(z) - f(z)\right)e^{-2ik_{\mathrm{air},z}z} \\ \left(g(z) - f(z)\right)e^{2ik_{\mathrm{air},z}z} & -i\left(p(z) - k_{\mathrm{air,z}}\right) \end{pmatrix}, \quad (2.29)$$

with the same parameters $f(z)$, $g(z)$ as in (2.21). The gradient functions $f(z)$ (related to propagation speed) and $g(z)$ (related to impedance) enter as a sum (for TE polarization) or as a difference (for TM one) into our coupled equations. Sharp steps of $n(z)$ and $Z(z)$ yield our result, equations (2.16).

The notion of reflection strength was originally introduced by us for non-absorbing media. It is remarkable, that the reflection by a sharp step with an absorbing second medium, or in the case of TIR, are both described by $S = -\text{arctanh}(r)$ and equations (2.15) and (2.16) are still valid. In particular, the TIR regime corresponds to

$$S_{\Delta Z} = \frac{1}{2}\ln\left(\frac{Z_1}{Z_2}\right), \quad S_{\Delta \mathrm{v}}(\theta_1) = i\frac{\pi}{4} + \frac{1}{2}\ln\left(\sqrt{(n_1/n_2)^2 \sin^2\theta_1 - 1}\Big/\cos\theta_1\right). \tag{2.30}$$

As expected, $|r| = |\tanh(i\pi/4 + \mathrm{Re}\, S)| = 1$ for the case of TIR.

Formalism of strength of reflection in other branches of physics

It is interesting to consider the reflection of longitudinal acoustic waves from the boundary between two liquids, which have densities ρ_1 and ρ_2, propagation speeds c_1 and c_2 and, therefore, acoustic impedances $Z_1 = \rho_1 c_1$ and $Z_2 = \rho_2 c_2$, respectively. A well-known expression for the reflection coefficient for the wave's pressure [31-Brekhovskikh 80, 96-Landau 87] is

$$r_{\text{longitud}} \equiv r(p \leftarrow p) = \frac{\cos\theta_1/Z_1 - \cos\theta_2/Z_2}{\cos\theta_1/Z_1 + \cos\theta_2/Z_2}. \tag{2.31}$$

For this acoustic case we see again that the reflection strength is given by the sum of two contributions,

$$r_{\text{longitud}} = -\tanh[S_p(\theta_1)], \qquad S_p(\theta_1) = S_{\Delta Z} + S_{\Delta c}(\theta_1). \tag{2.32}$$

The Schrödinger equation for the motion of an electron in a given Bloch band should generally account for two kinds of spatial inhomogeneity, see e.g. [97-Nelin 07]. One of them is $U(\mathbf{r})$ [Joule], i.e. the spatial profile of the bottom of the Brillouin zone. The other one must describe $m(\mathbf{r})$ [kg], i.e. the inhomogeneity of the coefficient $1/(2m)$ in the parabolic

approximation $E(\mathbf{p}) = p^2/(2m)$ of the dependence of electron energy in the vicinity of the bottom of Brillouin zone on the momentum $\mathbf{p}$. The corresponding hermitian Hamiltonian is

$$\hat{H} = \hat{\mathbf{p}} \frac{1}{2m(\mathbf{r})} \hat{\mathbf{p}} + U(\mathbf{r}); \tag{2.33}$$

which acts upon the wavefunction ψ. Consider now the motion of the electron with fixed energy E, i.e. $\psi(\mathbf{r},t) = \psi(\mathbf{r})\exp(-iEt/\hbar)$. Then the stationary Schrödinger equation takes the form

$$m(\mathbf{r})\nabla\left[\frac{1}{m(\mathbf{r})}\nabla\psi\right] + \frac{2m(\mathbf{r})}{\hbar^2}\left[E - U(\mathbf{r})\right]\psi = 0. \tag{2.34}$$

If $m(\mathbf{r})$ = const, then equation (2.34) is reduced to the conventional Schrödinger equation. It is convenient to introduce two quantities: a "kinematic parameter" $k(\mathbf{r})$ in m, i.e. the wavenumber, and a "dynamical parameter" $Z(\mathbf{r})$ in s/m, the analog of impedance by definitions

$$k(\mathbf{r}) = \frac{1}{\hbar}\sqrt{2m(\mathbf{r})\left[E - U(\mathbf{r})\right]}, \qquad Z(\mathbf{r}) = \frac{m(\mathbf{r})}{\hbar k(\mathbf{r})} = \sqrt{\frac{m(\mathbf{r})}{2\left[E - U(\mathbf{r})\right]}}. \tag{2.35}$$

Numerically, the parameter $Z(\mathbf{r})$ coincides with the local value of the inverse group velocity. With these notations equation (2.34) takes the form

$$Z(\mathbf{r})k(\mathbf{r})\nabla\left[\frac{1}{Z(\mathbf{r})k(\mathbf{r})}\nabla\psi\right] + k^2(\mathbf{r})\psi = 0. \tag{2.36}$$

Equation (2.36) has two interesting limiting cases. One of them is (2.36) with $Z = Z_0$ = const,

$$k(\mathbf{r})\nabla\left[\frac{1}{k(\mathbf{r})}\nabla\psi\right] + k^2(\mathbf{r})\psi = 0. \tag{2.37}$$

and we may call it the *Z*-Helmholtz equation to emphasize the condition $Z = Z_0 = \text{const}$. This *Z*-Helmholtz equation was first introduced in the talk by Prof. Zeldovich and Dr. Tsai [98-Tsai 06] in 2006.

The other limiting case is when $k = k_0 = \text{const}$, but the impedance is coordinate-dependent:

$$Z(\mathbf{r})\nabla\left[\frac{1}{Z(\mathbf{r})}\nabla\psi\right] + k_0^2\psi = 0\,. \qquad (2.38)$$

and for similar reasons (2.38) may be labeled as the *k*-Helmholtz equation. Finally, when both $Z = Z_0 = \text{const}$ and $k = k_0 = \text{const}$, we come to standard Helmholtz equation, $\nabla^2\psi + k_0^2\psi = 0$. The usual stationary Schrödinger equation $\nabla^2\psi + k^2(\mathbf{r})\psi = 0$ (i.e. with $\hbar kZ = m_0 = \text{const}$) is a certain intermediate case between the *Z*-Helmholtz and the *k*-Helmholtz equations.

The flux **J** [particles/(m^{2}s)] for a plane mono-energetic wave $\psi = \exp(-i\mathbf{kr})$ in a homogeneous part of the medium equals $\mathbf{J} = (\mathbf{k}/k)\mathrm{v}|\psi|^2 = (\mathbf{k}/k)|\psi|^2/Z$. The conservation law, which is valid as a consequence of the mono-energetic Schrödinger equation (2.36), is

$$\mathrm{div}\mathbf{J}(\mathbf{r},t) = 0, \quad \mathbf{J}(\mathbf{r},t) = \frac{i\hbar}{2m(\mathbf{r})}\left(\psi\nabla\psi^* - \psi^*\nabla\psi\right). \qquad (2.39)$$

The problem of reflection for a one-dimensional stationary Schrödinger equation,

$$\frac{d^2\psi}{dz^2} + k^2(z)\psi(z) = 0, \quad k^2(z) = \frac{2m}{\hbar^2}\left(E - V(z)\right), \qquad (2.40)$$

may also be solved by the coupled wave approach. Namely, we will assume for definiteness that $k^2(z) > 0$, and introduce local amplitudes $A(z)$ and $B(z)$ by

$$A(z)e^{ik_0 z} = \sqrt{k(z)}\psi - \frac{i}{\sqrt{k(z)}}\frac{d\psi}{dz}, \quad B(z)e^{-ik_0 z} = \sqrt{k(z)}\psi + \frac{i}{\sqrt{k(z)}}\frac{d\psi}{dz}, \quad k_0 = \frac{\sqrt{2mE}}{\hbar}. \tag{2.41}$$

The advantage of the amplitudes $A(z)$ and $B(z)$ is that the flux $J_z(z)$ is expressed very simply:

$$J(z) = \frac{i\hbar}{2m}\left(\psi\frac{d\psi^*}{dz} - \psi^*\frac{d\psi}{dz}\right) = \frac{\hbar}{4m}\left(|A(z)|^2 - |B(z)|^2\right), \tag{2.42}$$

This flux is conserved, $J(z) = \text{const}$, as a consequence of (2.34) with a real mass and potential. The uniqueness of the representation (2.41) is guaranteed, if one requires it, by the fact that in the homogenous part of the medium our waves A and B do not interact with each other. It is important, to note that (2.40) is exactly equivalent to the system of coupled first order equations:

$$\frac{d}{dz}\begin{pmatrix} A(z) \\ B(z) \end{pmatrix} = \begin{pmatrix} i(k(z)-k_0) & F(z)e^{-2ik_0 z} \\ F(z)e^{2ik_0 z} & -i(k(z)-k_0) \end{pmatrix}\begin{pmatrix} A(z) \\ B(z) \end{pmatrix}, \quad F(z) = \frac{1}{4}\frac{d}{dz}\ln k^2(z). \tag{2.43}$$

A numerical (or analytical, whenever possible) solution of this exact system in the form of an $\hat{M}$-matrix allows one to find the amplitudes of reflection and transmission. It should be emphasized that the boundary conditions for system (2.43) are applied only at one end, e.g. at $z = -\infty$, so that one should solve the Cauchy problem for which any standard code of integration of ODEs works very well. Figure 2 shows the example of the profiles of $|A(z)|^2$ and $|B(z)|^2$ normalized to $P(z) = 1$ for the problem with

$$k^2(z) = k_0^2 + \alpha^2 s(s+1)\big/\cosh^2(\alpha z), \tag{2.44}$$

at particular "non-reflective" value $s = 1$ at $k_0/\alpha = 0.3$ (see Landau & Lifshitz 1981).

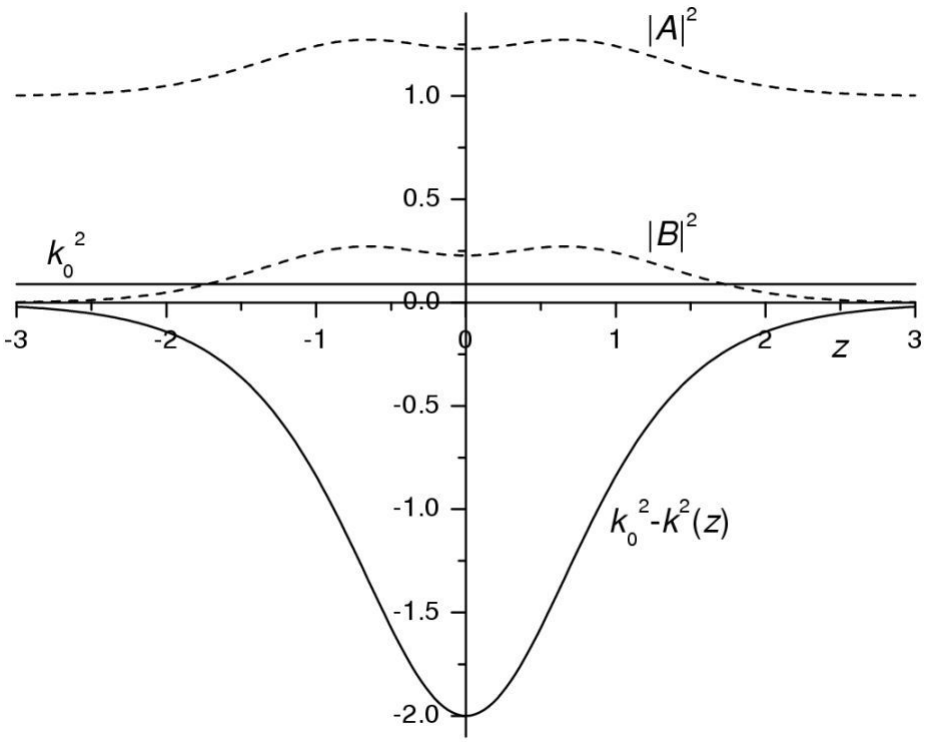

Figure 2. Solid lines: potential well $k_0^2 - k^2(z) = -2/\cosh^2 z$ yielding non-reflection and incident beam energy $k_0^2 = 0.09$. Dashed lines: fluxes $|A(z)|^2$ and $|B(z)|^2$ of counter-propagating wave function components.

Solving for the reflection of waves for tilted incidence by a sharp boundary between two media with different values (k_1, Z_1) and (k_2, Z_2) requires the analog of Snell's law: $k_1 \sin\theta_1 = k_2 \sin\theta_2$. Here θ_1 and θ_2 are the angles of the momentum normal to the boundary in the respective media. The boundary conditions of continuity of wave-function ψ and of the $(\partial\psi/\partial z)/(Zk)$ yield the following expression for the reflection coefficient:

$$r = -\tanh S, \quad S = S_{\Delta k} + S_{\Delta Z}, \quad S_{\Delta k} = \frac{1}{2}\ln\left(\frac{\cos\theta_2}{\cos\theta_1}\right), \quad S_{\Delta Z} = \frac{1}{2}\ln\left(\frac{Z_1}{Z_2}\right), \quad (2.45)$$

similar to expression (2.16) which we have for TE electromagnetic wave.

CHAPTER THREE: PROPERTIES OF UNIFORM VBG AND FRESNEL CORRECTIONS

SVEA equations for reflection by VBG

Consider now a non-magnetic (i.e. optical) medium with a volume Bragg grating (VBG) of refractive index $n(z)$:

$$\begin{aligned} n(z) &= n_0 + n_2(z) + n_1(z)\cos\big(Qz + \gamma(z)\big), \\ Z(z) &= \frac{Z_{\text{vac}}}{n(z)} \approx \frac{Z_{\text{vac}}}{n_0^2}\big(n_0 - n_2(z) - n_1'(z)\cos\big(Qz + \gamma(z)\big)\big). \end{aligned} \tag{3.1}$$

Here real $n_1(z)$ and $\gamma(z)$ are slow varying zero-to-top amplitude and phase of the "refractive" component of the VBG and $n_2(z)$ is small local correction to constant real refractive index n_0; that correction $n_2(z)$ includes possible loss $i\text{Im}[n_2(z)]$, so that the spatially-averaged power attenuation coefficient of the material is $\alpha_{\text{loss}}[1/\text{meter}] = 2\omega n_2''/c$.

We can calculate our coupling functions $f(z)$ and $g(z)$ according to (2.21) by approximate differentiation of fast oscillating terms of $n(z)$ only:

$$\begin{aligned} f(z) &= \frac{\frac{1}{2}n_{\text{air}}^2 \sin\theta_{\text{air}}^2}{n^2(z) - n_{\text{air}}^2 \sin\theta_{\text{air}}^2}\frac{d\ln n(z)}{dz}, \quad g(z) = \frac{1}{2}\frac{d\ln n(z)}{dz}, \\ \frac{d\ln n(z)}{dz} &\approx -Q\frac{n_1(z)\sin(Qz + \gamma(z))}{n_0}. \end{aligned} \tag{3.2}$$

Effective interaction between waves a and b occurs at the Bragg condition, when

$$Q \approx 2\frac{\omega}{c}n_0\cos\theta_{\text{in}}, \quad \cos\theta_{\text{in}} = \sqrt{1 - n_{\text{air}}^2 \sin\theta_{\text{air}}^2 \big/ n_0^2}\ . \tag{3.3}$$

Here θ_{in} is the angle between the z-axis and the propagation direction of light inside the VBG. Thus, Eq. (3.2) with account of the Bragg condition leads to coupling functions for TE and TM polarizations

$$g(z)+f(z)\approx-\frac{\omega}{c}\frac{n_1(z)\sin(Qz+\gamma(z))}{\cos\theta_{\text{in}}},$$
$$g(z)-f(z)\approx\big(g(z)+f(z)\big)\cos 2\theta_{\text{in}}\,. \tag{3.4}$$

We see a natural result: the coupling coefficient (which in optics is due to modulation of ε(*z*) only) is smaller by factor $\rho = (\mathbf{p}_a\cdot\mathbf{p}_b) = \cos 2\theta_{\text{in}}$ for TM polarization in comparison with the coupling for TE polarization, where that factor equals 1. Here $\mathbf{p}_a$ and $\mathbf{p}_b$ are unit polarization vectors of the electric field for waves *a* and *b*. The function sin(*Qz*+γ(*z*)) is equal to

$$\sin\big(Qz+\gamma(z)\big)=\frac{1}{2i}\Big(e^{iQz+i\gamma(z)}-e^{-iQz-i\gamma(z)}\Big), \tag{3.5}$$

and a similar expression for the function sin(*Qz*+δ(*z*)). The slowly varying envelope approximation, which we will use later, corresponds to keeping only one of the two exponential terms from (3.5) in the coupling terms from Eqs. (2.26) and (2.29); namely, the terms which will effect *z*-accumulated coupling. As a result, we get the equation for matrix $\hat{M}(z)$ expressing values *a*(*z*) and *b*(*z*) through *a*(0) and *b*(0):

$$\frac{d}{dz}\hat{M}(z)=\hat{V}_{\text{TE,TM}}(z)\hat{M}(z),\quad \hat{V}(z)=\begin{pmatrix} i\big(p(z)-k_{\text{air},z}\big) & i\kappa_+(z)e^{iQz-2ik_{\text{air},z}z} \\ -i\kappa_-(z)e^{-iQz+2ik_{\text{air},z}z} & -i\big(p(z)-k_{\text{air},z}\big)\end{pmatrix}, \tag{3.6}$$

$$\text{TE}:\quad \kappa_+(z)=\frac{\omega}{c}\frac{n_1(z)e^{i\gamma(z)}}{2\cos\theta_{\text{in}}},\quad \kappa_-(z)=\frac{\omega}{c}\frac{n_1(z)e^{-i\gamma(z)}}{2\cos\theta_{\text{in}}}\,. \tag{3.7}$$

The interaction coefficients κ_+ and κ_- have indexes (+) or (–), denoting the ± *z*-direction, in which the result of the corresponding scattering propagates. These coefficients for TM polarization are smaller by the polarization factor $\rho=\cos 2\theta_{\text{in}}$. As written in Eq. (3.6), the

interaction matrix still contains fast-oscillating phase factors. However, choosing a "central" value of the real parameter $p_0 = Q/2$, one can present the matrix $\hat{M}(z)$ in the form

$$\hat{M}(z) = \hat{K}\left((Q/2 - k_{\text{air},z})z\right)\hat{P}(z), \tag{3.8}$$

so that the equation for the $\hat{P}$-matrix becomes "slow varying" indeed:

$$\frac{d\hat{P}(z)}{dz} = \hat{W}(z)\hat{P}(z), \quad \hat{W}(z) = \begin{pmatrix} i\left(p(z) - Q/2\right) & i\kappa_+(z) \\ -i\kappa_-(z) & -i\left(p(z) - Q/2\right) \end{pmatrix}. \tag{3.9}$$

Then the Bragg condition is satisfied when $p(z) = Q/2$.

As we already discussed, a numerical (or analytic) solution of the Cauchy problem for this system placed between $z_1 = 0$ and $z_2 = L$ yields the matrix $\hat{P}(L)$, and thus $\hat{M}(L)$. If our glass plate with a VBG is placed at an arbitrary z_1, then, according to the definition of the amplitudes $a(z)$ and $b(z)$, the matrix $\hat{M}(z_2, z_1)$ will equal

$$\hat{M}\left(z_2 = z_1 + L, z_1\right) = \hat{K}\left(-k_{\text{air},z}z_1\right)\hat{M}(L)\hat{K}\left(k_{\text{air},z}z_1\right). \tag{3.10}$$

The value of the matrix $\hat{M}(z_2, z_1)$ at $z_2 = z_1 + L$, i.e. at the end of VBG, allows one to find the reflection and transmission coefficients.

Kogelnik's analytical solution for a uniform VBG

Consider a VBG medium placed between z_1 and $z_2 = z_1 + L$ with the previously considered above refractive index profile $n(z - z_1)$ with homogeneous (constant) parameters n_1, γ, δ, n_2', in_2'', and $\alpha_{\text{loss}}[1/\text{meter}] = 2\omega n_2''/c$ being the spatially-averaged attenuation coefficient for power. For

definiteness we consider here only the TE polarization. The function $p(z)$ from (2.21) in this case will be assumed constant with a small positive imaginary part:

$$p = \frac{\omega}{c}\sqrt{\left(n_0 + n_2\right)^2 - n_{\text{air}}^2 \sin\theta_{\text{air}}^2} \approx \frac{\omega}{c}\left(n_0 \cos\theta_{\text{in}} + \frac{n_2}{\cos\theta_{\text{in}}}\right) = p' + ip'', \quad p'' = \frac{\alpha_{\text{loss}}}{2\cos\theta_{\text{in}}}. \quad (3.11)$$

After that, the $\hat{W}$-matrix from (3.9) becomes z-independent, and Eq. (3.9) has the explicit solution:

$$\frac{d\hat{P}(z)}{dz} = \hat{W}\hat{P}(z),\ \hat{W} = \begin{pmatrix} i\Delta & i\kappa_+ \\ -i\kappa_- & -i\Delta \end{pmatrix} \quad \Rightarrow \quad \hat{P}(L) = e^{\hat{W}L} = \hat{1}\cosh G + \hat{W}L\frac{\sinh G}{G}, \quad (3.12)$$

$$\Delta = p' + ip'' - \tfrac{1}{2}Q, \quad G = \sqrt{S_+S_- - X^2}, \quad S_\pm = \kappa_\pm L = \kappa_\pm' L + i\kappa_\pm'' L, \quad X = \Delta \cdot L = X' + iX''. \quad (3.13)$$

The dimension of Δ is [1/meter]. In this manner, the matrix $\hat{P}(L)$ becomes

$$\hat{P}(L) = \begin{pmatrix} \cosh G + iX\dfrac{\sinh G}{G} & iS_+\dfrac{\sinh G}{G} \\ -iS_-\dfrac{\sinh G}{G} & \cosh G - iX\dfrac{\sinh G}{G} \end{pmatrix}. \quad (3.14)$$

Going back to Eqs. (3.10) and (3.8), we obtain the expression for the matrix $\hat{M}(z_2, z_1)$:

$$\hat{M}_{\text{VBG}}(z_2, z_1) = \hat{K}\left(-k_{\text{air},z}z_1 - \left(k_{\text{air},z} - \frac{Q}{2}\right)L\right)\hat{P}(L)\hat{K}\left(k_{\text{air},z}z_1\right), \quad (3.15)$$

As a result, the reflection coefficient for a VBG becomes

$$r(b \leftarrow a) = r_- = -\frac{M_{ba}}{M_{bb}} = -e^{2ik_{\text{air},z}z_1}\frac{P_{ba}}{P_{bb}} = e^{2ik_{\text{air},z}z_1}\frac{iS_-\sinh G/G}{\cosh G - iX\sinh G/G}. \quad (3.16)$$

Formulae (3.1)-(3.6) of this Section 3 allow one to find the reflection coefficient even in the presence of loss or gain. Equivalent results in different notation were first derived in the

fundamental work of H. Kogelnik [42-Kogelnik 69]. We have re-derived them in our notation, which facilitate the subsequent account of Fresnel reflections.

Imaginary detuning may be expressed via intensity an attenuation coefficient α_{loss}:

$$X'' \equiv Y = \frac{\alpha_{\text{loss}} L}{2\cos\theta_{\text{in}}}. \tag{3.17}$$

The relatively difficult part is to express the dimensionless quantity Re(X) via observables; this parameter signifies the detuning from the Bragg condition. Suppose that the Bragg condition is satisfied exactly at certain values of the incident angle $\theta_{air,0}$ at the wavelength $\lambda_{vac,0}$ for definite values of Q and n_2. Then, in the case of relatively small (but homogeneous) deviations from the Bragg condition one gets

$$\delta\,\mathrm{Re}(X) = \frac{-2\pi n_0 L\cos\theta_{\text{inside}}}{\lambda_{\text{vac},0}}\left(\frac{\delta\lambda_{\text{vac}}}{\lambda_{\text{vac}}} + \frac{\delta Q}{2Q} + \frac{1}{\cos^2\theta_{\text{inside}}}\left[\frac{n_{\text{air}}^2}{2n_0^2}\left(\sin^2\theta_{\text{air}} - \sin^2\theta_{\text{air},0}\right) - \frac{\delta n_2}{n_0}\right]\right). \tag{3.18}$$

While the appearance of expressions (3.11)-(3.18) is rather heavy, their calculation by any computer is quite straightforward. Moreover, accuracy of modern computers allows one to use the procedure, which is morally reprehensible, but numerically admissible: calculate p(detuned) – p(Bc) as a small difference of two large quantities. Such a procedure reduces the risk of making a typo in Eq. (3.18).

In the absence of loss or gain and with the modulation of real Re(n_1'), one gets $S_+=(S_-)^*=S_0e^{i\gamma}$ and Im(X) = 0, so that one can use the notion of reflection strength S, and then the reflection coefficient $R_{VBG} = R_+ = R_- = R$ becomes

$$R = \left|r\,(b \leftarrow a)\right|^2 = \tanh^2 S = \frac{\sinh^2 G}{\cosh^2 G - X^2/S_0^2};$$
$$S = \operatorname{arcsinh}\left(S_0 \frac{\sinh G}{G}\right),\ S_0 = \sqrt{S_+ S_-} = \left|S_+\right|,\ G = \sqrt{S_0^2 - X^2}. \qquad (3.19)$$

Finally, at the exact Bragg condition, $X = 0$, and without loss, the reflection strength S in (3.19) is

$$S = S_0 = \frac{\pi n_1 L}{\lambda_{\text{vac}} \cos\theta_{\text{in}}}, \qquad (3.20)$$

which constitutes the most important and most simple formula of Kogelnik's VBG theory.

Influence of Fresnel reflections

For a sharp boundary positioned at z_b, the process of Fresnel reflection of the waves with TE and TM polarizations is described, according to (2.12) and (3.10), by the matrix $\hat{M}$:

$$\hat{M}(z_b + 0, z_b - 0) = \hat{K}(-k_{\text{air},z} z_b)\hat{\Sigma}(S)\hat{K}(k_{\text{air},z} z_b) \qquad (3.21)$$

$$\hat{\Sigma}(S) = \begin{pmatrix} \cosh S & \sinh S \\ \sinh S & \cosh S \end{pmatrix},\quad S_{\text{TE,TM}} = \ln\sqrt{\frac{Z_1}{Z_2}} \pm \ln\sqrt{\frac{\cos\theta_2}{\cos\theta_1}} \equiv \ln\sqrt{\frac{n_2}{n_1}} \pm \ln\sqrt{\frac{\cos\theta_2}{\cos\theta_1}}. \qquad (3.22)$$

At normal incidence to the boundary between two optical media with n_1 and n_2, the reflection strength is the same for both polarizations: $S = \frac{1}{2}\ln(n_2/n_1)$, since $Z = Z_{\text{vac}}/n$. For the particular case $n_2/n_1 = 1.5$, one gets $S = 0.2027$.

Now consider the case of a VBG positioned between z_1 and $z_2 = z_1 + L$ with a background refractive index n_0; this VBG is surrounded by air, and $n_{\text{air}} = 1$. For a VBG with boundaries, the transformation matrix $\hat{M}$ given by Eq. (3.15) will be surrounded by two boundary matrices of the type (3.21):

$$\hat{M}(z_2+0, z_1-0) = \hat{K}(-k_{\text{air},z} z_2)\hat{\Sigma}(S_2)\hat{K}(k_{\text{air},z} z_2)\hat{M}_{\text{VBG}}(z_2, z_1)\hat{K}(-k_{\text{air},z} z_1)\hat{\Sigma}(S_1)\hat{K}(k_{\text{air},z} z_1)\,. \quad (3.23)$$

Here S_1 and S_2 are the strengths of reflections at the corresponding boundaries, and the matrix $\hat{M}_{\text{VBG}}(z_2, z_1)$ is given by Eq. (3.15). While the analytical expressions look quite heavy, one has to multiply the matrices given by explicit expressions only; such a procedure is very simple for a computer.

In case of a perfectly lossless VBG one has to take into account the phase relationships between contributions of the first boundary, the VBG and the second boundary. After a summation of the arguments in the corresponding $\hat{K}$-matrices, the total matrix of VBG with boundaries given by (3.23) will be

$$\hat{M} = \hat{K}(-k_{\text{air},z} z_2)\hat{\Sigma}(S_2)\hat{K}((\gamma + QL)/2)\hat{P}_{S_0,X}\hat{K}(-\gamma/2)\hat{\Sigma}(S_1)\hat{K}(k_{\text{air},z} z_1)\,, \quad (3.24)$$

$$\hat{P}_{S_0,X} = \begin{pmatrix} \cosh G + iX\dfrac{\sinh G}{G} & iS_0\dfrac{\sinh G}{G} \\ -iS_0\dfrac{\sinh G}{G} & \cosh G - iX\dfrac{\sinh G}{G} \end{pmatrix}, \quad G = \sqrt{S_0^2 - X^2}\,, \quad (3.25)$$

with S_0 and X defined in (3.13) and (3.19). We see that the character of the curve of reflectance versus detuning depends on two phases: γ and QL, both related to the properties of the specimen, which contains the grating. Their values fluctuate from one specimen to the other as a result of manufacturing of VBG. Quite often the specimens are coated with antireflection layers.

Far from resonance, when $X >> S_0$, the matrix $\hat{P}_{S_0,X}$ will transform into a diagonal phase matrix $\hat{K}(X)$. Then, after summation of the phases between the boundaries, we simplify the matrix (3.24) to

$$\hat{M} = \hat{K}(-k_{\text{air},z} z_2)\hat{\Sigma}(S_2)\hat{K}(\varphi)\hat{\Sigma}(S_1)\hat{K}(k_{\text{air},z} z_1), \quad \varphi = pL = \frac{\omega}{c} n_0 L\cos\theta_{\text{in}}\,, \quad (3.26)$$

which describes an ordinary glass plate with interferometric properties defined by the phase difference *pL*. When this relative boundary phase is equal to an integer number *m* of π, typically large, then the matrix $\hat{K}(\varphi)$ is proportional to the unit matrix, and the total reflection strength is $S = S_1+S_2 = 0$. This corresponds to perfectly resonant transmission in a Fabry-Perot interferometer based on reflections by the two boundaries. If at some particular frequency or angle point our VBG has zero strength, e.g. if $G = im\pi$, with *m* being integer non-zero number, then $\hat{P}_{S_0,X}$ is proportional to the unit matrix and the boundary strength matrices $\hat{\Sigma}$ are separated by the phase matrix so that the total reflectance will be defined only by the boundaries.

Let us return to the VBG without background loss or gain and with boundaries of different reflectances R_1 and R_2 in general case, so that their reflection strengths are $|S_{1,2}| = \operatorname{arctanh}\sqrt{R_{1,2}}$, respectively. Multiplication of the corresponding matrices of the first and of second boundaries of the VBG yielded the resulting matrix (3.24). The maximum and minimum values of the total resultant strength are realized when the boundary terms are added or subtracted from the VBG term,

$$R = \tanh^2 S, \quad S_{\max} = S_{\mathrm{VBG}} + |S_1| + |S_2|, \quad S_{\min} = S_{\mathrm{VBG}} - (|S_1| + |S_2|), \tag{3.27}$$

due to appropriate intermediate phases. We consider formula (3.27) to be one of the important results of the present work.

Figure 3 was obtained by direct multiplication of the relevant matrices and then by depicting all possible values of $|R_{\mathrm{total}}|^2$ at various combinations of the phases.

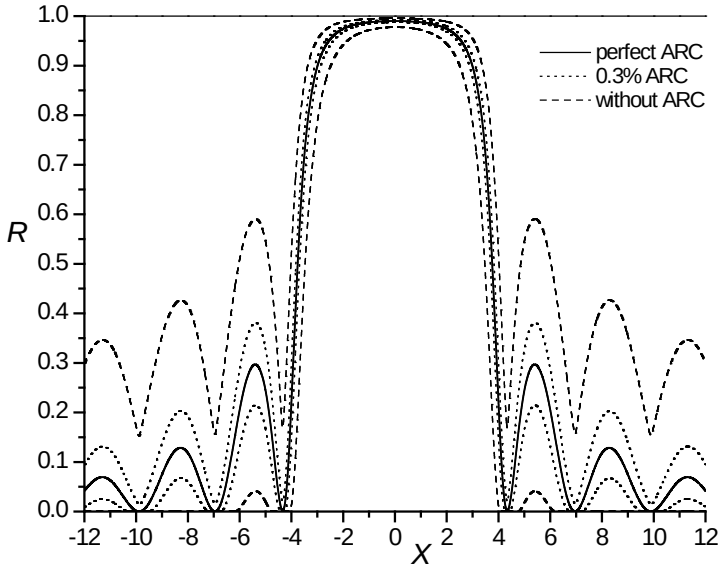

Figure 3. Reflectivity R of a VBG with account of the interference of reflection from the VBG alone with two extra contributions: from the two boundaries of the specimen, for all possible phase combinations. Values of R are between the dashed curves for Fresnel 4% reflections from bare boundaries, and are between dotted curves for anti-reflection coatings (ARC) at 0.3% each.

We see that in the region of perfect Bragg condition, $X = 0$, the reflectivity is not affected strongly by the boundaries. Even if one has to deal with Fresnel reflections, $R_1 = R_2 = 0.04$ (for $n_0 = 1.5$), the modified reflection at the exact Bragg condition is within the boundaries $0.9779 \le R_{\text{total}} \le 0.9956$ for $R_{\text{VBG}} = 0.9900$ (S = 2.993). On the contrary, in the spectral points of exactly zero R_{VBG}, where in (3.19) $X^2 = S_0^2 + m^2\pi^2$ with integer nonzero m, the residual reflection varies within the interval

$$\tanh^2(S_1 - S_2) \le R \le \tanh^2(S_1 + S_2), \quad S_i = \arctan\sqrt{R_i}\ . \tag{3.28}$$

In particular, if $R_1 = R_2 = 0.0400$, then there is a $0 \leq R \leq 0.1479$. Another example is if $R_1 = R_2 = 0.0030$; then $0 \leq R \leq 0.0119$. It means that there is a considerable advantage of the coating the VBG with an anti-reflection coating.

CHAPTER FOUR: NON-UNIFORM VBGS

Propagation of EM waves in a non-uniform VBG

The requirements for angular and spectral selectivities of VBGs define their necessary physical parameters such as thickness, depth of modulation of refractive index etc. The properties uniformly modulated VBGs are well known from Kogelnik's theory. Standard deliberately introduced non-uniformities are the apodization of refractive index modulation for reducing secondary lobes in the reflectance spectrum and chirping the grating period to compress short pulses. Parameters of real fabricated gratings can vary from the required ones and can significantly affect final properties. The influence of undesirable non-uniformities was studied for fiber gratings: the presence of a spatial quadratic term in the background refractive index and the observed asymmetries transmission spectrum of a fiber grating [65-Mizrahi 93] were discussed. An analysis of VBGs is more complicated because of the additional parameter, the angle of incidence.

The propagation of electromagnetic waves in layered media can be formulated in terms of counter-propagating waves $A(z)\exp(-i\omega t + ik_z z)$ and $B(z)\exp(-i\omega t - ik_z z)$ with a convenient normalization of Poynting vector: $P_z = |A|^2 - |B|^2$, (2.25). The matrix relationship for wave coupling in linear media is $A(z) = M_{AA}\cdot A(0) + M_{AB}\cdot B(0)$, $B(z) = M_{BA}\cdot A(0) + M_{BB}\cdot B(0)$. In the absence of losses, the matrix $\hat{M}$ belongs to the group SL(1,1) and the amplitude reflection coefficient for an element of length L is equal to $r = r(A \leftarrow B) = -M_{BA}(L)/M_{BB}(L) = -e^{-2i\eta}\tanh S$, where η is a phase parameter and S is the strength of reflection. Matrix $\hat{M}(z)$ can be found from equation

$$d\hat{M}/dz = \hat{V}(z)\hat{M}(z) \tag{4.1}$$

and the Maxwell equations for a TE wave inside a reflective VBG with $n(z) = n_0 + n_1(z)\cos[Qz+\gamma(z)] + n_2(z)$, which lead to matrix $\hat{V}$:

$$\begin{aligned} &V_{11} = V_{22} = 0, \quad V_{12} = V_{21}^{*} = i\frac{\omega n_1(z)}{2c\cos\theta_{\text{in}}}\exp(iQz + i\gamma(z) - 2ik_z z), \\ &k_z = \frac{\omega}{c}\sqrt{n(z)^2 - n_{\text{air}}^2\sin\theta_{\text{air}}^2}, \quad \cos\theta_{\text{in}} = \sqrt{1 - n_{\text{air}}^2\sin\theta_{\text{air}}^2/n_0^2}, \end{aligned} \tag{4.2}$$

And, after certain phase transformations, $\hat{V}$ goes to $\hat{W}$:

$$W_{11} = i\left[\frac{\omega}{c}\left(n_0\cos\theta_{\text{in}} + \frac{n_2(z)}{\cos\theta_{\text{in}}}\right) - \frac{1}{2}\left(Q + \frac{d\gamma}{dz}\right)\right] = W_{22}^{*}, \quad W_{12} = i\frac{\omega n_1(z)}{2c\cos\theta_{\text{in}}} = W_{21}^{*}. \tag{4.3}$$

The Bragg condition $\omega n_0\cos\theta_{\text{in}}/c - Q/2 = 0$ is affected by the term $\omega n_2(z)/(c\cos\theta_{\text{in}}) - \frac{1}{2}d\gamma/dz$, which is angular-dependent for VBGs.

Figure 4 represents an experimental transmission spectra from a fabricated, narrow-band reflective VBG fitted with a theoretical curve of a uniform grating with only a small additional quadratic term in $n_2(z)$ of the refractive index $n(z)$.

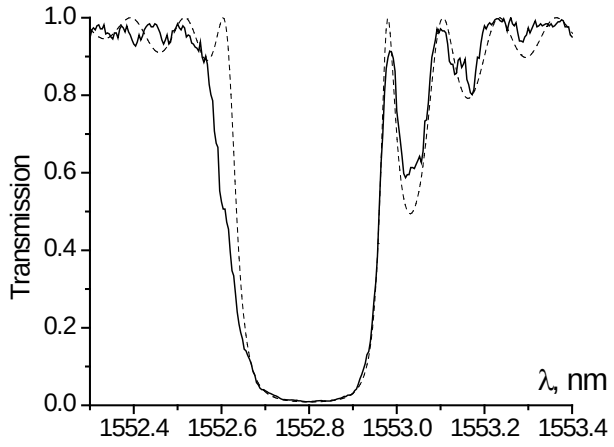

Figure 4. Asymmetry in transmission spectra. Solid line, our experiment; dotted line, our model.

The properties of a non-uniform VBG can be successfully simulated with a corresponding step-matrix algorithm.

Theory of light reflection from a chirped VBG

A chirped Bragg grating (CBG) allows for the stretching and subsequent compression of a short laser pulse, see experiments in [52-Liao 07]. Such a grating may be characterized by two parameters: z-dependence of resonant vacuum wavelength of reflection, $d\lambda_{res}/dz$, and coupling coefficient κ, of dimension m^{-1}. The profile of refractive index in such a CBG may be taken in the form $n(z) = n_0 + n_1(z)\cos[Qz+\gamma(z)]$. At a given point z of the CBG, the local Bragg condition corresponds to a certain vacuum wavelength $\lambda_{res}(z)$, which may be found from the equation

$$4\pi n_0 / \lambda_{res}(z) = Q + d\gamma/dz\,. \qquad (4.4)$$

In the approximation of relatively small deviations of $\lambda_{res}(z)$ from some central reflection wavelength $\lambda_0 = 4\pi n_0/Q$, the parameter $d\lambda_{res}/dz$ is related to the phase profile $\gamma(z)$ according to (4.4) by

$$\frac{d\lambda_{res}}{dz} = -\frac{\lambda_0^2}{4\pi n_0}\frac{d^2\gamma}{dz^2}\,. \qquad (4.5)$$

Coupled equations in slowly varying envelope approximation (SVEA) for a monochromatic wave $E(z,t) = \exp(-i\omega t)\left[A(z)\exp(ikz) + B(z)\exp(-ikz)\right]$ with wavelength λ_0 have the form

$$\frac{dA}{dz} = i\kappa e^{-i\gamma(z)}B,\quad \frac{dB}{dz} = -i\kappa e^{i\gamma(z)}A,\quad \kappa(z) = \frac{\pi n_1(z)}{\lambda_0},\quad \omega = \frac{2\pi c}{\lambda_0},\quad k = n_0\frac{\omega}{c}. \qquad (4.6)$$

Is it possible to find an analytic solution of these equations in the approximation that $\kappa(z) = \text{const}$ and $\gamma(z) = \beta(z-z_0)^2$, which corresponds to a homogeneously strong grating with constant chirp $d\lambda_{\text{res}}/dz = -\lambda_0^2\beta/(2\pi n_0)$.

The reflection coefficient r for a monochromatic wave may be found by analytical continuation of the coupled wave equations (4.6) into the complex plane of coordinate z. The result for reflectance is as follows

$$R = |r|^2 = 1 - \exp\left(-\pi\kappa^2/|\beta|\right). \tag{4.7}$$

Figure 5 represents the numerical simulation of reflection by a CBG with constant chirp in the range 10 nm on grating length 30 mm at $\lambda_0 = 1\mu\text{m}$ so that $\beta = 3.14\ \text{mm}^{-2}$ ($n_0 = 1.5$) and uniform coupling strength $\kappa = 1.57\ \text{mm}^{-1}$ by $n_1 = 5\cdot10^{-4}$. Weak oscillations of the reflection spectrum are connected with the influence of the un-apodized boundaries. The reflection value R obtained by these numerical simulations based on the transfer-matrix approach for chirped gratings [2-Glebov 08, 99-Ennser 97] coincides with our analytic result $R = 0.915$ given by (4.7).

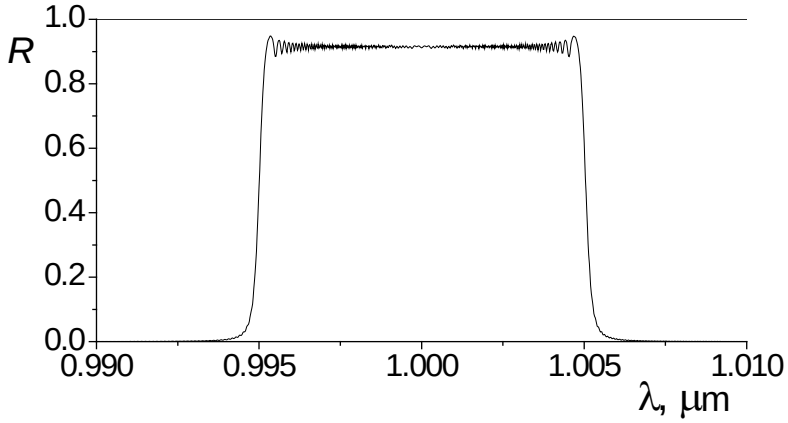

Figure 5. Reflection spectra of a uniformly chirped Bragg grating.

Figure 6 shows the intensity distributions inside the CBG.

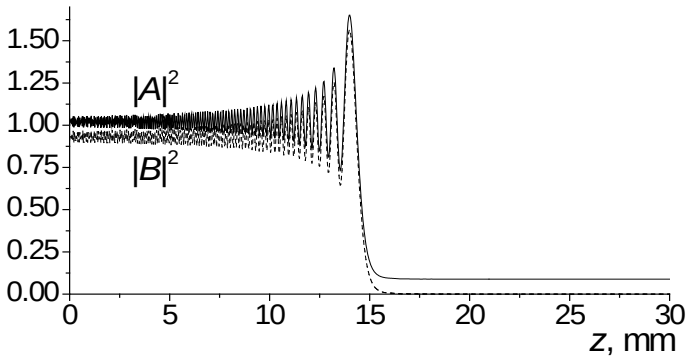

Figure 6. Intensity profiles $|A|^2$ and $|B|^2$ inside a chirped VBG for the central resonant wavelength.

Thus, the main result Eq. (4), which was actually obtained in [100-Belai 06], allows one to predict the parameters of CBG design for pulse stretching and pulse compression.

CHAPTER FIVE: RESONANT CAVITIES IN VBGS

Fabry-Perot resonator based on uniform VBGs

Consider a VBG made of two equally strong parts with each of them having the same values S_{VBG}. Then the reflection action of the compound VBG depends on the mutual phases of these two gratings. If there is no phase shift $\Delta\gamma$ between cosinusoidal modulations of refractive index inside these two gratings, then the combined VBG just acquires double the strength of each grating, $S_{tot} = 2S_{VBG}$. However, any intermediate shift, $0<\Delta\gamma<2\pi$, yields a narrow spectral transmission peak (or reflection dip) to $T = 1$ ($R = 0$). The physical sense of this 100% transmission peak is similar to the 100% transmission peak of a Fabry-Perot resonator with flat mirrors when the resonant condition is satisfied.

In order to describe such a configuration of two VBGs, we have to multiply consequently matrices of elements with corresponding phases. The experimental study was actually performed with two uncoated identical reflective VBGs placed very close to each other with a small gap l between them filled by an immersion liquid with the same background refractive index n_0 as the VBG. The coordinates of first grating's boundaries are $z_0 = 0$ and $z_1 = L$, and second grating is positioned between $z_2 = L+l$ and $z_3 = 2L+l$. Spectral parameters X and strengths S_0 are the same for both gratings, but the initial phases γ_1 and γ_2 are different. The boundary reflection strength from air to glass is S_b and the one from glass to air is $-S_b$. The transformation matrix determining waves a and b after this compound system, $z > z_3$, through values of a and b before it, $z < 0$, is a product of matrices of two types: (3.21) and (3.15) with $\hat{P}(L) = \hat{K}(\gamma/2)\hat{P}_{S_0,X}\hat{K}(-\gamma/2)$, see also (3.25). After simplifying the phase arguments, it becomes

$$\begin{pmatrix} a(z_3+0) \\ b(z_3+0) \end{pmatrix} = \hat{M}\begin{pmatrix} a(-0) \\ b(-0) \end{pmatrix}, \quad \hat{M} = \hat{K}(\beta_3)\hat{\Sigma}(-S_\mathrm{b})\hat{K}(\beta_2)\hat{P}_{S_0,X}\hat{K}\left(\frac{\Delta\gamma}{2}\right)\hat{P}_{S_0,X}\hat{K}(\beta_1)\hat{\Sigma}(S_\mathrm{b}),$$
$$\beta_1 = -\frac{\gamma_1}{2}, \quad \beta_2 = \frac{\gamma_2 + QL}{2}, \quad \beta_3 = -k_{\mathrm{air},z} z_3, \quad \Delta\gamma = QL + \gamma_1 - \gamma_2 + 2pl. \tag{5.1}$$

For small size *l* of the gap the phase *pl* (or *kl* at normal incidence) is approximately the same for all wavelengths in question. We see that the reflection characteristics of this compound system depend on three intermediate phases: the phase shift $\Delta\gamma$ between two cosinusoidal modulations in VBGs contacted via immersion layer and two outside boundary phases β_1 and β_2.

Our experimental collaborators from Prof. L. Glebov's group have presented an experimental demonstration of the coherent combination of two π-shifted VBGs in air. The VBG used for this demonstration were recorded inside PTR glass [2-Glebov 08]. They have their central wavelengths at 1063.4 nm, thicknesses of 2.76 mm and refractive index modulation of 154 ppm, middle-to-top. They were recorded inside PTR glass without slant, and the diffraction efficiency was equal to 72%, so S_0 = 1.25. The two VBGs were fixed on mirror holders, and one holder was motorized with a piezo-electric transducer that allowed fine translation and fine angle tuning. The setup is shown in Figure 7 for the measurement of the spectral response using a tunable laser having a 1 pm spectral resolution.

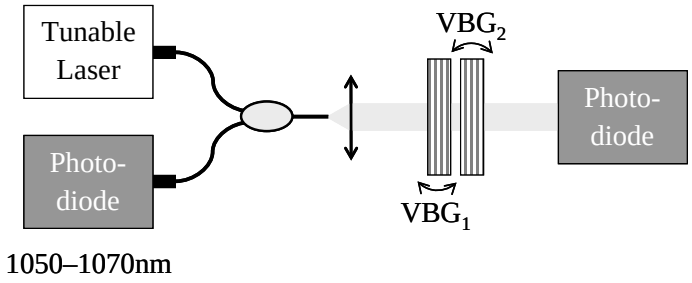

Figure 7. Experimental setup for the coherent combination of two VBGs in PTR glass.

Details of the experiment are described in our paper [2-Glebov 08].

The typical spectral dependence of the transmission filter is shown in Figure 8. Oscillations in transmission outside the resonance are due to the phase interplay between uncovered Fresnel reflections and the secondary evanescent lobes of gratings. This filter presents a transmission higher than 90%, with a bandwidth approximately equal to 25 pm (FWHM) and a rejection width equal to 200 pm. Rejection outside the resonance was better than 10 dB and can be improved by combining it with an additional VBG or using VBGs with higher diffraction efficiencies [101-Lumeau 06].

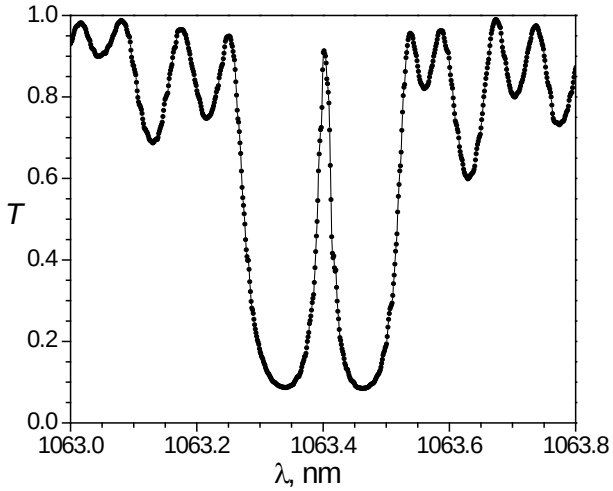

Figure 8. Experimental transmission of two π-shifted VBGs.

To illustrate the principle of phase matching between the two VBG, the distance between them was changed and the transmission for each distance was recorded in Figure 9a,b,c. One can see that depending on the distance between the two VBG, the resonance moved inside the main

lobe of the diffraction efficiency of the VBG. When distance was optimized and the phase shift $\Delta\gamma$ set equal to π, the resonance was centered in the middle of this lobe. When this phase was different from π, resonance was shifted to the edge of the lobe.

The solid curves at Figure 9 correspond to experimental data, while dashed curves are theoretical fits with optimized $\Delta\gamma$ for these actual gratings.

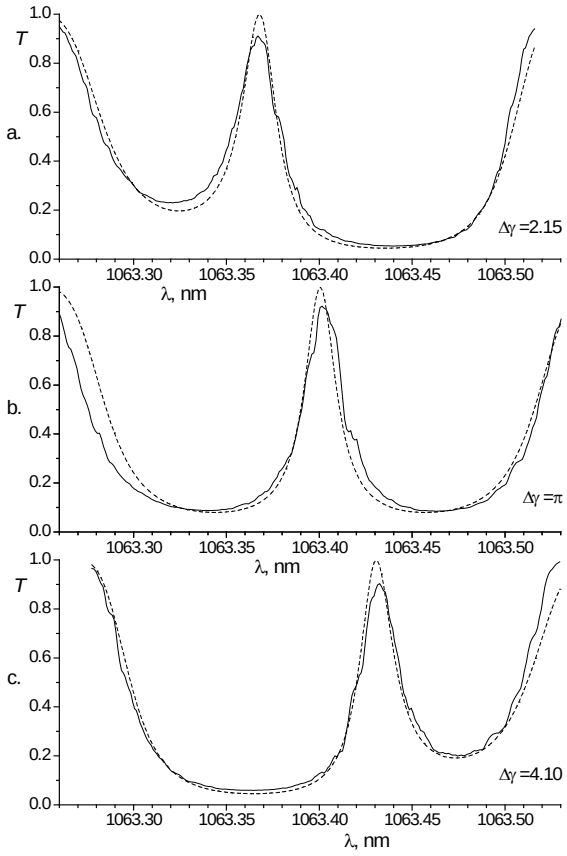

Figure 9. Spectral shift of resonant transmission due to phase shift $\Delta\gamma$ between two grating modulations.

We see reasonable agreement of the theory with experiment.

Resonant cavity in moiré VBG

The spectral profile of a reflective VBG strongly depends on the actual profile of its refractive index modulation. By reducing the modulation amplitude at the ends of the grating, the secondary lobes of the reflection spectra are suppressed. This apodization can be realized in different ways. One of them is based on the moiré effect which occurs at imposing two periodic oscillations with slightly different periods in media. As a result, the total recorded pattern has carrier average spatial frequency, while amplitude envelope varies slowly with spatial frequency equal to half of the difference of the two partial frequencies, namely

$$\cos(Q_1 z) + \cos(Q_2 z) = 2\cos(Qz)\cos(qz), \quad Q = (Q_1 + Q_2)/2, \quad q = (Q_1 - Q_2)/2 . \quad (5.2)$$

Such slow periodic variation of refractive index modulation has been implemented for fiber Bragg gratings [102-Legoubin 91]. The properties of moiré fiber Bragg gratings were studied before [103-Campbell 91, 104-Everall 97].

Here, we discuss moiré structure recorded in bulk material. Consider two uniform gratings with equal amplitude, slightly different vacuum resonant frequencies λ_1 and λ_2, and wave vectors along *z*-axis recorded in the same medium. Then, total modulation of refractive index is

$$\begin{gathered} n(z) = n_0 + n_1(z)\cos(Qz), \quad Q = \frac{4\pi n_0}{\lambda_0}, \quad \lambda_0 = \frac{\lambda_1 + \lambda_2}{2}, \\ n_1(z) = N_1 \sin\frac{\pi z}{t_\pi}, \quad t_\pi = \frac{\lambda_0^2}{2n_0\Delta\lambda}, \quad \Delta\lambda = \lambda_2 - \lambda_1, \end{gathered} \quad (5.3)$$

here, n_0 is the background refractive index of material, λ_0 is the vacuum Bragg resonant wavelength of the moiré grating, and $n_1(z)$ is the slowly varying envelope of modulation amplitude with constant N_1 and spatial semi-period t_π.

Propagation of electromagnetic waves inside VBG may be formulated in terms of counter-propagating waves $A(z)\exp(-i\omega t+ik_z z)$ and $B(z)\exp(-i\omega t-ik_z z)$ with $k_z = n_0\cos\theta_{in}\omega/c$, where θ_{in} is the angle of propagation inside a VBG in the case of tilted incidence. Coupled equations for slowly varying envelopes $A(z)$ and $B(z)$ are the following:

$$\frac{dA}{dz} = i\kappa(z)Be^{-2iDz}, \quad \frac{dB}{dz} = -i\kappa(z)Ae^{2iDz}, \quad \kappa(z) = \frac{\omega n_1(z)}{2c\cos\theta_{in}}, \quad D = \frac{\omega n_0}{c}\cos\theta_{in} - \frac{Q}{2}, \quad (5.4)$$

where $\kappa(z)$ is the coupling parameter and D is a z-independent parameter of detuning from the Bragg condition, $D = 0$. This condition is angular dependent, so at skew propagation the resonant wavelength is shifted to $\lambda_{res} = \lambda_0\cos\theta_{in}$.

The solution of the system (5.4) for linear media can be represented in matrix form by

$$A(z) = M_{AA}(z)A(0) + M_{AB}(z)B(0), \quad B(z) = M_{BA}(z)A(0) + M_{BB}(z)B(0). \quad (5.5)$$

In the absence of loss, the matrix $\hat{M}$ belongs to the group SL(1,1) and, with account of boundary condition $B(L) = 0$, the amplitude reflection coefficient for an element of length L equals

$$r = r(A \leftarrow B) = -M_{BA}(L)/M_{BB}(L) = -e^{-2i\eta}\tanh S, \quad R = \tanh^2 S, \quad (5.6)$$

where η is a phase parameter, S is the strength of reflection, and R is the reflectance.

The solution of (5.4) for a uniform grating is given by the well-known result of Kogelnik. Propagation of electromagnetic waves in non-uniform VBG in the general case with z-dependent $n_0(z)$, $n_1(z)$ and $Q(z)$ may be studied numerically only.

If the coupling $\kappa(z)e^{-2iDz}$ is a real function, e.g. at $\kappa = \kappa^*$, $D = 0$, then the matrix $M(z)$ for system (5.4) can be found in simple way and we get the reflection coefficient r:

$$\hat{M}\Big|_{D=0} = \begin{pmatrix} \cosh S_0 & i\sinh S_0 \\ -i\sinh S_0 & \cosh S_0 \end{pmatrix}, \qquad r_0 = i\tanh S_0, \quad S_0 = \int_0^L \kappa(z)dz = \frac{\omega}{2c}\int_0^L n_1(z)dz\,. \quad (5.7)$$

We see that gratings with slow varying envelopes $n_1(z)$ with zero integral values, $S_0 = 0$ (5.7), demonstrate 100% theoretical transmittance at Bragg resonance, $T_{res} = 1 - R_0 = 1$. We have such a situation for $n_1(z)$ from (5.3) with $L = 2t_\pi$. This result can be interpreted as perfect transmission through a Fabry-Perot filter of two identical reflective elements. Figure 10 illustrates a moiré filter with one sinusoidal period of $n_1(z)$ and its spectral transmittance.

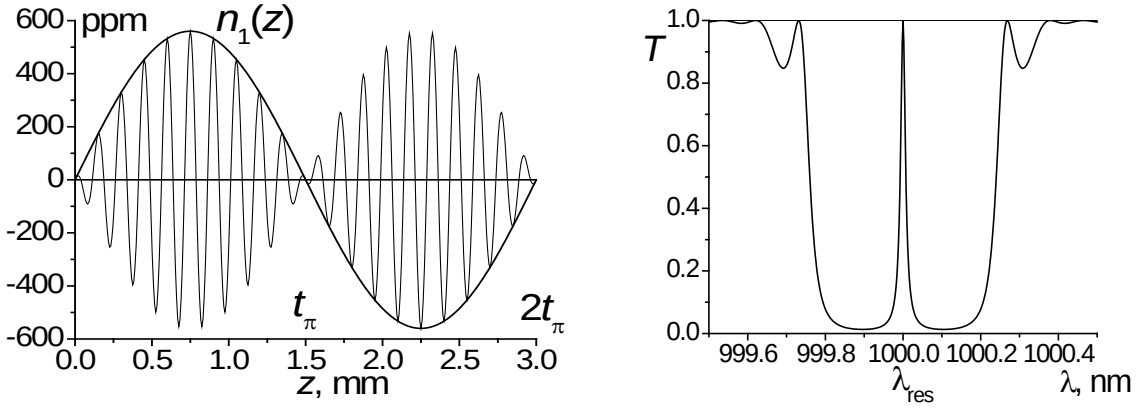

Figure 10. Sketch of the envelope and simulated transmittance of a moiré filter.

The first moiré VBG filter was fabricated in photo-thermo-refractive (PTR) glass by sequentially recording two gratings with close resonance wavelengths near 1550 nm in the same wafer. Figure 11 presents experimental transmission spectrum of this coated sample with two semi-periods of the moiré pattern. The bandwidth was 50 pm with 95% maximum transmittance.

The estimated modulation of the recorded gratings is 120 ppm, which is not high for PTR glass. Our simulations show that with higher modulation amplitudes it is possible to obtain bandwidths of less than 10 pm.

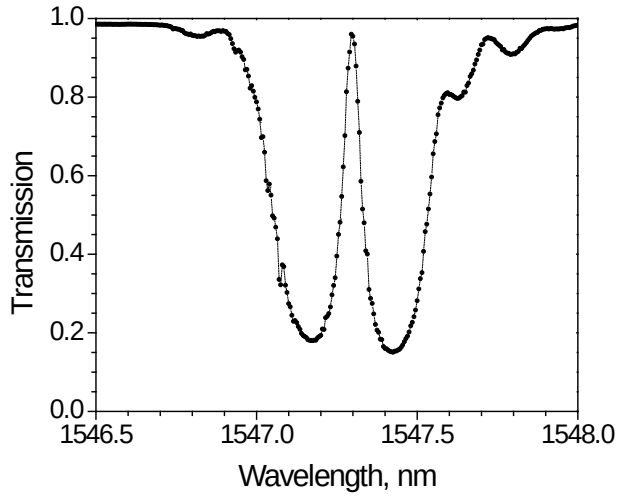

Figure 11. Experimental spectral selectivity of a moiré VBG filter.

The presence of transverse degrees of freedom in a VBG gives new possibilities for operations with laser beams. First of all, a small rotation of the grating at an angle θ_{air} shifts the spectral profile to a new Bragg wavelength according to

$$\lambda_{res} = \lambda_0 \cos\theta_{in} \approx \lambda_0[1 - \tfrac{1}{2}(n_{air}/n_0)^2\theta_{air}^2]. \qquad (5.8)$$

Even more attractive is the possibility to create VBG filters with non-trivial transverse profiles when the vectors of the moiré pattern **q** and the Bragg reflection **Q** are not co-linear. Shifting the grating perpendicularly within a laser beam or cavity will provide different filtering spectral properties of such VBGs. Consider a one-full-period moiré VBG, $L = 2t_\pi$, with an envelope $n_1(z,x)$ that changes linearly from sin(z) to cos(z) when the VBG shifts in the x-direction from L_x

to 0, see Figure 12. An important feature of a VBG with such a moiré pattern is the zero resonance strength at any illuminated x-position according to (5.7), $S_0(x) = 0$. As a result, this grating will have a narrow transmission peak at the same frequency λ_{res}, but with a tunable bandwidth and peak top flatness in the vicinity of resonance. In the case of a cos(z) profile, we have a coherently doubled Fabry-Perot filter with a fourth-power detuning dependence in the vicinity of the peak top, while a single Fabry-Perot filter yields a quadratic dependence. The plot on the right side of Figure 12 presents the transmittances at the corresponding illumination points.

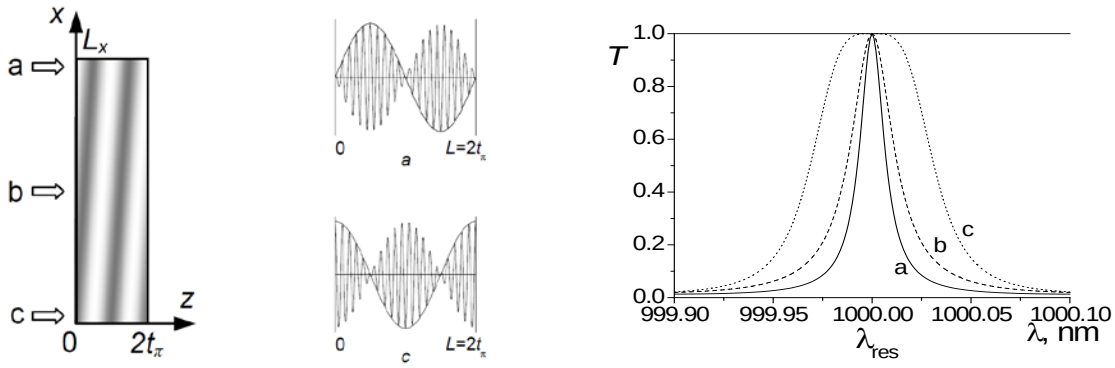

Figure 12. Transmission spectra of a tunable moiré VBG filter at different illumination points.

To conclude, robust solid-state high-aperture moiré VBG filters tolerant to high-power laser irradiation with tunable filtering characteristics are suggested as optical elements for laser design and for significantly narrowing the emission spectra of lasers of different types. They also can be used in high-resolution spectroscopy applications.

Bandwidth of resonant cavities in terms of strength of reflection

The most important characteristic of any spectral filter is its transmission spectral bandwidth. In the case of a symmetric cavity formed by two identical elements, the transmission peak profile has a Lorentzian form [105-Lipson 95]

$$T = \frac{1}{1 + F \cdot X^2}, \quad X = n_0 \frac{\omega - \omega_0}{c} L = -2\pi n_0 \frac{\lambda - \lambda_0}{\lambda_0^2} L, \tag{5.9}$$

where X is the dimensionless detuning (3.13) from resonant wavelength λ_0 at which transmission is 100%, and F is a dimensionless parameter, called "finesse", characterizing the narrowness of the transmission peak.

Let us first re-derive an expression for the finesse of an ordinary Fabry-Perot filter in terms of the reflection strength concept which we introduced earlier. Suppose that we have two surfaces with sharp reflection strengths $\pm S_h$ (subscript "h" stands for "half"), placed at $z = 0$ and $z = L$; we have chosen strengths with opposite signs in order the reflection goes to zero when these surfaces coincide, that is, when the separation L goes to zero. A typical example of such a filter is a glass plate with surface Fresnel reflection strength $S_h = \frac{1}{2}\ln n_0$ (2.15) for propagation from air to glass with refractive index n_0. If a transverse electric field, propagating normally to the reflective surface, is represented in terms of counter-propagating waves

$$E = A(z)e^{i\frac{\omega}{c}\int_0^z n(z')dz'} + B(z)e^{-i\frac{\omega}{c}\int_0^z n(z')dz'}, \tag{5.10}$$

then the wave amplitudes just after this surface at $z = 0$ will be expressed through a simple propagation matrix

$$\begin{pmatrix} A \\ B \end{pmatrix}_{z=+0} = \hat{\Xi}(S_{\rm h}) \begin{pmatrix} A \\ B \end{pmatrix}_{z=-0}, \quad \hat{\Xi}(S) = \begin{pmatrix} \cosh S & \sinh S \\ \sinh S & \cosh S \end{pmatrix}. \tag{5.11}$$

An identical expression for another wave representation of the same electric field can be written for the second reflective surface at $z = L$ with strength $-S_{\rm h}$ in a coordinate system shifted along the z-axis:

$$E = \widetilde{A}(\widetilde{z}) e^{i\frac{\omega}{c}\int_0^{\widetilde{z}} n(\widetilde{z}')d\widetilde{z}'} + \widetilde{B}(\widetilde{z}) e^{-i\frac{\omega}{c}\int_0^{\widetilde{z}} n(\widetilde{z}')d\widetilde{z}'}, \quad \begin{pmatrix} \widetilde{A} \\ \widetilde{B} \end{pmatrix}_{\widetilde{z}=+0} = \hat{\Xi}(-S_{\rm h}) \begin{pmatrix} \widetilde{A} \\ \widetilde{B} \end{pmatrix}_{\widetilde{z}=-0}, \quad \widetilde{z} = z - L, \tag{5.12}$$

Comparing of the two different representations of the same electric field (5.10) and (5.12), we can find a relation between two sets of counter-propagating waves

$$\int_0^{\widetilde{z}} n(\widetilde{z}')d\widetilde{z}' = \int_L^z n(z')dz' = \int_0^z n(z')dz' - \int_0^L n(z')dz' = \int_0^z n(z')dz' - n_0 L \quad \rightarrow \quad \begin{matrix} \widetilde{A}(\widetilde{z}) = A(z) e^{+in_0\frac{\omega}{c}L} \\ \widetilde{B}(\widetilde{z}) = B(z) e^{-in_0\frac{\omega}{c}L} \end{matrix}, \tag{5.13}$$

And, finally, we can write the propagation matrix for the total process of coherent reflection from two surfaces of dielectric plate (dp):

$$\begin{pmatrix} A \\ B \end{pmatrix}_{z=L+0} = \hat{M}_{\rm dp} \begin{pmatrix} A \\ B \end{pmatrix}_{z=-0}, \quad \hat{M}_{\rm dp} = \hat{K}(-\alpha)\hat{\Xi}(-S_{\rm h})\hat{K}(\alpha)\hat{\Xi}(S_{\rm h}), \quad \hat{K}\left(\alpha = \frac{n_0 \omega L}{c}\right) = \begin{pmatrix} e^{i\alpha} & 0 \\ 0 & e^{-i\alpha} \end{pmatrix}, \tag{5.14}$$

Suppose at wavelength $\lambda = 2\pi c/\omega$ equal to some particular resonant value λ_0 there is no reflection at all which means that the total propagation matrix is a trivial unity-matrix, $\hat{1}$. This is possible when the K-matrix is proportional to the unity-matrix itself:

$$\hat{K}\left(\frac{2\pi n_0 L}{\lambda_0}\right) = \pm\hat{1} \quad \rightarrow \quad \frac{2\pi n_0 L}{\lambda_0} = \pi m, \quad m = 0,1,... \quad \rightarrow \quad L = \frac{m\lambda_0}{2n_0}. \tag{5.15}$$

We have got a well-known result that 100% transmission of transparent dielectric plate occurs when its thickness equals to an integer number of light half-waves in this medium.

The reflective surfaces of a dielectric plate have strengths of opposite signs. If we have resonant cavity formed by identical non-absorbing reflective surfaces (rs) with the same strengths S_h of the same sign separated by distance d, then the total propagation matrix

$$\begin{pmatrix} A \\ B \end{pmatrix}_{z=L+0} = \hat{M}_{rs} \begin{pmatrix} A \\ B \end{pmatrix}_{z=-0}, \quad \hat{M}_{rs} = \hat{K}(-\beta)\hat{\Xi}(S_h)\hat{K}(\beta)\hat{\Xi}(S_h), \quad \beta = \frac{n_0 \omega d}{c}, \tag{5.16}$$

will be a unity matrix when

$$\hat{K}\left(\frac{2\pi n_0 d}{\lambda_0}\right) = \pm\sigma_z = \pm\begin{pmatrix} 1 & 0 \\ 0 & -1 \end{pmatrix} \quad \rightarrow \quad \frac{2\pi n_0 d}{\lambda_0} = \pi(m + \tfrac{1}{2}), \quad m = 0,1,... \quad \rightarrow \quad d = \frac{(m+\tfrac{1}{2})\lambda_0}{2n_0}. \tag{5.17}$$

Therefore in the case of two identical reflectors, the resonant transmission condition occurs when the separation between them equals an integer number plus one half wavelength.

Let us consider the propagation of a wave with a wavelength slightly different from the resonant transmission wavelength, $\lambda = \lambda_0 + \Delta\lambda$. Then, the propagation phase between the two surfaces of a dielectric plate will be equal to $\alpha = \pi m + X$, where X is the detuning defined before (5.9), and the total propagation matrix will be equal to

$$\begin{aligned} \hat{M}_{dp} &= \hat{K}(-\alpha)\hat{\Xi}(-S_h)\hat{K}(\alpha)\hat{\Xi}(S_h) = \hat{K}(-X)\hat{\Xi}(-S_h)\hat{K}(X)\hat{\Xi}(S_h) = \\ &= \hat{K}(-X)\begin{pmatrix} \cos X + i\cosh(2S_h)\sin X & i\sinh(2S_h)\sin X \\ -i\sinh(2S_h)\sin X & \cos X - i\cosh(2S_h)\sin X \end{pmatrix}. \end{aligned} \tag{5.18}$$

It is easy to check that the expression for the propagation matrix for two identical reflective surfaces will be the same, $\hat{M}_{rs}(S_h, X) = \hat{M}_{dp}(S_h, X)$, in the vicinity of resonant transmission with the corresponding propagation phase $\beta = \pi(m + ½) + X$ with the same X but with separation d (5.17) instead of thickness L (5.15).

Knowing the propagation matrix we can find amplitude transmission coefficient as the ratio of the transmitted amplitude $A_{z=L+0}$ to the incident amplitude $A_{z=0-}$ with the condition that there is no incident of *B*-wave, $B_{z=L+0} = 0$, from (5.14)

$$\begin{cases} A_{L+0} = M_{AA}A_{0-} + M_{AB}B_{0-} \\ B_{L+0} = M_{BA}A_{0-} + M_{BB}B_{0-} = 0 \end{cases} \rightarrow \quad r_{B\leftarrow A} = \frac{B_{0-}}{A_{0-}} = -\frac{M_{BA}}{M_{BB}}, \quad t_{B\leftarrow A} = \frac{A_{L+0}}{A_{0-}} = \frac{\det \hat{M}}{M_{BB}} = \frac{1}{M_{BB}}, \quad (5.19)$$

Finally, the intensity transmission coefficient will equal

$$T_{B\leftarrow A} = \left|t_{B\leftarrow A}\right|^2 = \frac{1}{\left|M_{BB}\right|^2} = \frac{1}{\left|\cos X - i\cosh(2S_{\mathrm{h}})\sin X\right|^2} = \frac{1}{1 + F\cdot\sin^2 X}, \quad F = \sinh^2(2S_{\mathrm{h}}), \quad (5.20)$$

In the literature [33-Hecht 01] we can find following expression for the finesse based on the reflectivity *R* of one reflective surface element with an additional expression for the maximum reflectivity of two coherently combined elements:

$$F = \frac{4R}{(1-R)^2}, \quad R_{\max} = \frac{4R}{(1+R)^2}, \quad (5.21)$$

It is easy to check that we got the same expression (5.16) if we take into account that the reflectivity of one reflective element is equal to $R = \tanh^2 S_{\mathrm{h}}$. Also, when we substitute this expression into the expression for $R_{\max}$ we get natural result that the maximum reflectivity corresponds to $2S_{\mathrm{h}}$, double the strength of one element, as it has to be according to the addition law for reflection strength (2.4), which states that the maximum strength is equal to the sum of moduli of two particular strengths

$$R = \tanh^2 S_{\mathrm{h}} \quad \rightarrow \quad F = \frac{4R}{(1-R)^2} = \sinh^2(2S_{\mathrm{h}}), \quad R_{\max} = \frac{4R}{(1+R)^2} = \tanh^2(2S_{\mathrm{h}}), \quad (5.22)$$

Thus, we have presented expressions for the finesse F and the maximum reflectivity R_{max} of a Fabry-Perot filter formed by two thin reflective elements in new way through reflection strength of each element S_h.

In case of large finesse, $F >> 1$, in the vicinity of a transmission peak where the transmission T is not much smaller than 1, in expression (5.20) we can substitute X for $\sin X$. Finally, from the value of dimensionless detuning at which transmission intensity equals its half maximum (HM),

$$T = \frac{1}{1 + F \cdot X_{HM}^2} = \frac{1}{2} \quad \rightarrow \quad X_{HM} = \frac{1}{\sqrt{F}}, \tag{5.23}$$

we will find the full width at half maximum (FWHM) of the transmission peak intensity in terms of wavelength units

$$X_{HM} = -2\pi n_0 \frac{\Delta\lambda_{HM}}{\lambda_0^2} L = \frac{1}{\sqrt{F}} \quad \rightarrow \quad \Delta\lambda_{FWHM} = 2\left|\Delta\lambda_{HM}\right| = \frac{1}{\sqrt{F}} \frac{\lambda_0^2}{\pi n_0 L}. \tag{5.24}$$

In the case of resonant cavity (C) formed by two surfaces with the same reflective strength S_h, the finesse is defined by (5.20) and, therefore, the width of the transmission peak is equal to

$$\Delta\lambda_{C,FWHM} = \frac{1}{\sqrt{F}} \frac{\lambda_0^2}{\pi n_0 L} = \frac{\lambda_0^2}{\pi n_0 L \sinh(2S_h)}. \tag{5.25}$$

Now, let us calculate the bandwidth based on the corresponding finesse of a resonant cavity based on two identical uniform VBGs with a mutual π-shift between their refractive index modulations. The results of experiments performed in Prof. Glebov's group for this compound VBG system were discussed in the beginning of this chapter. We presented the propagation matrix for this cavity in (5.1). If we consider two strong VBGs with antireflection coating, then we do not need to complicate our consideration by additional boundary Fresnel reflections,

$S_b = 0$. And, then, according to (5.1) the propagation matrix for two VBGs of thickness L, each with particular reflective strength S_h and with phase modulation separation between them γ ($\gamma_1 = 0$, $\gamma_2 = \gamma$), will equal

$$\begin{pmatrix} A \\ B \end{pmatrix}_{2L} = \hat{M}\begin{pmatrix} A \\ B \end{pmatrix}_0, \quad \hat{M} = \hat{K}(-2X)\hat{K}(-\gamma/2)\hat{P}_{S_h,X}\hat{K}(\gamma/2)\hat{P}_{S_h,X},$$
$$\hat{P}_{S,X} = \begin{pmatrix} \cosh G + iX\sinh G/G & iS\sinh G/G \\ -iS\sinh G/G & \cosh G - iX\sinh G/G \end{pmatrix}, \quad G = \sqrt{S^2 - X^2}. \tag{5.26}$$

If the phase mismatch between the modulations of the two gratings is equal to $\gamma = 2\pi m$, then the phase matrix between the two gratings will be equal to the unity matrix multiplied by a factor ±1, namely $\hat{K}(\gamma/2) = (-1)^m\hat{1}$, and we will obtain the expected propagation matrix of a uniform VBG of thickness $2L$ with total strength $2S_h$. On the contrary, with phase mismatch equal $\gamma = 2\pi(m + ½)$, we will get 100% transmission at the exact Bragg condition, $X = 0$, and, the corresponding propagation matrix, with omitting trivial first phase matrix factor $\hat{K}(-2X)$, will have the form

$$\hat{m} = \begin{pmatrix} \cosh G + iX\dfrac{\sinh G}{G} & -iS\dfrac{\sinh G}{G} \\ iS\dfrac{\sinh G}{G} & \cosh G - iX\dfrac{\sinh G}{G} \end{pmatrix}\begin{pmatrix} \cosh G + iX\dfrac{\sinh G}{G} & iS\dfrac{\sinh G}{G} \\ -iS\dfrac{\sinh G}{G} & \cosh G - iX\dfrac{\sinh G}{G} \end{pmatrix} \tag{5.27}$$

As we mentioned before, the transmission of a lossless optical system is defined by its propagation matrix element as $1/|m_{22}|^2$; see, for example, (5.20). In our case the matrix element of interest is equal to

$$m_{22} = \left(\cosh G - iX\frac{\sinh G}{G}\right)^2 - S^2\frac{\sinh^2 G}{G^2} = 1 - i\frac{\sinh(2S)}{S}X - 2\frac{\sinh^2 S}{S^2}X^2 + O(X^3). \tag{5.28}$$

Here we keep terms up to the second order of detuning in order to be able reproduce the Lorentzian shape of transmission peak

$$T = \frac{1}{\left|m_{22}\right|^2} = \frac{1}{1 + F_{\mathrm{U}} \cdot X^2 + O(X^4)}, \quad F_{\mathrm{U}} = \frac{4\sinh^4 S_{\mathrm{h}}}{S_{\mathrm{h}}^2}. \tag{5.29}$$

According to (5.24), the bandwidth of a resonant cavity formed by two uniform VBGs with mutual modulation π-shift will equal

$$\Delta\lambda_{\mathrm{U,FWHM}} = \frac{1}{\sqrt{F_{\mathrm{U}}}} \frac{\lambda_0^2}{\pi n_0 L} = \frac{\lambda_0^2 S_{\mathrm{h}}}{2\pi n_0 L \sinh^2 S_{\mathrm{h}}}. \tag{5.30}$$

In the experiment discussed before, see Figure 8, the measured bandwidth was $\Delta\lambda = 25$pm. Let us compare this value with the theoretical one using the following data mentioned before: resonant wavelength $\lambda_0 = 1063.4$ nm, corresponding refractive index of PTR glass $n_0 = 1.485$, thickness of each VBG $L = 2.76$ mm, and strength $S_{\mathrm{h}} = 1.25$ according to the reflectivity $R = \tanh^2 S_{\mathrm{h}} = 72\%$ of each VBG. Substitution of this data into (5.30) gives theoretical value $\Delta\lambda = 21$pm. A small experimental widening of the bandwidth and a reduction of the peak from 100% transparency can be naturally explained by small inhomogeneities inside the VBG which results some blurring of transmission peak with corresponding spreading out of its width and washing out perfect 100% resonant transmission in measured transmittance across aperture.

The experimental results presented in Figure 9 show the wavelength shift of the transmission peak with change of shift γ between the refractive index modulations of two gratings in the vicinity of π-value. For considered symmetric case $\gamma = \pi$, the transmission peak occurs at exact Bragg resonance with zero detuning $X = 0$. Now, with arbitrary modulation mismatch $\gamma = \pi + \delta$, we determine the wavelength detuning X_δ at which 100% transmission will

occur. For these purposes let us expand matrix coupling waves inside VBG $\hat{P}_{S_h,X}$ (5.26) up to the first order of detuning X

$$\hat{P}_{S,X} = \begin{pmatrix} \cosh S\left(1 + iX\,\dfrac{\tanh S}{S}\right) & i\sinh S \\ -i\sinh S & \cosh S\left(1 - iX\,\dfrac{\tanh S}{S}\right) \end{pmatrix} + O(X^2) \approx \\ \approx \hat{K}\left(X\,\frac{\tanh S}{2S}\right)\hat{P}_{S,0}\hat{K}\left(X\,\frac{\tanh S}{2S}\right). \tag{5.31}$$

As a result, using the definition $\gamma = \pi + \delta$ and the additivity of arguments of phase matrices, the propagation matrix (5.26) will equal

$$\hat{M} \approx \hat{K}(-2X)\hat{K}\left(-\frac{\pi+\delta}{2} + X\,\frac{\tanh S_h}{2S_h}\right)\hat{P}_{S_h,0}\hat{K}\left(-\frac{\pi+\delta}{2} + X\,\frac{\tanh S_h}{S_h}\right)\hat{P}_{S_h,0}\hat{K}\left(X\,\frac{\tanh S_h}{2S_h}\right). \tag{5.32}$$

As we saw before in (5.26), 100% transmission occurred when the argument of the phase matrix $\hat{K}(-\gamma/2)$ between matrices $\hat{P}_{S_h,0}$ with zero detuning was equal to $-\pi/2$, which leads to the 100% transmission condition in the case of Equation (5.32) with γ shifted from π:

$$-\frac{\delta}{2} + X_\delta\,\frac{\tanh S_h}{S_h} = 0 \quad \rightarrow \quad X_\delta = \frac{S_h}{2\tanh S_h}\delta, \quad \delta = \gamma - \pi\,. \tag{5.33}$$

So, we get a first order dependence of the dimensionless detuning shift of the transmission peak when γ varies from π by δ. And, according to the conversion factor from (5.24), the wavelength shift of the transmission peak will equal

$$\Delta\lambda_\delta = -\frac{\lambda_0^2}{2\pi n_0 L}X_\delta = -\frac{\lambda_0^2}{2\pi n_0 L}\frac{S_h}{2\tanh S_h}\delta\,. \tag{5.34}$$

Substitution of the parameters of the VBGs specified after Equation (5.30) into (5.34) gives the same value of the peak position shift with mutual grating modulation mismatch $\Delta\lambda_\delta/\delta$ = 32 pm/rad which was experimentally observed and presented in Figure 9.

Bandwidth of a tunable moiré filter

The main feature of a VBG is its high spectral selectivity, or, in other words small rejection bandwidth. This property together with its large operation aperture makes a VBG recorded in PTR glass a unique, robust, spectral selective element for high power laser applications. As we discussed before, spectral selectivity of a VBG-based element can be improved by more than an order of magnitude by creating a resonant cavity with two uniform VBGs with a mutual π-shift between their modulations. Unfortunately, this compound structure is very sensitive to alignment, which makes its implementation problematic for many practical applications. On the other hand, the proposed moiré filter is characterized by similarly improved spectral selectivity, but it is mechanically as robust as one uniform VBG, because it is recorded in one piece of glass. As a result, there are no problems with mutual alignment of both cavity reflectors. But, in the case of the moiré filter, the precision required to record holographic gratings is quite high, because both gratings; recorded in the same glass sample with a precise, small difference between their periods; have to be uniform enough to produce a high quality resonator. Any non-uniformity, like a small drift of the grating periods across the aperture, which is an undesirable small chirp, will lead to "washing out" of the narrow transmission peak.

Now, let us derive an expression for the transmission peak bandwidth of a tunable moiré Bragg filter with a full envelope period of length $2L_\pi$. The corresponding coupled wave equations are:

$$\frac{d}{dz}\begin{pmatrix} A \\ B \end{pmatrix} = \hat{V}\begin{pmatrix} A \\ B \end{pmatrix}, \quad \hat{V} = \begin{pmatrix} 0 & i\kappa(z)e^{-2i\Delta\cdot z} \\ -i\kappa(z)e^{2i\Delta\cdot z} & 0 \end{pmatrix}, \quad \kappa(z) = \frac{\pi}{\lambda}n_1(z), \quad \Delta = \frac{2\pi}{\lambda}n_0 - \frac{Q}{2}, \\ 0 \le z \le 2L_\pi, \quad n_1(z) = n_M \sin(\pi z/L_\pi + \varphi), \quad S_h = \int_0^{L_\pi} \sin(\pi z/L_\pi)dz = 2n_M L_\pi/\lambda. \tag{5.35}$$

For convenience, we will adjust the wave amplitudes with appropriate detuning phase dependence in order to have differential equations, which are linear in terms of the detuning Δ:

$$\begin{pmatrix} A \\ B \end{pmatrix} = \hat{K}(-\Delta\cdot z + \pi/4)\begin{pmatrix} \tilde{A} \\ \tilde{B} \end{pmatrix} \quad \rightarrow \quad \frac{d}{dz}\begin{pmatrix} \tilde{A} \\ \tilde{B} \end{pmatrix} = \begin{pmatrix} i\Delta & \kappa(z) \\ \kappa(z) & -i\Delta \end{pmatrix}\begin{pmatrix} \tilde{A} \\ \tilde{B} \end{pmatrix}. \tag{5.36}$$

We will also rewrite the coupled equations in terms of a dimensionless variable ζ, instead of the *z*-coordinate

$$\frac{d}{d\varsigma}\begin{pmatrix} \tilde{A} \\ \tilde{B} \end{pmatrix} = \hat{w}(\varsigma)\begin{pmatrix} \tilde{A} \\ \tilde{B} \end{pmatrix}, \quad \hat{w}(\varsigma) = \hat{w}_0(\varsigma) + iX\tilde{\sigma}, \quad 0 \le \varsigma = \frac{\pi}{L_\pi}z \le 2\pi, \\ \hat{w}_0(\varsigma) = \frac{L_\pi}{\pi}\kappa(\varsigma) = \tfrac{1}{2}S_h \sin(\varsigma + \varphi)\begin{pmatrix} 0 & 1 \\ 1 & 0 \end{pmatrix}, \quad \tilde{\sigma} = \frac{1}{\pi}\begin{pmatrix} 1 & 0 \\ 0 & -1 \end{pmatrix}, \quad X = \Delta\cdot L_\pi. \tag{5.37}$$

In order to determine the width of the Lorentzian peak, we have to solve equation (5.37) by sequential approximations up to the second order of detuning *X*; in other words, we have to find the elements of the propagation matrix $\hat{m}$ at $\varsigma = 2\pi$ in quadratic form of *X*

$$\begin{pmatrix} \tilde{A}(\varsigma) \\ \tilde{B}(\varsigma) \end{pmatrix} = \hat{m}(\varsigma)\begin{pmatrix} \tilde{A}(0) \\ \tilde{B}(0) \end{pmatrix}, \quad \frac{d}{d\varsigma}\hat{m}(\varsigma) = \hat{w}(\varsigma)\hat{m}(\varsigma), \quad \hat{m}(0) = \hat{1}, \quad \hat{m}(2\pi) = ? \tag{5.38}$$

For this purpose, we represent the propagation matrix power series with respect to the detuning *X*

$$\hat{m}(\varsigma) = \hat{m}_0(\varsigma)\left[\hat{1} + iX\hat{u}^{(1)}(\varsigma) + (iX)^2\hat{u}^{(2)}(\varsigma)\right], \quad \hat{m}_0(0) = \hat{1}, \quad \hat{u}^{(1,2)}(0) = 0\,. \tag{5.39}$$

After substitution of this expansion into the matrix differential equation (5.38), we will get series of matrix differential equations for each power of the detuning X

$$\begin{aligned}
&\frac{d\hat{m}_0}{d\varsigma}\left[\hat{1} + iX\hat{u}^{(1)} - X^2\hat{u}^{(2)}\right] + \hat{m}_0\left[iX\frac{d\hat{u}^{(1)}}{d\varsigma} - X^2\frac{d\hat{u}^{(2)}}{d\varsigma}\right] = (\hat{w}_0 + iX\tilde{\sigma})\hat{m}_0\left[\hat{1} + iX\hat{u}^{(1)} - X^2\hat{u}^{(2)}\right]: \\
&\frac{d\hat{m}_0}{d\varsigma} = \hat{w}_0\hat{m}_0; \qquad \frac{d\hat{m}_0}{d\varsigma}\hat{u}^{(1)} + \hat{m}_0\frac{d\hat{u}^{(1)}}{d\varsigma} = \hat{w}_0\hat{m}_0\hat{u}^{(1)} + \tilde{\sigma}\hat{m}_0 \quad \rightarrow \quad \frac{d\hat{u}^{(1)}}{d\varsigma} = \hat{m}_0^{-1}\tilde{\sigma}\hat{m}_0; \\
&\frac{d\hat{m}_0}{d\varsigma}\hat{u}^{(2)} + \hat{m}_0\frac{d\hat{u}^{(2)}}{d\varsigma} = \hat{w}_0\hat{m}_0\hat{u}^{(2)} + \tilde{\sigma}\hat{m}_0\hat{u}^{(1)} \quad \rightarrow \quad \frac{d\hat{u}^{(2)}}{d\varsigma} = \hat{m}_0^{-1}\tilde{\sigma}\hat{m}_0\hat{u}^{(1)} = \frac{d\hat{u}^{(1)}}{d\varsigma}\hat{u}^{(1)}.
\end{aligned} \tag{5.40}$$

The solution of the differential equation for the propagation matrix at zero detuning is the result already discussed; it has the form equivalent to (5.7):

$$\begin{aligned}
&\frac{d\hat{m}_0}{d\varsigma} = \hat{w}_0\hat{m}_0 \quad \rightarrow \quad \hat{m}_0(\varsigma) = \begin{pmatrix} \cosh S(\varsigma) & \sinh S(\varsigma) \\ \sinh S(\varsigma) & \cosh S(\varsigma) \end{pmatrix}, \\
&S(\varsigma) = \frac{L_\pi}{\pi}\int_0^\varsigma \kappa(\varsigma')d\varsigma' = \frac{S_\mathrm{h}}{2}\big(\cos\varphi - \cos(\varsigma + \varphi)\big), \qquad \hat{m}_0(2\pi) = \hat{1}.
\end{aligned} \tag{5.41}$$

We see that the propagation matrix for a full 2π moiré period length is a unity matrix, as it should be for 100% resonant transmission. But we also will need its ς-dependent expression in order to calculate the higher order terms on detuning, which will then be used to calculate the matrix element $m_{22}(2\pi)$ which defines transmission as $T = 1/|m_{22}|^2$ according to (2.6)

$$\hat{m}(2\pi) = \hat{1}\left[\hat{1} + iX\hat{u}^{(1)}(2\pi) - X^2\hat{u}^{(2)}(2\pi)\right], \quad m_{22}(2\pi) = 1 + iXu_{22}^{(1)}(2\pi) - X^2u_{22}^{(2)}(2\pi)\,. \tag{5.42}$$

For the next first order term we will have

$$\frac{d\hat{u}^{(1)}}{d\varsigma} = \hat{m}_0^{-1}\tilde{\sigma}\hat{m}_0 = \frac{1}{\pi}\begin{pmatrix} c(\varsigma) & s(\varsigma) \\ -s(\varsigma) & -c(\varsigma) \end{pmatrix}, \quad \hat{u}^{(1)}(\varsigma) = \frac{1}{\pi}\begin{pmatrix} \int_0^{\varsigma} c(\varsigma')d\varsigma' & \int_0^{\varsigma} s(\varsigma')d\varsigma' \\ -\int_0^{\varsigma} s(\varsigma')d\varsigma' & -\int_0^{\varsigma} c(\varsigma')d\varsigma' \end{pmatrix},$$
$$c(\varsigma) = \cosh\big(2S(\varsigma)\big), \quad s(\varsigma) = \sinh\big(2S(\varsigma)\big), \qquad (5.43)$$
$$\hat{u}^{(1)}(2\pi) = 2I_0(S_{\rm h})\begin{pmatrix} \cosh(S_{\rm h}\cos\varphi) & \sinh(S_{\rm h}\cos\varphi) \\ -\sinh(S_{\rm h}\cos\varphi) & -\cosh(S_{\rm h}\cos\varphi) \end{pmatrix}, \quad I_0(S_{\rm h}) = \frac{1}{2\pi}\int_0^{2\pi} e^{\pm S_{\rm h}\cos(\varsigma'+\varphi)}d\varsigma',$$

where $I_0(S_{\rm h})$ is a zero-order modified Bessel function.

Moreover, for the approximation term proportional to X^2 we have

$$\frac{d\hat{u}^{(2)}}{d\varsigma} = \hat{m}_0^{-1}\tilde{\sigma}\hat{m}_0\hat{u}^{(1)} = \frac{d\hat{u}^{(1)}}{d\varsigma}\hat{u}^{(1)} = \frac{1}{2}\frac{d\big(\hat{u}^{(1)}\hat{u}^{(1)}\big)}{d\varsigma} + \frac{1}{2}\left[\frac{d\hat{u}^{(1)}}{d\varsigma}\hat{u}^{(1)} - \hat{u}^{(1)}\frac{d\hat{u}^{(1)}}{d\varsigma}\right],$$
$$\frac{d\hat{u}^{(1)}}{d\varsigma}\hat{u}^{(1)} - \hat{u}^{(1)}\frac{d\hat{u}^{(1)}}{d\varsigma} = \frac{2}{\pi^2}\begin{pmatrix} 0 & 1 \\ 1 & 0 \end{pmatrix}\left(c(\varsigma)\int_0^{\varsigma} s(\varsigma')d\varsigma' - s(\varsigma)\int_0^{\varsigma} c(\varsigma')d\varsigma'\right) \qquad (5.44)$$
$$\rightarrow \quad \hat{u}_{22}^{(2)}(2\pi) = \tfrac{1}{2}\big(\hat{u}^{(1)}(2\pi)\cdot\hat{u}^{(1)}(2\pi)\big)_{22} = 2I_0^2(S_{\rm h}).$$

As a result, we get the matrix element of interest from (5.43-44)

$$m_{22}(2\pi) = 1 - 2iI_0(S_{\rm h})\cosh(S_{\rm h}\cos\varphi)X - 2I_0^2(S_{\rm h})X^2 + i\cdot O(X^3), \qquad (5.45)$$

which defines Lorentzian shape of the moiré filter transmission peak with a finesse parameter $F_{\rm M}$

$$T = \frac{1}{\left|m_{22}(2\pi)\right|^2} = \frac{1}{1 + F_{\rm M}X^2 + O(X^4)}, \quad F_{\rm M} = 4I_0^2(S_{\rm h})\sinh^2(S_{\rm h}\cos\varphi). \qquad (5.46)$$

According to (5.24), the bandwidth of the moiré filter is equal to

$$\Delta\lambda_{\rm M,FWHM} = \frac{1}{\sqrt{F_{\rm M}}}\frac{\lambda_0^2}{\pi m_0 L} = \frac{\lambda_0^2}{2\pi m_0 L I_0(S_{\rm h})\sinh(S_{\rm h}\cos\varphi)}. \qquad (5.47)$$

The phase shift $\varphi = \pi/2$ in the moiré 2π-period corresponds to the cosine-profile of the moiré modulation envelope, as opposed to the initial sine-profile with $\varphi = 0$. And, in this case of a cosine-profile, the parameter $F_{\rm M}$ is going to zero (5.46) with $\varphi = 0$, which leads to an infinite

bandwidth according to (5.47). In order to have a physically reasonable value of the bandwidth, we have to take into account next non-zero power term on detuning X^4 in (5.46).

Let us calculate the approximation up to fourth power for a particular cosine profile:

$$\begin{gathered}
\frac{d}{d\varsigma}\hat{m}(\varsigma)=\left(\hat{w}_0^c(\varsigma)+iX\tilde{\sigma}\right)\hat{m}(\varsigma),\quad \hat{w}_0^c(\varsigma)=\tfrac{1}{2}S_{\mathrm{h}}\cos\varsigma\begin{pmatrix}0&1\\1&0\end{pmatrix},\\
\hat{m}(\varsigma)=\hat{m}_0(\varsigma)\left[\hat{1}+\sum_{j=1}^{4}(iX)^j\hat{u}^{(j)}(\varsigma)\right],\quad \hat{m}_0(0)=\hat{1},\quad \hat{u}^{(j)}(0)=0,\\
\frac{d\hat{m}_0}{d\varsigma}=\hat{w}_0^c\hat{m}_0\quad\rightarrow\quad \hat{m}_0(\varsigma)=\begin{pmatrix}\cosh S(\varsigma)&\sinh S(\varsigma)\\\sinh S(\varsigma)&\cosh S(\varsigma)\end{pmatrix},\quad S(\varsigma)=\tfrac{1}{2}S_{\mathrm{h}}\sin\varsigma,\\
\frac{d\hat{u}^{(1)}}{d\varsigma}=\hat{m}_0^{-1}\tilde{\sigma}\hat{m}_0,\quad \frac{d\hat{u}^{(j)}}{d\varsigma}=\hat{m}_0^{-1}\tilde{\sigma}\hat{m}_0\hat{u}^{(j-1)},\quad j=2,3,4.
\end{gathered}\qquad (5.48)$$

Similar to (5.43) in the first order we have the following:

$$\begin{gathered}
\frac{d\hat{u}^{(1)}}{d\varsigma}=\hat{m}_0^{-1}\tilde{\sigma}\hat{m}_0=\frac{1}{\pi}\begin{pmatrix}\cosh(2S(\varsigma))&\sinh(2S(\varsigma))\\-\sinh(2S(\varsigma))&-\cosh(2S(\varsigma))\end{pmatrix}=\hat{r}\varepsilon^{+}(\varsigma)+\hat{c}\varepsilon^{-}(\varsigma),\\
\varepsilon^{\pm}(\varsigma)=\tfrac{1}{2\pi}e^{\pm S_{\mathrm{h}}\sin\varsigma},\quad \hat{r}=\begin{pmatrix}1&1\\-1&-1\end{pmatrix},\quad \hat{c}=\begin{pmatrix}1&-1\\1&-1\end{pmatrix}\quad\rightarrow\quad \hat{u}^{(1)}(\varsigma)=\hat{r}I^{+}(\varsigma)+\hat{c}I^{-}(\varsigma),\\
I^{\pm}(\varsigma)=\int_0^{\varsigma}\varepsilon^{\pm}(\varsigma')d\varsigma',\quad I^{\pm}(2\pi)=I_0(S_{\mathrm{h}}),\quad \hat{u}^{(1)}(2\pi)=2I_0(S_{\mathrm{h}})\begin{pmatrix}1&0\\0&-1\end{pmatrix}.
\end{gathered}\qquad (5.49)$$

Expressions for second order are

$$\begin{gathered}
\frac{d\hat{u}^{(2)}}{d\varsigma}=\frac{d\hat{u}^{(1)}}{d\varsigma}\hat{u}^{(1)}=\left(\hat{r}\varepsilon^{+}+\hat{c}\varepsilon^{-}\right)\left(\hat{r}I^{+}+\hat{c}I^{-}\right)=2\hat{d}\varepsilon^{+}(\varsigma)I^{-}(\varsigma)+2\hat{p}\varepsilon^{-}(\varsigma)I^{+}(\varsigma),\\
\hat{r}^2=\hat{c}^2=0,\quad \hat{d}=\tfrac{1}{2}\hat{r}\hat{c}=\begin{pmatrix}1&-1\\-1&1\end{pmatrix},\quad \hat{p}=\tfrac{1}{2}\hat{c}\hat{r}=\begin{pmatrix}1&1\\1&1\end{pmatrix},\quad\rightarrow\\
\hat{u}^{(2)}(\varsigma)=2\hat{p}I^{-+}(\varsigma)+2\hat{d}I^{+-}(\varsigma),\quad I^{\mp\pm}(\varsigma)=\int_0^{\varsigma}\varepsilon^{\mp}(\varsigma')\int_0^{\varsigma'}\varepsilon^{\pm}(\varsigma'')d\varsigma''d\varsigma'.
\end{gathered}\qquad (5.50)$$

The diagonal matrix elements of the second order matrix term are easy to calculate

$$u_{11}^{(2)}=u_{22}^{(2)}=2I^{-+}(\varsigma)+2I^{-+}(\varsigma)=2\int_0^{\varsigma}\varepsilon^{-}(\varsigma')d\varsigma'\cdot\int_0^{\varsigma}\varepsilon^{+}(\varsigma'')d\varsigma'',\quad u_{11,22}^{(2)}(2\pi)=2I_0^2(S_{\mathrm{h}}),\qquad (5.51)$$

but calculation of the off-diagonal matrix elements is much more challenging. We present here final the result from the detailed derivation, which can be done by the approach, based on differentiation parameter under the integral sign:

$$u_{12}^{(2)} = u_{21}^{(2)} = 2I^{-+}(\varsigma) - 2I^{-+}(\varsigma), \quad u_{12,21}^{(2)}(2\pi) = 4\sum_{k=0}^{\infty} \frac{I_0(S_\text{h})S_\text{h}^{2k+1}}{\pi[(2k+1)!!]^2}. \tag{5.52}$$

The third and fourth order approximation terms are expressed as

$$\begin{aligned}
&\frac{d\hat{u}^{(3)}}{d\varsigma} = \frac{d\hat{u}^{(1)}}{d\varsigma}\hat{u}^{(2)} = \left(\hat{r}\varepsilon^{+} + \hat{c}\varepsilon^{-}\right)2\left(\hat{p}I^{-+} + \hat{d}I^{+-}\right) = \left| \begin{matrix} \hat{r}\hat{p} = 2\hat{r},\ \hat{c}\hat{d} = 2\hat{c}, \\ \hat{r}\hat{d} = \hat{c}\hat{p} = 0 \end{matrix} \right| = 4\hat{r}\varepsilon^{+}I^{-+} + 4\hat{c}\varepsilon^{-}I^{+-}, \\
&\hat{u}^{(3)}(\varsigma) = 4\hat{r}I^{+-+}(\varsigma) + 4\hat{c}I^{-+-}(\varsigma), \quad I^{\pm\mp\pm}(\varsigma) = \int_0^{\varsigma} \varepsilon^{\pm}(\varsigma')I^{\mp\pm}(\varsigma')d\varsigma', \quad I^{+-+}(2\pi) = I^{-+-}(2\pi). \\
&\frac{d\hat{u}^{(4)}}{d\varsigma} = \frac{d\hat{u}^{(1)}}{d\varsigma}\hat{u}^{(3)} = \left(\hat{r}\varepsilon^{+} + \hat{c}\varepsilon^{-}\right)4\left(\hat{r}I^{+-+} + \hat{c}I^{-+-}\right) = 8\hat{p}\varepsilon^{-}I^{+-+} + 8\hat{d}\varepsilon^{+}I^{-+-}, \\
&\hat{u}^{(4)}(\varsigma) = 8\hat{p}I^{-+-+}(\varsigma) + 8\hat{d}I^{+-+-}(\varsigma), \quad I^{\mp\pm\mp\pm}(\varsigma) = \int_0^{\varsigma} \varepsilon^{\mp}(\varsigma')I^{\pm\mp\pm}(\varsigma')d\varsigma'.
\end{aligned} \tag{5.53}$$

Now we can write the total expression for the propagation matrix of a moiré filter with a cosine profile up to the fourth power of detuning

$$\begin{aligned}
\hat{m}(2\pi) = \hat{1} + iX\hat{u}^{(1)} - X^2\hat{u}^{(2)} - iX^3\hat{u}^{(3)} + X^4\hat{u}^{(4)} = 1 + 2iXI_0(S_\text{h})\begin{pmatrix} 1 & 0 \\ 0 & -1 \end{pmatrix} - \\
- X^2\begin{pmatrix} 2I_0^2(S_\text{h}) & u_{12}^{(2)}(2\pi) \\ u_{12}^{(2)}(2\pi) & 2I_0^2(S_\text{h}) \end{pmatrix} - 8iX^3I^{+-+}(2\pi)\begin{pmatrix} 1 & 0 \\ 0 & -1 \end{pmatrix} + \\
+ 8X^4I^{-+-+}(2\pi)\begin{pmatrix} 1 & 1 \\ 1 & 1 \end{pmatrix} + 8X^4I^{+-+-}(2\pi)\begin{pmatrix} 1 & -1 \\ -1 & 1 \end{pmatrix}.
\end{aligned} \tag{5.54}$$

The square of the diagonal matrix element $|m_{22}(2\pi)|^2$, which defines the transmission peak shape, up to the fourth power of detuning, is equal to

$$\left|m_{22}(2\pi)\right|^2 = 1 + \left(4I_0^4(S_\text{h}) - 32I_0(S_\text{h})I^{+-+}(2\pi) + 16[I^{-+-+}(2\pi) + I^{+-+-}(2\pi)]\right)X^4 \tag{5.55}$$

On the other hand, the determinant of the propagation matrix for an arbitrary lossless element has to be equal unity according to (2.3) with ψ = 0. So the calculation of the determinant of the current propagation matrix (5.54) up to fourth power of detuning X^4 gives an expression which has to be equal one without any functional dependence on the parameters, such as detuning, which means that the coefficients at detuning powers have to be identically zero

$$\begin{aligned} &\left|\hat{m}(2\pi)\right|^2 = 1 + \left(4I_0^4(S_\mathrm{h}) - 32I_0(S_\mathrm{h})I_{(2\pi)}^{+-+} + 16[I_{(2\pi)}^{-+-+} + I_{(2\pi)}^{+-+-}] - [u_{12}^{(2)}(2\pi)]^2\right)X^4 = 1 \\ &\quad\rightarrow\quad 4I_0^4(S_\mathrm{h}) - 32I_0(S_\mathrm{h})I_{(2\pi)}^{+-+} + 16[I_{(2\pi)}^{-+-+} + I_{(2\pi)}^{+-+-}] = [u_{12}^{(2)}(2\pi)]^2. \end{aligned} \tag{5.56}$$

The last relation in (5.56) significantly simplifies expression (5.55). As a result, with account of the value of the off-diagonal elements (5.52), we get an analytical expression for the transmission peak profile of a cosine moiré filter

$$\begin{aligned} &\left|m_{22}(2\pi)\right|^2 = 1 + H\cdot X^4, \quad H = [u_{12}^{(2)}(2\pi)]^2, \quad u_{12}^{(2)}(2\pi) = 4\sum_{k=0}^{\infty}\frac{I_0(S_\mathrm{h})S_\mathrm{h}^{2k+1}}{\pi[(2k+1)!!]^2}, \\ &T = \frac{1}{\left|m_{22}(2\pi)\right|^2} = \frac{1}{1 + H\cdot X^4}. \end{aligned} \tag{5.57}$$

Such detuning dependence of the transmission peak profile has a much more flat-topped peak shape than a regular Lorentzian peak profile. It can be explained as the equivalence of a cosine moiré filter to a new physical transmission element – the double coherent cavity.

Finally, the wavelength full width at half maximum (FWHM) of this doubly coherent moiré (DCM) cavity transmission peak can expressed using the half width (HW) detuning parameter according to (5.57)

$$T(X_{\mathrm{HW}})=\frac{1}{2}\quad\rightarrow\quad X_{\mathrm{HWHM}}=\frac{1}{\sqrt[4]{H}}=\left(2\sqrt{\sum_{k=0}^{\infty}\frac{I_0(S_{\mathrm{h}})S_{\mathrm{h}}^{2k+1}}{\pi[(2k+1)!!]^2}}\right)^{-1}=-\frac{\Delta\lambda_{\mathrm{HW}}}{\lambda_0^2}2\pi n_0L_\pi,$$
$$\Delta\lambda_{\mathrm{DCM,FWHM}}=2\left|\Delta\lambda_{\mathrm{HW}}\right|=\frac{\lambda_0^2}{\pi n_0L_\pi}X_{\mathrm{HWHM}}=\frac{\lambda_0^2}{\pi n_0L_\pi}\cdot\left(2\sqrt{\sum_{k=0}^{\infty}\frac{I_0(S_{\mathrm{h}})S_{\mathrm{h}}^{2k+1}}{\pi[(2k+1)!!]^2}}\right)^{-1}. \tag{5.58}$$

To the best of my knowledge, the theory of doubly coherent cavities is not well-researched. We think such cavities could be useful for some quantum optics or quantum information applications. While regular Fabry-Perot cavities are widely available, the fabrication of double cavity looks to be challenging. The realization of such cavities based on a particular moiré cosine profile in principle can be a realistic way to implement a doubly coherent cavity.

CHAPTER SIX: MULTIPLEXED VBGS IN PTR GLASS

Properties of PTR glass

Photo-thermo-refractive glass is a photosensitive material developed [106-Glebov 02] for the recording of volume holographic elements such as high-efficiency volume Bragg gratings [49-Efimov 04]. UV laser radiation causes a chemical recombination processes in the compounds of this glass; after subsequent thermal developing the permanent change of refractive index of the glass matrix can be achieved up to $\delta n \approx 10^{-3} \equiv 10^{3}$ppm. Robust optical elements made of this glass are characterized by low absorption and scattering in the visible and IR spectral ranges and a high tolerance to operating laser irradiation. VBGs recorded in PTR glass are widely used for spectral narrowing of radiation from laser cavities; they are promising candidates for the implementation of spectral beam combining (SBC). In particular, we discuss in this chapter PTR glass for recording transmitting, non-diffractive phase elements.

PTR glass is a unique photosensitive material for recording optical phase plates. Homogeneous optical flats with apertures as large as $100\times100\ \text{mm}^2$ and fluctuation of the refractive index of a few ppm across the aperture can be fabricated in PTR glasses. The change of the average refractive index across the PTR glass aperture (x,y) allows one to change the optical path length along z-coordinate. As a result, different phase shifts $\varphi(x,y)$ can be achieved, and the phase of the transmitted beam can be modulated across its aperture. In addition, PTR glass has a broad transmission spectral range, high mechanical, chemical and thermal stability, and good tolerance to high power radiation.

Let us consider a PTR glass window of constant thickness L. This plate will be used for recording a phase plate operating at wavelength λ. Suppose that we want a relative phase shift of $\Delta\varphi = 2\pi$ between the different aperture points. It can be achieved with relative variation $\Delta n(x,y)$ of the refractive index of the glass in these aperture points. If the refractive index depends also on coordinate z, then $\Delta n(x,y)$ is the average value along the thickness, so

$$\Delta\varphi = 2\pi = L\Delta k = L\Delta n_{2\pi}\frac{2\pi}{\lambda} \quad \rightarrow \quad \Delta n_{2\pi} = \frac{\lambda}{L}, \tag{6.1}$$

Thus, the variation of the recorded refractive index change across the aperture for a plate of thickness $L = 3$mm and operating wavelength $\lambda = 1.06$μm has to be $\Delta n_{2\pi} = \lambda/L = 355$ppm. This value is within the range of the linear photosensitivity of PTR glass, see Figure 13. Researchers in the glass fabrication laboratory of Prof. L. Glebov's group have measured this experimental curve.

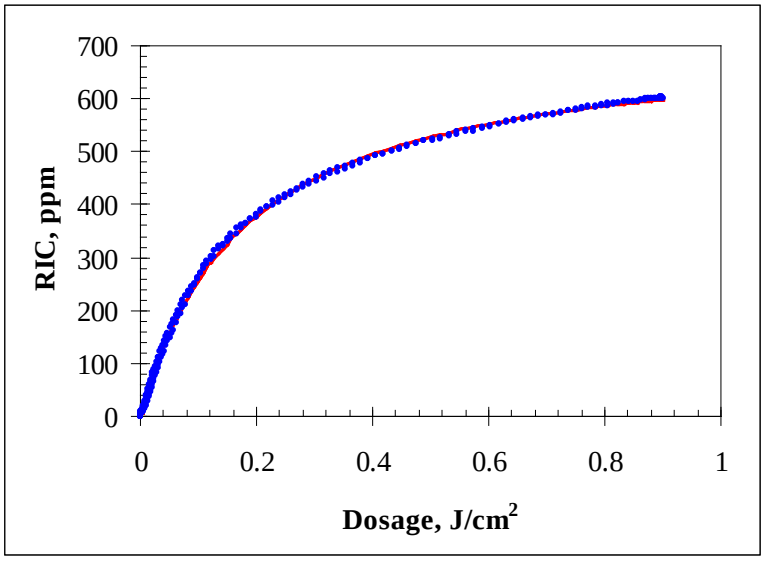

Figure 13. Photosensitivity curve of PTR glass depending on the exposure dosage.

The process of creating local refractive index change in PTR glass is described in detail in [107-Efimov 03]. It consists of two major steps: first, a PTR glass sample is exposed to radiation using, for example, a He-Cd laser, and then the sample is thermally developed at a temperature above the glass transition temperature for several hours.

The change of the local refractive index of the recorded phase plate is determined by the UV dosage at this aperture point. Therefore, in order to create a desirable distribution of the phase variation $\varphi(x,y)$ across aperture, it is necessary to control the spatial distribution of the UV dosage according to the curve of Figure 13.

Probabilistic amplitude masks for phase plates in PTR glass

In general, an amplitude mask with a gradually varying transmittance is required for recording an arbitrary phase plate. During the digital generation and printing process, amplitude masks often have small regular structural elements, “dots”, with sizes larger than the wavelength of UV exposure. In this case, laser radiation transmitted through such an amplitude mask has an additional, undesirable diffraction pattern from those structural elements. For example, ordinary lithographic methods allow one to create amplitude masks with only binary transparent/nontransparent areas. Gradual variation of the transmittance across the mask aperture can be achieved by creating small areas with a corresponding probabilistic distribution of their binary transmittance. Figure 14 demonstrates an amplitude mask of such a probabilistic type.

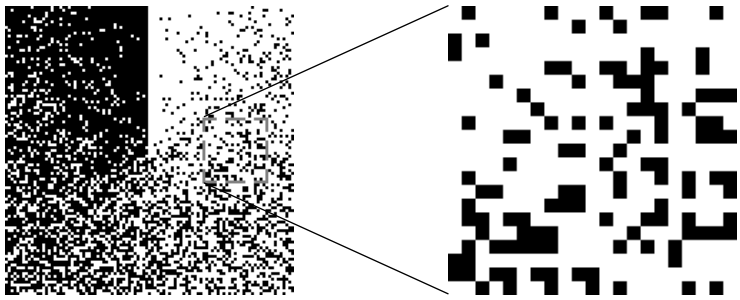

Figure 14. The central area of a probabilistic amplitude mask for recording vortex phase plate (left) and the local area with a filling factor 0.25 (right).

If the size of small micro-areas is larger than the wavelength, then the final recorded coherent intensity radiation pattern inside the PTR blank will demonstrate a parasitic, highly divergent diffraction structure at the operating wavelength of the fabricated phase plate. There are several approaches to eliminate this parasitic diffraction pattern from microstructures. First, when contact recording is used, an incoherent source, e.g. a lamp, can be used as the source of recording radiation instead of a UV laser. The spectral filter can be used to eliminate the unnecessary part of the spectrum, restricting it to the spectral range in which the PTR glass is photosensitive, and, thus, reducing heating. An alternative method consists in using recording UV laser with small translational or angular relative shifts, varying with time, between the master amplitude mask and the PTR blank in order to average the coherent intensity distribution during the contact recording process.

Besides the contact recording process, imaging systems can be applied. In this scheme the amplitude mask intensity distribution is imaged on a PTR glass blank, while high-angular diffraction frequencies, caused by the small structural elements, are eliminated using a spatial filter. As a result, the PTR glass blank is illuminated by a cleaned-up, smooth intensity

distribution. One optical setup of such type is a classical *4f*-system. This system consists of two lenses separated by a distance equal to the sum of the two focal lengths, different in general case. A pinhole is added in the beam path between the two lenses (i.e. at the image focal plane of the first lens, or the object focal plane of the second lens, which overlap). The amplitude mask is located in the object focal plane of the 1st lens while the recording material is placed in the image focal plane of the 2nd lens, see Figure 15. Finally, this optical system is illuminated by a collimated uniform beam. In this setup, the mask is imaged using the two lenses in the PTR glass window and the aperture "filters out" the high angular diffraction frequencies from small printing "dots" on the amplitude mask.

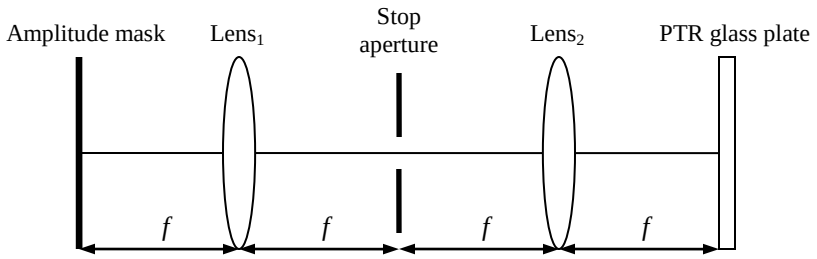

Figure 15. 4*f* optical system for spatial filtering.

The method of spatial filtering was applied to record a phase mask with an azimuthally increasing phase shift. The experimental part of this work was done in the holography laboratory of Prof. L. Glebov's group and it is not discussed in this dissertation.

To conclude, the refractive index change across the aperture can be controlled using two parameters: the dosage of UV exposure and the thermal treatment duration/temperature. Thus, after recording the phase plate, the only controlling parameter is the thermal duration. It is

possible to develop the sample at a given temperature and for a given time and to control this phase plate after such a heat-treatment. If the local refractive index change of the exposed area is less than the required change, and the phase change is also less than the required change, then the phase plate can be additionally thermally developed in order to make the local phase shift larger. To the contrary, if the refractive index change that was achieved is larger than the required one, and therefore the phase change is larger than the required one, it is possible to decrease the phase change to the required one by finely polishing the phase plate. Finally, for phase plates that are developed for specific operational wavelengths, after fabrication their surfaces can be anti-reflection coated to reduce Fresnel reflection losses.

Slanted reflective and transmissive VBGs

We have previously discussed VBGs of the reflective type, which can be described by one-dimensional coupled equations for counter-propagating waves. The same theoretical results are applicable for fiber Bragg gratings (FBGs). The main advantage of reflective VBGs in comparison with FBG used for high-power lasers is that their large aperture and, as a result, the couplers are unnecessary, that reducing coupling losses. Another additional, important feature of VBGs is the possibility of tuning the Bragg condition by changing the angle of incidence upon the grating. Another possibility for tuning is the moiré filter in VBG with the recorded pattern shown in Figure 12, which conserves the resonant wavelength of the transmission peak with a transverse shift of the illumination point along the aperture while still allowing for a change in the shape and width of the transmission peak.

The next step is to consider volume Bragg grating geometries, which cannot be realized in the case of FBG. They are transmissive gratings, characterized by high angular selectivity, and volume elements with multiple gratings recorded simultaneously, mostly reflective VBGs with different slanted angles between Bragg wave vectors and normals to grating surfaces. The Bragg diffraction processes again can be efficiently described by coupled wave theory – actually with equations of the same type and with slightly different, more generalized boundary conditions.

Previously, we used coupled wave equations derived for layered media with only *z*-dependent properties. Now, consider a VBG with its refractive index uniformly modulated along the grating vector **Q** for an arbitrary orientation

$$n(\mathbf{r}) = n_0 + n_1 \cos(\mathbf{Q}\mathbf{r}), \quad n_1 << n_0: \quad n^2(\mathbf{r}) \approx n_0^2 + 2 n_0 n_1 \cos(\mathbf{Q}\mathbf{r}). \tag{6.2}$$

We can rederive the coupled equations from the Helmholtz wave equation for the electric field presented as a superposition of two waves, $A(\mathbf{r})$ and $B(\mathbf{r})$, with different polarizations and wave vectors approximately satisfying the Bragg condition

$$(\nabla \cdot \nabla)\mathbf{E} + k_0^2 n^2(\mathbf{r})\mathbf{E} = 0, \quad \mathbf{E} = \mathbf{e}_A A e^{i\mathbf{k}_A \mathbf{r}} + \mathbf{e}_B B e^{i\mathbf{k}_B \mathbf{r}}, \quad \left|\mathbf{k}_{A,B}\right| = k_0 = \frac{2\pi}{\lambda}, \quad \mathbf{k}_B = \mathbf{k}_A - \mathbf{Q}. \tag{6.3}$$

With the standard assumption of slow variance for *A* and *B*, the second derivatives can be neglected, so

$$2i\mathbf{e}_A e^{i\mathbf{k}_A \mathbf{r}} (\mathbf{k}_A \nabla) A + 2i\mathbf{e}_B e^{i\mathbf{k}_B \mathbf{r}} (\mathbf{k}_B \nabla) B + k_0^2 n_0 n_1 (e^{i\mathbf{Q}\mathbf{r}} + e^{-i\mathbf{Q}\mathbf{r}})(\mathbf{e}_A A e^{i\mathbf{k}_A \mathbf{r}} + \mathbf{e}_B B e^{i\mathbf{k}_B \mathbf{r}}) = 0. \tag{6.4}$$

According to the Bragg condition from (6.2), we keep only two corresponding terms after expanding the brackets in (6.4) and, finally, we will get two separate, coupled equations with slow, spatially oscillating factors

$$\begin{cases}(\mathbf{m}_A\nabla)A = ip\kappa B e^{-2i\mathbf{Dr}}, \\ (\mathbf{m}_B\nabla)B = ip\kappa A e^{2i\mathbf{Dr}}, \end{cases} \quad \kappa = \frac{\pi n_1}{\lambda}, \quad p = (\mathbf{e}_A\mathbf{e}_B), \quad D = \frac{\mathbf{k}_A - \mathbf{k}_B - \mathbf{Q}}{2}. \tag{6.5}$$

The polarization factor p is equal to one for TE polarization, and for TM polarization coupling is reduced by the cosine of the mutual angle between the wave vectors. In particular, for TM waves propagating in orthogonal directions there will be no coupling.

Now, consider a reflective VBG of thickness L with vector $\mathbf{Q}$ in xz-plane with an angle γ relative to the normal of the front face of the VBG plate, see Figure 16. For definiteness, consider only TE incident and reflected plane waves, which, in particular, means that the amplitudes A and B are constant outside the VBG and at the boundaries of the VBG.

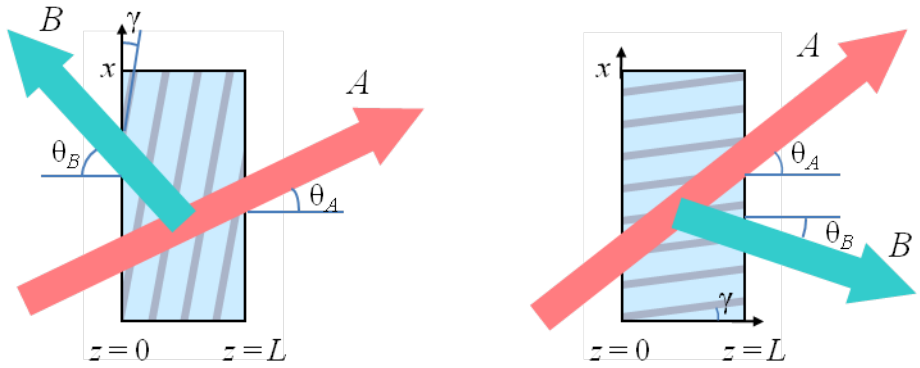

Figure 16. Beam geometries of slanted reflective and transmissive VBGs.

If the boundary conditions for the amplitudes do not depend on coordinate x, then it is natural to look for only z-dependent solutions, $A(z)$ and $B(z)$, of the coupled equations (6.5). After that, the only explicit functional dependence on the x-coordinate will remain in the oscillating factor, and, in order to eliminate it, the phase-matching condition $D_x = 0$ must be satisfied. It means that for a certain incident angle θ_A, the direction of the reflected wave will be

determined from this phase-matching boundary condition. Finally, we come to the following system of equations for the amplitudes of the incident and reflected waves

$$\begin{gathered}
\mathbf{k}_A = (\sin\theta_A, 0, \cos\theta_A), \quad \mathbf{k}_B = (\sin\theta_B, 0, -\cos\theta_B), \quad |\theta_{A,B}| < \frac{\pi}{2}, \quad \mathbf{Q} = (\sin\gamma, 0, \cos\gamma), \\
D_x = \tfrac{1}{2}(k\sin\theta_A - k\sin\theta_B - Q\sin\gamma) = 0 \quad \rightarrow \quad \theta_B = \arcsin(\sin\theta_A - Q/k\sin\gamma), \qquad (6.6) \\
\begin{cases} \cos\theta_A \dfrac{dA}{dz} = i\kappa B e^{-2iD_z z}, & \kappa = \dfrac{\pi n_1}{\lambda}, \quad D_z = \tfrac{1}{2}(k\cos\theta_A + k\cos\theta_B - Q\cos\gamma), \\ -\cos\theta_B \dfrac{dB}{dz} = i\kappa A e^{2iD_z z}, & \rightarrow \quad \dfrac{d}{dz}\left(\cos\theta_A |A|^2 - \cos\theta_B |B|^2\right) = 0. \end{cases}
\end{gathered}$$

All of the angles θ_A, θ_B, γ are defined inside the VBG glass plate, while outside the VBG the propagation angles of the waves in air can be recalculated according to Snell's law. In order to avoid consideration of this trivial extra step, we can assume that the grating is surrounded by a refractive-index-matched liquid, for example.

The coupled wave equations (6.6) can be easily transformed to linear equations with constant coefficients by the following substitution for wave amplitudes. After that, we can write a solution very similar to the already discussed one, and with the boundary condition of no-incoming wave *B* into the VBG we can get expression for the diffraction efficiency:

$$\begin{gathered}
\begin{matrix} A = e^{-iD_z z}\, a \Big/ \sqrt{\cos\theta_A}\,, \\ B = e^{iD_z z}\, b \Big/ \sqrt{\cos\theta_B}, \end{matrix} \quad \rightarrow \quad \frac{d}{dz}\begin{pmatrix} a \\ b \end{pmatrix} = \begin{pmatrix} iD_z & i\tilde{\kappa} \\ -i\tilde{\kappa} & -iD_z \end{pmatrix}, \quad \tilde{\kappa} = \frac{\kappa}{\sqrt{\cos\theta_A \cos\theta_B}} \quad \rightarrow \\
\begin{pmatrix} a \\ b \end{pmatrix}_{z=L} = \left(\hat{1}\cosh\sqrt{S^2 - X^2} + \begin{pmatrix} iX & iS \\ -iS & -iX \end{pmatrix} \frac{\sinh\sqrt{S^2 - X^2}}{\sqrt{S^2 - X^2}} \right) \begin{pmatrix} a \\ b \end{pmatrix}_{z=0}, \quad \begin{matrix} S = \tilde{\kappa} L, \\ X = D_z L, \end{matrix} \qquad (6.7) \\
b\big|_{z=L} = 0 \qquad \rightarrow \qquad R = \frac{\cos\theta_B |B_0|^2}{\cos\theta_A |A_0|^2} = \frac{|b_0|^2}{|a_0|^2} = \frac{\sinh^2\sqrt{S^2 - X^2}}{\cosh^2\sqrt{S^2 - X^2} - X^2/S^2}.
\end{gathered}$$

Such a reflection spectrum was discussed before, see the solid line (no additional Fresnel corrections from boundaries) in Figure 3.

A typical value of the reflective strength of a VBG is $S = 3$, which corresponds to a reflectivity of $R = 0.99$ at the exact Bragg resonance. The numerical value of detuning corresponding to half of this maximal reflectivity is

$$\frac{0.99}{2} = \frac{\sinh^2\sqrt{3^2 - X^2}}{\cosh^2\sqrt{3^2 - X^2} - X^2/3^2} \quad \rightarrow \quad X_{\mathrm{HWHM}}(S = 3) = 3.77. \qquad (6.8)$$

Then, the spectral bandwidth of a non-slanted, reflective VBG, $\gamma = 0$, can be estimated as

$$X = D_z L = \left(k - \frac{Q}{2}\right)L \approx -2\pi n_0 \frac{\Delta\lambda}{\lambda_0^2} L \quad \rightarrow \quad \Delta\lambda_{\mathrm{FWHM}} = \frac{X_{\mathrm{HWHM}}\lambda_0^2}{\pi n_0 L}.. \qquad (6.9)$$

For example, for numerical values $\lambda_0 = 1.06$ μm, $n_0 = 1.5$, $L = 3$ mm and $S = 3$, the spectral bandwidth is equal to $\Delta\lambda_{\mathrm{FWHM}} = 300$ pm.

Now, let us discuss a transmissive grating in similar way. The main difference between a transmissive VBG and a reflective one is that the wave *B* generated by volume diffraction is not reflected back in the negative *z*-direction, opposite to the incident wave *A*, but, in this case, the wave *B* leaves VBG in the same direction as wave *A*, see Figure 16. Such a diffraction process can be realized when the Bragg wave vector **Q** is directed mostly along the surface of the grating, so that it changes the transverse *x*-component of incident wave vector $\mathbf{k}_A$, while the *z*-components of both waves have the same sign. The power of incident wave *A* will be redistributed between two coupled, co-propagating waves *A* and *B* along the thickness of the grating. Because this redistribution process is oscillating, we obtain a so-called “pendulum” solution.

With the following notation for the (*x*, *y*, *z*)-components of the wave vectors we will derive a system of coupled equations. Again, if we assume that the wave amplitudes are constant

outside of the VBG and at its boundaries, then the phase-matching boundary condition $D_x = 0$ must be satisfied, and the angle of diffraction θ_B will be determined from it.

$$\begin{gathered}
\mathbf{k}_A = (\sin\theta_A, 0, \cos\theta_A), \quad \mathbf{k}_B = (-\sin\theta_B, 0, \cos\theta_B), \quad |\theta_{A,B}| < \frac{\pi}{2}, \quad \mathbf{Q} = (\cos\gamma, 0, \sin\gamma), \\
D_x = \tfrac{1}{2}(k\sin\theta_A + k\sin\theta_B - Q\cos\gamma) = 0 \quad \rightarrow \quad \theta_B = \arcsin(Q/k\cos\gamma - \sin\theta_A), \\
\begin{cases}
\cos\theta_A \dfrac{dA}{dz} = i\kappa B e^{-2iD_z z}, & \kappa = \dfrac{\pi n_1}{\lambda}, \quad D_z = \tfrac{1}{2}(k\cos\theta_A - k\cos\theta_B - Q\sin\gamma), \\
\cos\theta_B \dfrac{dB}{dz} = i\kappa A e^{2iD_z z}, & \rightarrow \quad \dfrac{d}{dz}\left(\cos\theta_A |A|^2 + \cos\theta_B |B|^2\right) = 0.
\end{cases}
\end{gathered} \tag{6.10}$$

A transmissive VBG will be called non-slanted if $\gamma = 0$.

The system of differential equations from (6.10) also can be transformed to a linear systemwith constant coefficients by the same substitutions as in (6.7), and, after that, the solution can be written down analytically

$$\begin{gathered}
A = e^{-iD_z z}\, a \Big/ \sqrt{\cos\theta_A}, \qquad \frac{d}{dz}\begin{pmatrix} a \\ b \end{pmatrix} = \begin{pmatrix} iD_z & i\tilde{\kappa} \\ i\tilde{\kappa} & -iD_z \end{pmatrix}, \quad \tilde{\kappa} = \frac{\kappa}{\sqrt{\cos\theta_A \cos\theta_B}} \quad \rightarrow \\
B = e^{iD_z z}\, b \Big/ \sqrt{\cos\theta_B}, \\
\begin{pmatrix} a \\ b \end{pmatrix}_{z=L} = \hat{M}\begin{pmatrix} a \\ b \end{pmatrix}_{z=0}, \quad \hat{M} = \left(\hat{1}\cos\sqrt{S^2 + X^2} + \begin{pmatrix} iX & iS \\ iS & -iX \end{pmatrix}\frac{\sin\sqrt{S^2 + X^2}}{\sqrt{S^2 + X^2}}\right), \quad \begin{matrix} S = \tilde{\kappa}L, \\ X = D_z L. \end{matrix}
\end{gathered} \tag{6.11}$$

Power flows in the positive *z*-direction for both waves *A* and *B*. This is manifested in the trigonometric functions in matrix $\hat{M}$, instead of the hyperbolic functions seen in the case of a reflective grating (6.7).

In order to find the diffraction efficiency η we have to apply the boundary condition of zero amplitude to the incoming wave *B*, which, in the case of a transmissive grating, is defined at the same grating surface *z* = 0 for incoming wave *A*:

$$b_0 = 0 \quad \rightarrow \quad b_L = M_{21} a_0, \quad \eta = \frac{|b_L|^2}{|a_0|^2} = |M_{21}|^2 = \frac{S^2}{S^2 + X^2}\sin^2\sqrt{S^2 + X^2}. \tag{6.12}$$

We see that at the exact Bragg resonance, $X = 0$, the diffraction efficiency is equal to $\eta = \sin^2 S$, where the coupling strength parameter is proportional to the thickness, so that at certain periodic values of the thickness, corresponding to $S = \frac{1}{2}\pi + \pi m$, we will have 100% diffraction efficiency in theory. This is what is meant by the "pendulum" nature of the oscillating solution of coupled equations for co-propagating waves.

The functional dependence of the diffraction efficiency η on the detuning D_z for the same coupling constant κ can be demonstrated in the following way. For illustration purposes, consider three values of the coupling strength $S_m = m\frac{1}{2}\pi = \kappa L_m$, m =1,2,3, corresponding to three different lengths of a VBG $L_m = mL_1$. Let us plot the diffraction efficiency η which depends upon the dimensionless parameter $X_1 = D_z L_1$, ½ππproportional to varying detuning D_z. If we want to have values on argument axis corresponding to the same D_z, or for convenience dimensionless parameter X_1, then for two other cases of other thicknesses the corresponding dimensionless parameters used in (6.12) should be normalized $X_m = D_z L_m = X_1 L_m / L_1 = mX_1$ in order to keep dimensionless coordinate of argument axis proportional to the same detuning constant D_z for different gratings. These dependences are presented on Figure 17.

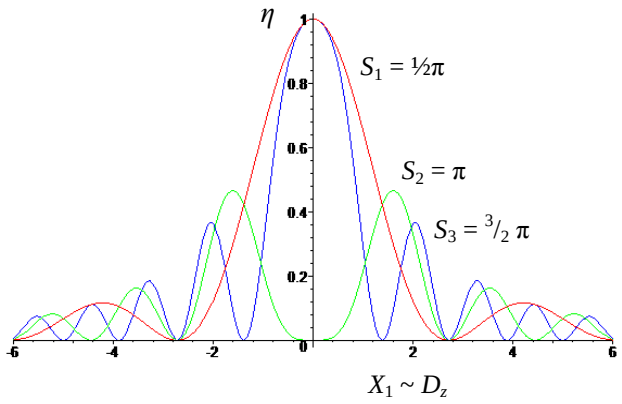

Figure 17. Diffraction efficiency of transmissive VBG depending on detuning for different coupling strengths.

The detuning half width at half maximum of the diffraction efficiency of a transmissive grating with coupling strength ½π can be found numerically in terms of the dimensionless detuning parameter

$$0.5 = \frac{(\frac{\pi}{2})^2}{(\frac{\pi}{2})^2 + X^2} \sin^2 \sqrt{(\tfrac{\pi}{2})^2 + X^2} \quad \rightarrow \quad X_{\mathrm{HWHM}\frac{1}{2}\pi} = 1.255. \tag{6.13}$$

This detuning value can be converted to a spectral width or an angular width for some particular grating. For clarity, consider a non-slanted transmissive VBG, $\gamma = 0$, with its corresponding approximate Bragg condition, $2k{\cdot}\sin\theta_A \approx Q$. The boundary phase-matching condition (6.10) defines the angle of the diffracted wave

$$D_x = \tfrac{1}{2}(k\sin\theta_A + k\sin\theta_B - Q) = 0 \quad \rightarrow \quad \sin\theta_B = Q/k - \sin\theta_A. \tag{6.14}$$

After that, the small detuning parameter X can be calculated as

$$\begin{aligned} X &= D_z L = \tfrac{1}{2} Lk(\cos\theta_A - \cos\theta_B) = \tfrac{1}{2} Lk\left(\cos\theta_A - \sqrt{1-(Q/k - \sin\theta_A)^2}\right) = \\ &= \tfrac{1}{2} Lk\cos\theta_A \left(1 - \sqrt{1 + \frac{Q}{k^2\cos^2\theta_A}(2k\sin\theta_A - Q)}\right) \approx \left|2k\sin\theta_A \approx Q\right| \approx \\ &\approx \tfrac{1}{2} L \tfrac{1}{2} \frac{Q}{k\cos\theta_A}(Q - 2k\sin\theta_A) \approx \tfrac{1}{2} L\tan\theta_A (Q - 2k\sin\theta_A). \end{aligned} \tag{6.15}$$

Suppose that the exact Bragg condition occurs at a certain wavelength λ_0 and angle θ_{A0} of wave A, so that $Q = 2k_0{\cdot}\sin\theta_{A0}$ and $k_0 = 2\pi n_0/\lambda_0$, then with angular or/and spectral deviation we get an expression for detuning

$$X \approx \frac{L\tan\theta_A}{2}\left[Q - 2k_0\left(1 - \frac{\Delta\lambda}{\lambda_0}\right)(\sin\theta_A + \cos\theta_A\Delta\theta_A)\right] \approx L\frac{2\pi n_0}{\lambda_0}\sin\theta_A\left(\frac{\Delta\lambda}{\lambda_0}\tan\theta_A - \Delta\theta_A\right). \tag{6.16}$$

Then, the full width at half maximum in terms of wavelength detuning or in terms of angle deviation in air, $\theta_{\mathrm{air}} \approx n_0\theta_A$, is equal to

$$\Delta\lambda_{\mathrm{FWHM}} = \frac{X_{\mathrm{HWHM}\frac{1}{2}\pi}\lambda_0^2 n_0}{\pi L \sin\theta_{\mathrm{air}} \tan\theta_{\mathrm{air}}}, \quad \Delta\theta_{\mathrm{FWHM}} = \frac{X_{\mathrm{HWHM}\frac{1}{2}\pi}\lambda_0 n_0}{\pi L \sin\theta_{\mathrm{air}}}. \tag{6.17}$$

For example, the corresponding full widths for a transmissive grating with coupling strength ½π and parameters $\lambda_0 = 1.06$ μm, $n_0 = 1.5$, $\theta_{\mathrm{air}} = 5°$, and $L = 3$ mm will be equal to $\Delta\lambda \approx 29$ nm and $\Delta\theta_{\mathrm{air}} \approx 0.14°$. We see that the spectral width of a transmissive grating is much higher than the width of a reflective grating because of the inverse square dependence on the incident angle.

The foregoing mathematical approach to the problems of coupled waves in VBG of reflective or transmissive type is a basic tool in theory of volume refraction. Now, consider one possible application of a highly multiplexed, efficient holographic element.

Multiplexed reflective VBG for coherent beam combining

The need for compact, high-power laser sources stimulates active research in fiber lasers because these lasers can produce high-power beams due to their effective thermal management. However, the ultimate output power is restrained by thermal and nonlinear optical effects in fibers. Therefore, coherent beam combining (CBC) of the radiation from separate lasers is of strong interest; the output power can be scaled up by subsequent SBC [108-Andrusyak 09].

Several approaches for passively coherent-locking fiber lasers have been proposed and realized with some success. One of the common approaches to CBC is based on using fiber couplers, but in such schemes the power limit of a single fiber remains and the number of lasers is limited because of the large super-mode spacing [109-Chang 10]. Fiber laser arrays placed in a self-Fourier cavity can also be coherently combined, but the far-field pattern side lobes will carry

out significant power due to the limited fill-factor [110-Corcoran 08]. One of the most powerful realizations is a two-dimensional array of lasers coupled in a ring with small, spatially cleaned-up power feedback reflected by a tilted aperture [111-Rothenberg 08], but one of the limitations of this approach again is the actual fill factor of the fiber array.

Prof. L. Glebov has proposed a Multiplexed Volume Bragg Grating (MVBG) for coherent combining because laser beams can be reflected in the same aperture spot and direction simultaneously by partial volume gratings. As a result, one can avoid intrinsic problems connected with the limited aperture fill factor of fiber arrays. The background of this approach consists of a well-developed technology for recording volume Bragg gratings in photo-thermo-refractive glass for different high power laser applications.

The problem of reflection of a beam by N gratings recorded in the same volume, when all of them satisfy the exact Bragg resonance condition simultaneously, was discussed before [112-Solymar 77]. Here, we reformulate this problem in terms of a convenient parameter for reflection problems – S , the strength of reflection, which, for a single reflective VBG of thickness L with refractive index profile $n(z) = n_0 + n_1\cos(4\pi n_0/\lambda_0 \cdot z)$, equals

$$S_1 = \kappa \cdot L, \quad \kappa = \pi\, n_1 / \lambda_0 \,. \tag{6.18}$$

Suppose that each of N waves $A, B, \ldots, D$ is coupled with just one common wave F in the case of MVBG, so for their slowly varying envelopes we have coupled equations at the exact Bragg resonance:

$$\frac{dA}{dz} = i\kappa F(z), \quad \frac{dB}{dz} = i\kappa F(z), \quad ..., \quad \frac{d}{dz}F(z) = -i\kappa[A(z) + B(z) + ... + D(z)], \tag{6.19}$$

To simplify the notation, we have assumed all coupling coefficients κ to be real, positive numbers. Then, an explicit solution of this equation at $z = L$ can be represented in the form of a transfer matrix:

$$\begin{pmatrix} A(L) \\ B(L) \\ ... \\ D(L) \\ F(L) \end{pmatrix} = \hat{\mathrm{M}} \begin{pmatrix} A(0) \\ B(0) \\ ... \\ D(0) \\ F(0) \end{pmatrix}, \quad \hat{\mathrm{M}} = \begin{pmatrix} 1+\frac{-1+\cosh S}{N} & \frac{-1+\cosh S}{N} & ... & \frac{-1+\cosh S}{N} & \frac{i\sinh S}{\sqrt{N}} \\ \frac{-1+\cosh S}{N} & 1+\frac{-1+\cosh S}{N} & ... & \frac{-1+\cosh S}{N} & \frac{i\sinh S}{\sqrt{N}} \\ ... & ... & ... & ... & ... \\ \frac{-1+\cosh S}{N} & \frac{-1+\cosh S}{N} & ... & 1+\frac{-1+\cosh S}{N} & \frac{i\sinh S}{\sqrt{N}} \\ -\frac{i\sinh S}{\sqrt{N}} & -\frac{i\sinh S}{\sqrt{N}} & ... & -\frac{i\sinh S}{\sqrt{N}} & \cosh S \end{pmatrix}, \quad S = \sqrt{N}\kappa L. \quad (6.20)$$

Here $S = \sqrt{N} S_1$ is the effective strength of a MVBG with N gratings of identical strengths S_1.

Appropriate boundary conditions allow one to find all the necessary reflection and transmission coefficients. For example, if only the F-wave is incident, so that the corresponding boundary conditions are $F(0) = 1$, A, B, …, $D(L) = 0$, then the power P_F is diffracted in equal portions into reflected powers P_A, P_B, …, P_D:

$$P_A = P_B = ... = P_D = \eta(A \leftarrow F) P_F, \quad \eta(A \leftarrow F) = \frac{\tanh^2 S}{N} \approx \frac{1}{N}. \quad (6.21)$$

If only the A-wave is incident upon the MVBG with interaction of all $N + 1$ waves, then the boundary conditions are $A(L) = 1$, B,…,$D(L) = 0$, $F(0) = 0$, and the efficiencies of diffraction and transmission are

$$\begin{aligned} &\eta(F \leftarrow A) = \frac{\tanh^2 S}{N} \approx \frac{1}{N}, \quad \eta(B,...,D \leftarrow A) = \frac{1}{N^2}\left(\frac{1}{\cosh S} - 1\right)^2 \approx \frac{1}{N^2}, \\ &\tau(A(L) \leftarrow A(0)) = \left(1 + \frac{1}{N}\left(\frac{1}{\cosh S} - 1\right)\right)^2 \approx \left(\frac{N-1}{N}\right)^2. \end{aligned} \quad (6.22)$$

The sum of all of those η and transmission τ is equal to 1 for both the exact expressions and for the approximate ones, if $S \geq 3$.

MVBG, which was experimentally studied by Dr. O. Andrusyak, consists of two gratings symmetrically recorded at ±3.3^{o} inside PTR glass, each with a separate diffraction efficiency of 99% at resonance, with FWHM spectral bandwidth about 210 pm, see Figure 18a. The corresponding three-wave (*A*, *B*, *F*) coherent spectral profiles are present on Figure 18b,c , which are in good agreement with theoretical predictions for $N + 1 = 2 + 1$: b) for incident wave *F* we have $\eta(A,B \leftarrow F) = ½$; c) for incident one-channel wave *A* we have $\eta(F \leftarrow A) = ½$, $\eta(B \leftarrow A) = ¼$, $\tau(A \leftarrow A) = ¼$.

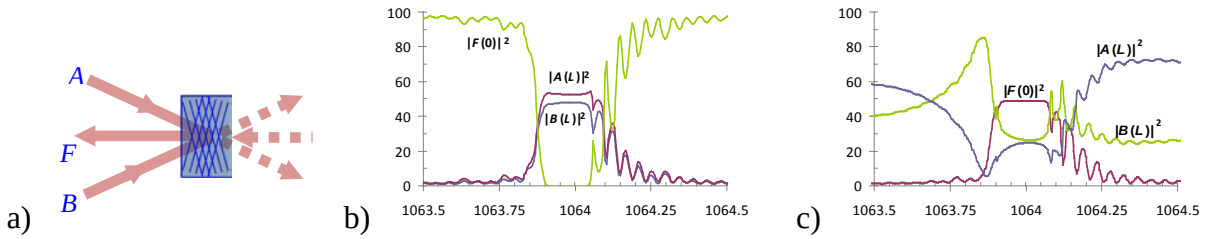

Figure 18. Spectral properties of a double MVBG with three-wave coherent coupling: a) notation of waves; b) incident wave *F*; c) incident wave *A*.

The diffraction efficiencies of several waves incident upon a MVBG simultaneously can be calculated as well using the transfer matrix $\hat{M}$ and the results will strongly depend on their mutual phases at the boundaries.

In conclusion, we would like to emphasize that the coherent operation of a MVBG cannot be represented by a sequence of regular beam splitters; therefore, this optical element offers new possibilities for laser system design.

CHAPTER SEVEN: HIGH-POWER SPECTRAL BEAM COMBINING WITH VBGS UNDER THERMAL DISTORTIONS

Beam quality parameter based on second moments

Due to the wave nature of light, optical beams diverge with propagation in free space. In the far-field zone, the angular amplitude profile of a particular beam can be calculated by the Huygens integral, which is actually the Fourier transform of the amplitude profile at a certain initial propagation plane. With free space propagation, the angular content of beam is conserved and, as result, the beam size grows linearly in the far-field zone. For example, the linear divergence of a beam diffracted by an aperture is determined by the angle, which is proportional to the ratio of the wavelength to the aperture size. Analogously, one can characterize the process of free propagation of a beam by the product of the minimal observed beam size multiplied by the divergence angle and divided by the wavelength [113-Siegman 93]. By eliminating the scale factors of the governing linear diffraction equation, this dimensionless propagation parameter should depend only on the inner structure of the beam profile.

To derive a rigorous expression for such a propagation invariant, people usually start their consideration with the parabolic wave equation (PWE) for a slowly *z*-varying amplitude $A(\vec{r},z)$ of the electric field amplitude $E(\vec{r},z)$:

$$E(\vec{r},z)=A(\vec{r},z)\cdot e^{ikz},\quad \frac{\partial A(\vec{r},z)}{\partial z}-\frac{i}{2k}\left(\nabla_{\vec{r}}\cdot\nabla_{\vec{r}}\right)A(\vec{r},z)=0,\quad \vec{r}=(x,y). \tag{7.1}$$

Here $\vec{r}$ denotes the two transverse coordinates *x* and *y*, and *k* is the wave vector in a linear lossless medium. If the transverse profile of the complex amplitude *A* is known at some propagation point $z = z_1$, then this boundary condition determines solution of (7.1) at any *z*. As a

result, the final expression for propagation invariant discussed above can be expressed only through known $A(\vec{r}, z_1)$.

For further analysis of how the coordinate and angular content of a beam are redistributed with free propagation, it is convenient to introduce the Wigner function, see e.g. [114-Zeldovich 85],

$$W(\vec{r} = \tfrac{1}{2}\vec{r}_1 + \tfrac{1}{2}\vec{r}_2, \vec{\rho} = \vec{r}_2 - \vec{r}_1, z) = A^*(\vec{r}_1, z)A(\vec{r}_2, z), \quad \frac{\partial W}{\partial z} - \frac{i}{k}\left(\nabla_{\vec{r}} \cdot \nabla_{\vec{\rho}}\right)W(\vec{r}, \vec{\rho}, z) = 0, \quad (7.2)$$

which satisfies the propagation equation (7.2) derived from PWEs for amplitudes $A^*(\vec{r}_1, z)$ and $A(\vec{r}_2, z)$.

The Fourier transform of a Wigner function performed with respect to the relative transverse coordinates is

$$\tilde{W}(\vec{r}, \vec{\theta}, z) = \frac{k^2}{4\pi^2}\int W(\vec{r}, \vec{\rho}, z)e^{-ik\vec{\rho}\cdot\vec{\theta}}d\vec{\rho}, \quad \vec{\theta} = (u, v), \quad W(\vec{r}, \vec{\rho}, z) = \int \tilde{W}(\vec{r}, \vec{\theta}, z)e^{ik\vec{\rho}\cdot\vec{\theta}}d\vec{\theta}. \quad (7.3)$$

The Wigner function also satisfies the first-order propagation equation given by (7.2) with a corresponding solution

$$\frac{\partial}{\partial z}\tilde{W}(\vec{r}, \vec{\theta}, z) + \left(\vec{\theta} \cdot \nabla_{\vec{r}}\right)\tilde{W}(\vec{r}, \vec{\theta}, z) = 0 \quad \rightarrow \quad \tilde{W}(\vec{r}, \vec{\theta}, z) = \tilde{W}(\vec{r} - \vec{\theta}(z - z_1), \vec{\theta}, z_1). \quad (7.4)$$

The moments of the spatial and angular coordinates can be calculated as

$$\begin{aligned} &\left\langle x^n y^m u^p v^q \right\rangle = \frac{1}{P}\iint \tilde{W}(\vec{r}, \vec{\theta}, z)x^n y^m u^p v^q d\vec{\theta}d\vec{r}, \\ &P = \iint \tilde{W}(\vec{r}, \vec{\theta}, z)d\vec{\theta}d\vec{r} = \int \left|A(\vec{r}, z)\right|^2 d\vec{r} = \text{const.} \end{aligned} \quad (7.5)$$

Here, the normalization value P is proportional to the total beam power. Spatial moments have simple expressions with clear physical interpretation and pure moments of the angle variables can be derived from (7.5, 7.3) as

$$\begin{aligned}
&\left\langle x^n y^m \right\rangle = \frac{1}{P}\int \left|A(\vec{r},z)\right|^2 x^n y^m d\vec{r}, \\
&\left\langle u^n v^m \right\rangle = \frac{1}{P}\int \left|C(\vec{\theta},z)\right|^2 u^n v^m d\vec{\theta}, \quad C(\vec{\theta},z) = \frac{k}{2\pi}\int A(\vec{r},z) e^{-ik\vec{r}\cdot\vec{\theta}} d\vec{r},
\end{aligned} \tag{7.6}$$

where $\left|C(\vec{\theta},z)\right|^2$ is the intensity distribution in angular space. The interpretation of arbitrary moments of both coordinates and angles is less obvious, but some of them are important for the calculation of others because, due to (7.4), there is a propagation equation for moments:

$$\begin{aligned}
\frac{\partial}{\partial z}\left\langle x^n y^m u^p v^q \right\rangle &= -\frac{1}{P}\iint x^n y^m u^p v^q (\vec{\theta}\cdot\nabla_{\vec{r}})\tilde{W}(\vec{r},\vec{\theta},z) d\vec{\theta} d\vec{r} = \\
&= n\left\langle x^{n-1} y^m u^p v^q \right\rangle + m\left\langle x^n y^{m-1} u^p v^q \right\rangle.
\end{aligned} \tag{7.7}$$

For the x-related second moments, the positive, dimensionless propagation invariant can be obtained, which is usually noted as M_x^2, and it was proposed as parameter characterizing beam duality some time ago [113-Siegman 93]

$$\begin{aligned}
&\frac{\partial}{\partial z}\left\langle x^2 \right\rangle = \left\langle xu \right\rangle, \quad \frac{\partial}{\partial z}\left\langle xu \right\rangle = \left\langle u^2 \right\rangle, \quad \frac{\partial}{\partial z}\left\langle u^2 \right\rangle = 0 \\
&\rightarrow \quad \frac{\partial}{\partial z} M_x^2 = 0, \quad M_x^2 = 2k\sqrt{\left\langle x^2 \right\rangle\left\langle u^2 \right\rangle - \left\langle xu \right\rangle^2}.
\end{aligned} \tag{7.8}$$

In the last formula and below we will assume that first order moments are equal to zero $\left\langle x \right\rangle = \left\langle u \right\rangle = \left\langle y \right\rangle = \left\langle v \right\rangle = 0$; these conditions can be easily realized by an appropriate linear transformation of the coordinate frame.

It can be shown that the minimal value $M_x^2 = 1$ and, therefore, the smallest divergence and best beam quality is achieved only by Gaussian beams [115-Bastiaans 79]. Any phase distortion of a Gaussian beam leads to increasing M_x^2. This parameter has well-studied analytical properties. It is widely used for characterizing beam quality in experiments, and corresponding measurement devices are commercially available.

The work [116-Serna 91] has introduced a parameter based on both the coordinates *x* and *y*, which is invariant to transverse rotation. It has following explicit form:

$$\langle x^2\rangle\langle u^2\rangle - \langle xu\rangle^2 + \langle y^2\rangle\langle v^2\rangle - \langle yv\rangle^2 + 2\langle xy\rangle\langle uv\rangle - 2\langle xv\rangle\langle yu\rangle . \qquad (7.9)$$

The main advantage of this generalized propagation invariant introduced for two-dimensional transverse space is that it is conserved after any astigmatic quadratic phase distortion $e^{i(\alpha x^2+\beta y^2+\gamma xy)}$, but notion of this parameter is less established. In practice, astigmatic beams are usually characterized just by two separate values, M_x^2 and M_y^2.

All information about beam propagation is defined by a particular profile cross-section $A(\vec{r}, z_1)$, as we mentioned before. An arbitrary moment (7.5) at this particular z_1 can be calculated through corresponding amplitude profile in explicit form

$$\left\langle x^n y^m u^p v^q \right\rangle_{z_1} = \frac{1}{P}\left(-\frac{i}{k}\right)^{p+q} \iint A^*(\vec{r}_1, z_1)\delta(\vec{r}_2 - \vec{r}_1)\frac{\partial^p}{\partial x_2^p}\frac{\partial^q}{\partial y_2^q}\left[A^*(\vec{r}_2, z_1)\left(\tfrac{x_1+x_2}{2}\right)^n\left(\tfrac{y_1+y_2}{2}\right)^m\right] d\vec{r}_1 d\vec{r}_2 . \quad (7.10)$$

The formula (7.10) with propagation equation (7.7) allows one to find the value of an arbitrary moment at any propagation coordinate *z*.

Hermite-Gaussian and Laguerre-Gaussian modes

An important example of self-similar solutions of the parabolic wave equation are orthogonal Gaussian mode sets with two indices corresponding to mode excitations in the transverse plane. Depending on which coordinate system is used, Cartesian or cylindrical, these mode sets are Hermite-Gaussian $\psi_{nx,ny}(x,y)$ or Laguerre-Gaussian $\psi_{n,m}(r,\varphi)$. These basic functions are used in different areas of physics. In optics they have following definitions with corresponding normalization [117-Siegman 86]

$$\begin{aligned}
&\psi_{n_x n_y}(x,y) = \psi_{n_x}(x)\psi_{n_y}(y), \quad \psi_n(x) = \frac{1}{\sqrt{\sqrt{\pi}\,2^{n-\frac{1}{2}}\,n!\,w_0}}\, e^{-\frac{x^2}{w_0^2}} H_n\!\left(\frac{\sqrt{2}x}{w_0}\right),\\
&\int_{-\infty}^{\infty} \psi_n(x)\psi_{n'}(x)dx = \delta_{nn'},\\
&\psi_{nm}(r,\varphi) = (-1)^n \sqrt{\frac{n!}{\pi(n+|m|)!}} \left(\frac{\sqrt{2}r}{w_0}\right)^{|m|} L_n^{|m|}\!\left(\frac{2r^2}{w_0^2}\right) e^{-\frac{r^2}{w_0^2}} e^{im\varphi}\, \frac{\sqrt{2}}{w_0},\\
&\int_0^{\infty} r dr \int_0^{2\pi} d\varphi \psi_{nm}^*(r,\varphi)\psi_{n'm'}(r,\varphi) = \delta_{nn'}\delta_{mm'}.
\end{aligned} \tag{7.11}$$

These notations do not contain phase factors corresponding to wave front curvature in the *z*-direction, so these formulae describe mode profiles at the beam waist.

With propagation along the *z*-direction, the mutual orthogonality of these modes will be preserved because the conservation of the scalar product of two different solutions of the PWE for slowly varying amplitudes (7.1) is an intrinsic property of the PWE.

$$\langle A|B\rangle = \int A^*(\vec{r},z)B(\vec{r},z)d\vec{r}, \quad \vec{r}=(x,y):$$

$$\frac{\partial}{\partial z}\langle A|B\rangle = \int\left(\frac{\partial A^*}{\partial z}B + A^*\frac{\partial B}{\partial z}\right)d\vec{r} \overset{\text{PWE}}{=} \int\left(\frac{1}{2ik}(\nabla_{\vec{r}}\cdot\nabla_{\vec{r}})A^*\cdot B + A^*\frac{\partial B}{\partial z}\right)d\vec{r} = \quad (7.12)$$

$$\overset{\text{Integr-n by parts}}{=} \int\left(A^*\frac{1}{2ik}(\nabla_{\vec{r}}\cdot\nabla_{\vec{r}})B + A^*\frac{\partial B}{\partial z}\right)d\vec{r} \overset{\text{PWE}}{=} 0.$$

Explicit expressions of Gaussian modes for arbitrary propagation distance z from the beam waist are presented in a very limited number of textbooks [30-Haus 84], and we would like to present rigorous derivation of them here.

The solution of the PWE for a slowly varying amplitude $A(x,y,z)$ with the boundary condition $A(x,y,0)$ is actually the Huygens integral [117-Siegman 86]

$$A(\vec{r},z) = \frac{-i}{\lambda z}\int A(\vec{r}',0)e^{ik\frac{(\vec{r}-\vec{r}')^2}{2z}}d\vec{r}', \qquad \frac{\partial A}{\partial z} - \frac{i}{2k}(\nabla_{\vec{r}}\cdot\nabla_{\vec{r}})A = 0. \quad (7.13)$$

For simplicity, let us use the generating function of the Hermite-Gaussian basis [118-Bateman 1953]

$$\Phi(\vec{r},z=0,\vec{R}) = \sqrt{\frac{2}{\pi}}\frac{1}{w_0}\exp\left(-\frac{r^2}{w_0^2} + 2\frac{\vec{r}\vec{R}}{w_0} - \frac{R^2}{2}\right) = \sum_{n_x n_y=0}^{\infty}\psi_{n_x n_y}(\vec{r})\Psi_{n_x n_y}(\vec{R}),$$
$$\vec{R}=(X,Y), \quad \Psi_{n_x n_y}(\vec{R}) = \frac{X^{n_x}Y^{n_y}}{\sqrt{n_x!n_y!}}. \quad (7.14)$$

This function Φ consists whole set of orthonormal functions $\psi_{nx,ny}(x,y)$ which are linearly independent coefficients at corresponding powers of the generating parameters X and Y. The normalization of these mode functions can be checked through the calculation of overlap integrals of two generating functions with different generating parameters:

$$\int\Phi(\vec{r},0,\vec{R})\Phi(\vec{r},0,\vec{U})d\vec{r} = e^{\vec{R}\vec{U}} = \sum_{n_x n_y=0}^{\infty}\Psi_{n_x n_y}(\vec{R})\Psi_{n_x n_y}(\vec{U}). \quad (7.15)$$

Now, in order to find each Hermite-Gaussian mode expression at $z \neq 0$, the Huygens integral (7.13) should be applied to the generating function:

$$\begin{aligned}
&\Phi(\vec{r}, z, \vec{R}) = \frac{-i}{\lambda z}\int \Phi(\vec{r}',0,\vec{R}) e^{ik\frac{(\vec{r}-\vec{r}')^2}{2z}} d\vec{r}' = \left| z_0 = \frac{k w_0^2}{2} \right| = \\
&= \sqrt{\frac{2}{\pi}} \frac{1}{w_0(1+i\,z/z_0)} \exp\left(-\frac{r^2}{w_0^2(1+i\,z/z_0)} + \frac{2\vec{r}\vec{R}}{w_0(1+i\,z/z_0)} - \frac{R^2}{2}\frac{1-i\,z/z_0}{1+i\,z/z_0} \right) = \\
&\quad = \left| \gamma = \sqrt{\frac{1-i\,z/z_0}{1+i\,z/z_0}} = \frac{1-i\,z/z_0}{\sqrt{1+z^2/z_0^2}}, \quad w(z) = w_0\sqrt{1+z^2/z_0^2} \right| = \\
&= \sqrt{\frac{2}{\pi}} \frac{\gamma}{w(z)} \exp\left(-\frac{r^2}{w_0^2(1+i\,z/z_0)} + \frac{2\vec{r}\gamma\vec{R}}{w(z)} - \frac{\gamma^2 R^2}{2} \right) = \sum_{n_x n_y=0}^{\infty} G_{n_x n_y}(\vec{r}, z)\Psi_{n_x n_y}(\vec{R}).
\end{aligned} \tag{7.16}$$

Each separate function $G_{n_x n_y}(\vec{r}, z)$ satisfies the PWE separately due to the linear independence of the powers of generating parameters and, according to (7.14), we see that functions $G_{n_x n_y}(\vec{r}, z)$ are propagating Hermite-Gaussian modes, which we were looking for. By comparing (7.16) with (7.14) we can write down explicit expression for Hermite-Gaussian mode at arbitrary *z*:

$$\begin{aligned}
&G_{n_x n_y}(\vec{r}, z) = \frac{\gamma^{n_x+n_y+1} e^{-\frac{r^2}{w_0^2(1+iz/z_0)}}}{\sqrt{\pi 2^{n_x+n_y-1} n_x! n_y!}\, w(z)} H_{n_x}\left(\frac{\sqrt{2}x}{w(z)}\right) H_{n_y}\left(\frac{\sqrt{2}y}{w(z)}\right), \\
&\gamma = (1-i\,z/z_0)\Big/\sqrt{1+z^2/z_0^2}, \quad z_0 = \tfrac{1}{2}k w_0^2, \quad w(z) = w_0\sqrt{1+z^2/z_0^2}, \\
&\left[\frac{\partial}{\partial z} - \frac{i}{2k}\left(\nabla_{\vec{r}}\cdot\nabla_{\vec{r}}\right)\right] G_{n_x n_y}(\vec{r}, z) = 0, \quad \int G^*_{n_x n_y}(\vec{r}, z) G_{n_x n_y}(\vec{r}, z) d\vec{r} = \delta_{n_x' n_x}\delta_{n_y' n_y}.
\end{aligned} \tag{7.17}$$

In a similar manner, we can rederive expressions for orthonormal Laguerre-Gaussian modes in a cylindrical coordinate system:

$$F_{nm}(r,\varphi)=(-1)^n\sqrt{\frac{n!}{\pi(n+|m|)!}}\gamma^{2n+|m|+1}\left(\frac{\sqrt{2}r}{w(z)}\right)^{|m|}L_n^{|m|}\left(\frac{2r^2}{w^2(r)}\right)e^{-\frac{r^2}{w_0^2(1+iz/z_0)}}e^{im\varphi}\frac{\sqrt{2}}{w(r)},$$
$$\left[\frac{\partial}{\partial z}-\frac{i}{2k}\left(\nabla_{\vec{r}}\cdot\nabla_{\vec{r}}\right)\right]F_{n'm'}(r,\varphi,z)=0,\quad\int_0^\infty rdr\int_0^{2\pi}d\varphi F_{nm}^*(r,\varphi,z)F_{n'm'}(r,\varphi,z)=\delta_{nn'}\delta_{mm'}. \tag{7.18}$$

Sometimes explicit expressions of propagating Gaussian modes at an arbitrary *z* can be useful in propagation problems. For example, if the initial wave amplitude *A* can be represented as a sum of several transverse Gaussian modes, then it can be easily found at an arbitrary propagation distance *z* as a sum of propagating Gaussian modes with the corresponding complex weight coefficients found at initial plane.

Variation of losses with detuning in reflective VBG

Bragg gratings are used in many applications. The key characteristics of these optical elements are the absorption coefficient and the scattering coefficient, which together define the total optical losses. In high-power laser applications, such as spectral beam combining realized with volume Bragg gratings (VBGs), the heating due to absorption is the main limiting factor of the whole system's performance. The amount of power lost per unit length is proportional to the loss coefficient and the local intensity. Depending on the resonant conditions, the intensity profile along distributed feedback systems, such as Bragg gratings, changes dramatically. Therefore, the absorption heating of a grating operated at some power level will be different depending on the wavelength detuning from Bragg resonance. In other words, the effective absorption length for a Bragg grating depends on wavelength detuning and, therefore, at the

same incident power the amount of absorbed power varies correspondingly with the effective length.

In this part of work, we study this detuning dependence of losses inside reflective Bragg gratings. Our results and conclusions are based on an analytical approach to the problem of a uniform Bragg grating. Additionally, the fabrication of Bragg gratings is usually based on the creation of refractive index modulation through photo-induced processes. Photo-induced refractive index change is often accompanied by change in the losses, usually increasing one. As a result, the optical loss coefficient in fabricated Bragg gratings will also be modulated with the Bragg period which leads to additional non-trivial detuning dependence of the losses.

If we consider the case with a relatively small loss coefficient $\alpha[m^{-1}]$, so that $\alpha L \ll 1$, where L is the length of the grating, we can use the following approach. First, we find the intensity profile $I(z)$ along the grating length without any losses. Then we calculate intensity lost due to losses as a product of α times the integrated $I(z)$ over the length of the grating. For constant α_0, an incident beam with intensity I_0, and with a wavelength far from Bragg resonance, this integral yields a simple product $\alpha_0 L I_0$. So, $\alpha_0 L$ is the fraction of intensity lost in grating. Then we investigate the relative variation of this fraction in the vicinity of the Bragg resonance in a uniform grating with a modulated refractive index profile $n_0 + n_1\cos(Qz)$, $Q = 4\pi n_0/\lambda_0$, where λ_0 is the resonant Bragg wavelength.

The propagation of electromagnetic waves inside Bragg gratings may be formulated in terms of counter-propagating waves $A(z)\exp(-i\omega t + ikz)$ and $B(z)\exp(-i\omega t - ikz)$ with $k = n_0\omega/c = 2\pi n_0/\lambda$. Coupled equations for slowly varying envelopes $A(\zeta)$ and $B(\zeta)$, where we have introduced the normalized dimensionless coordinate $\zeta = z/L$, are the following:

$$\frac{dA}{d\varsigma} = iS \cdot B(\varsigma)e^{-2iX\varsigma}, \quad \frac{dB}{d\varsigma} = -iS \cdot A(\varsigma)e^{2iX\varsigma}, \quad S = \frac{\pi n_1}{\lambda_0} L, \quad X = (k - \tfrac{1}{2}Q)L \approx -2\pi n_0 \frac{\Delta\lambda}{\lambda_0^2} L, \quad (7.19)$$

Here, the dimensionless S is the called strength of reflection and X is the dimensionless wavelength detuning, these both parameters were used before. Because we are interested in the detuning dependence of relative values, assume for convenience that the amplitude of the incident beam $A(0) = 1$. Another standard boundary condition for the reflection problem: $B(\zeta{=}1) = 0$.

According to the above mentioned boundary conditions and based on the well-known analytical solution of the system (7.19) for uniform Bragg gratings, we can write down expressions for the wave amplitudes along the ζ-coordinate inside the grating in the following form:

$$\begin{aligned} A(\zeta) &= e^{-iX\zeta} \frac{\cosh[G(1-\zeta)] - i\,X/G \cdot \sinh[G(1-\zeta)]}{\cosh G - i\,X/G \cdot \sinh G}, \\ B(\zeta) &= e^{iX\zeta} \frac{i\,S/G \cdot \sinh[G(1-\zeta)]}{\cosh G - i\,X/G \cdot \sinh G}, \quad G = \sqrt{S^2 - X^2}. \end{aligned} \qquad (7.20)$$

It is easy to check that the second expression in (7.20) agrees with the well-known formula for spectral reflectivity of a uniform Bragg grating, $R = |B(0)|^2 = \sinh^2 G/(\cosh^2 G - X^2/S^2)$, which gives $R_0 = \tanh^2 S$ at the exact Bragg resonance. This theoretical spectral behavior of reflectivity is shown on Figure 19 together with an experimental spectrum of an actual VBG recorded for 99% resonant reflectivity in photo-thermo-refractive glass with the following parameters: $L = 3.6$ mm, $\lambda_0 = 1066.14$ nm, $n_0 = 1.49$, $n_1 = 265{\cdot}10^{-6}$. The corresponding reflection strength is $S = 2.81$. The asymmetry of the

experimental reflection profile and the washing out of its zeros can be explained by longitudinal non-uniformities within the fabricated VBG.

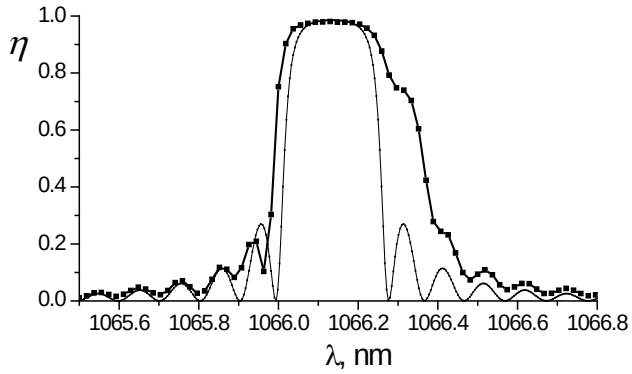

Figure 19. Experimental spectral reflection profile of a VBG compared with simulation (thin line).

The next step is the calculation of the intensity profile, $I(\zeta)$, inside the Bragg grating with the use of (7.20) and integrating this profile along whole length of the grating:

$$I(\zeta) = |A|^2 + |B|^2 = \frac{\cosh[2G(1-\zeta)] - \frac{X^2}{S^2}}{\cosh^2 G - \frac{X^2}{S^2}}, \quad f(S,X) = \int_0^1 I(\zeta)d\zeta = \frac{\frac{\sinh(2G)}{2G} - \frac{X^2}{S^2}}{\cosh^2 G - \frac{X^2}{S^2}}. \quad (7.21)$$

Since we are using normalized incident intensity $|A(0)|^2 = 1$, the last integral gives us the necessary relative function $f(S,X)$ of the fraction of total losses in the Bragg grating with wavelength detuning. Far from resonance, $f|_{X\to\infty} = 1$.

The lowest value of this function is $f_{\min} = f(S,0) = \sinh(2S)/[2S\cdot\cosh^2 S] \approx 1/S \approx 0.35$ at the exact Bragg resonance for the parameters of grating mentioned before. The lower losses in this case can be explained by the exponential decrease of the reflected and transmitted power inside the grating. The highest value, $f_{\max} \approx 1.91$, occurs near the first zero of the reflection spectrum due to the increased resonant capacity of the grating, similar to a Fabry-Perot resonator.

We see that relative variation of loses can differ up to a factor of 6 for the same grating with resonant reflectivity about 99%.

Figure 20 illustrates the experimental relative variation of losses versus wavelength detuning from Bragg resonance and the corresponding numerical simulation of this loss ratio variation (7.21). Despite some systematic errors of measurement and previously mentioned in-homogeneities inside the VBG, both curves from Figure 20 clearly demonstrate similar spectral behavior. This variation of losses was measured in a VBG at a small incidence angle, and in this case can resolve the incident and reflected beams while precisely measuring the power balance in the experimental setup using beam sampler to calibrate the incident power. The absolute value of losses was less than 10^{-2}.

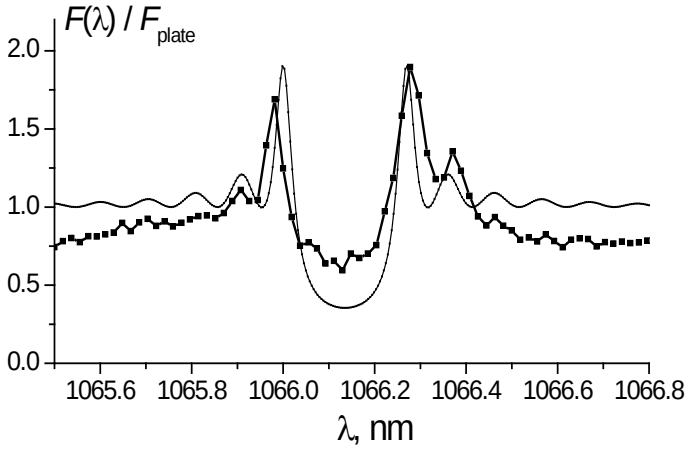

Figure 20. Experimental variation of the absorption ratio versus the detuning and the analytical expression (thin line).

Experimental measurements presented on both pictures were done in laser laboratory of Prof. L. Glebov's group.

Now let's consider the modulation of the loss coefficient with Bragg period $\alpha(z) = \alpha_0[1-\varepsilon\cdot\cos(Qz)]$, where α_0 is the average loss coefficient and $0 \le \varepsilon \le 1$ is the depth of modulation. We have chosen a minus sign because our recording material has negative photosensitivity and with increase of the absolute value of the refractive index change, the losses are increasing, so the minima of the refractive index modulation correspond to the maxima of losses.

In order to get the correct value of losses we have to calculate the corresponding integral along the grating length $\int\alpha(z)/\alpha_0\cdot|A(z)e^{ikz} + B(z)e^{-ikz}|^2dz$, which will give us an additional odd-functional term $\varepsilon\cdot g(S,X)$ for the relative variation of losses with detuning:

$$f_\varepsilon = f + \varepsilon\cdot g, \quad g(S,X) = -\frac{1}{2}\int_0^1 (AB^* e^{2iX\zeta} + A^* B e^{-2iX\zeta})d\zeta = \frac{X}{2S}\frac{\sinh(2G)/(2G)-1}{\cosh^2 G - X^2/S^2}. \quad (7.22)$$

The odd function $g(S,X)$ is positive for positive X and goes to zero at large detuning. This means that for Bragg gratings recorded in our material, the losses for wavelengths smaller than λ_0, $X > 0$ (7.19), are higher than the losses for correspondingly longer wavelengths. At the maximum modulation depth of $\varepsilon = 1$, the maxima of the relative losses f_{max} is increased up to 2.61.

Heat transfer in a VBG plate under laser beam exposure

The problem under consideration was as follows: to calculate the heating of a volume Bragg grating (VBG) by the transmitted or reflected beam of a given power P_{tot} [Watt], given the transverse radius w_0 of Gaussian profile of intensity w_0 [meter] = Δx[HWe^{-2}IM] =Δy[HWe^{-2}IM], and given the heat removal coefficient h [Watt/(m^{2}K)] from the surface.

In the case of CW laser operation, the process of heating is described by the stationary thermal conductivity equation

$$-\Lambda(\nabla\cdot\nabla)T = Q(x,y,z)\,. \qquad (7.23)$$

Here T denotes the local increase of temperature in comparison with the temperature of the surrounding air T_{room} or the temperature of a cooling gas, and Λ = 1.05 Joule/(m·K) is thermal conductivity coefficient of glass.

The power deposited $Q(r)$ [W/m^3] in the VBG by the beam being transmitted through the VBG at a wavelength out of resonance equals

$$Q(r) = 2.3\cdot\alpha_{10}\cdot I(r),\quad I(r) = I_0\cdot\rho(r),\quad I_0 = \frac{2}{\pi w_0^2}P_{\text{tot}},\quad \rho(r) = \exp\left(-2\frac{r^2}{w_0^2}\right). \qquad (7.24)$$

Here $I(r)$ [W/m^2] is the transverse distribution of intensity with maximum value I_0 at the center and relative transverse profile $\rho(r)$.

The VBG plate has the following physical dimensions: aperture d by d and thickness l, and we use the coordinate system with its center in the center of this rectangular plate. The boundary conditions are assumed for convectional heat removal from surfaces in the form [119-Lienhard 08]:

$$-\Lambda\frac{\partial T}{\partial x}\bigg|_{x=\pm\frac{d}{2}} = \pm h\cdot T\big|_{x=\pm\frac{d}{2}},\quad -\Lambda\frac{\partial T}{\partial x}\bigg|_{x=\pm\frac{d}{2}} = \pm h\cdot T\big|_{x=\pm\frac{d}{2}},\quad -\Lambda\frac{\partial T}{\partial z}\bigg|_{z=\pm\frac{l}{2}} = \pm h\cdot T\big|_{z=\pm\frac{l}{2}}\,. \qquad (7.25)$$

We establish that for typical values of the heat removal coefficient: h = 100 W/(m^{2}K) through h = 800 W/(m^{2}K); the value of h = 250 W/(m^{2}K) corresponds to the cooling gas velocity v = 80 m/s.

For a laser beam with P_{tot} and w_0, and reflected by the VBG at exact Bragg resonance, the corresponding power deposition will be additionally z-dependent:

$$Q(r) = 2.3 \cdot \alpha_{10} \cdot I_0 \cdot \rho(r) \cdot \sigma(z), \quad \sigma(z) = \frac{\cosh^2[2S(\frac{1}{2} - z/l)]}{\cosh^2 S}. \tag{7.26}$$

According to transverse symmetry of problem, the even eigenfunctions depending on x and y and satisfying (7.25) will be used:

$$g_n(x) = \cos(p_n x): \quad \cot(\theta_n) = \theta_n/\Theta, \quad \Theta_n = p_n l/2, \quad \Theta = p_n d/(2\Lambda) \quad \rightarrow \quad \{p_n\}, \quad n \geq 0. \tag{7.27}$$

Meanwhile, the z-dependent even eigenfunctions of the Laplace operator and the additional odd eigenfunctions necessary for reflective beam problem are

$$\begin{aligned} &f_m(z) = \cos(q_m z): \quad \cot(\varphi_m) = \varphi_m/\Phi, \quad \varphi_m = q_m l/2, \quad \Phi = q_m l/(2\Lambda) \quad \rightarrow \quad \{q_m\}, \quad m \geq 0, \\ &\tilde{f}_m(z) = \sin(\tilde{q}_m z): \quad \tan(\phi_m) = -\phi_m/\Phi, \quad \phi_m = \tilde{q}_m \frac{l}{2}, \quad \rightarrow \quad \{\tilde{q}_m\}, \quad m \geq 1. \end{aligned} \tag{7.28}$$

Here p_n, q_m and $\tilde{q}_m$ are the solutions of the corresponding transcendental equations.

With the definition of the basis of functions satisfying the boundary conditions, the solution of second-order PDE (7.23) can be represented as a sum of the basis functions. For the problem with the transmitted beam out of resonance the representation of solution is

$$T(x, y, z) = \sum_{n_x, n_y, m} C_{n_x n_y m} g_{n_x}(p_{n_x} x) g_{n_y}(p_{n_y} y) f_m(q_m z). \tag{7.29}$$

After substituting (7.29) into (7.23) we will get the coefficients

$$\begin{aligned} &C_{n_x n_y m} = \frac{Q_0 G_{n_x} G_{n_y} \bar{f}_m}{\Lambda N_{n_y} N_{n_y} M_m (p_{n_x}^2 + p_{n_y}^2 + q_m^2)}, \quad Q_0 = 2.3\alpha_{10} I_0, \\ &G_n = \int_0^{d/2} f_n(x) \exp(-\tfrac{2x^2}{w_0^2}) dx, \quad \bar{f}_m = \int_0^{l/2} f_m(z) dz, \quad N_n = \int_0^{d/2} g_n^2(x) dx, \quad M_m = \int_0^{l/2} f_n^2(z) dz. \end{aligned} \tag{7.30}$$

So, we have presented a solution of (7.23) for a transmitted beam in analytical form.

The temperature distribution inside the VBG with a laser beam reflected at Bragg resonance can be found in a similar manner. Below, we will discuss mostly the problem of heating in transmissive VBG because it is more important for realization of SBC.

In foregoing simulations, we used the parameters $l = 2.5$ mm, absorption $\alpha = \ln 10 \cdot \alpha_{10} = 2.3 \cdot 10^{-2}$ m^{-1}, total power $P_0 = 100$ kW and various values of the heat removal coefficient, $h = 100$ W/(m^{2}K) through $h = 800$ W/(m^{2}K). The error of our approximation is found to be less than 15% even for the worst case considered with $h = 100$ W/(m^{2}K).

Simulated temperature distributions inside thin glass plate heated by a wide laser beam and intensively cooled from surfaces are presented in Figure 21 in normalized form. The normalized forms show the common behavior of the intensity and temperature profiles. The actual increase of temperature at the center of aperture typically is about 15°C.

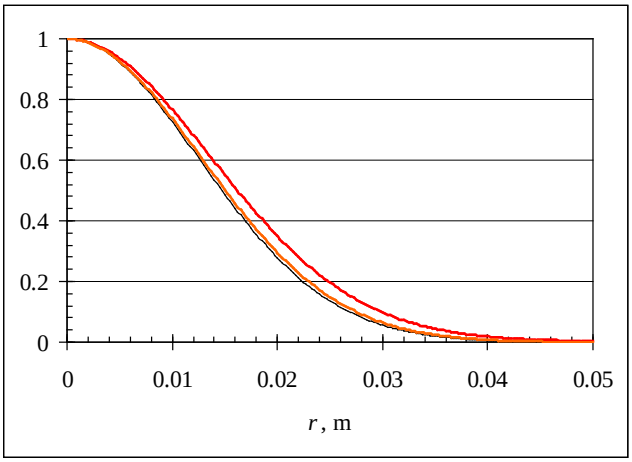

Figure 21. Normalized temperature profiles $T(r)$ inside a VBG across aperture for two different values of heat removal coefficient: the upper line corresponds to $h = 100$ W/(m^{2}K), the curve below corresponds to $h = 800$ W/(m^{2}K) and it is closer to the normalized profile intensity, which is depicted by the thin black line.

These results show that the heat transfer problem can be efficiently reduced to a one-dimensional approximation along the *z*-direction of the grating thickness, because of the relatively small heat flow in the radial direction. The input data for new ordinary differential equation is the heat deposition rate, which varies across the aperture according to a Gaussian intensity distribution proportional to $\rho(r)$.

This one-dimensional approximation for the problem (7.23) means that transverse coordinate *r* may be considered as external parameter without differentiation with it. Thus we came to ODE with corresponding boundary condition, which describes *z*-dependence of the temperature profile in the center of the aperture at $x = y = 0$, and $T_c(z)$:

$$T(r,z) = T_c(z)\rho(r), \quad -\Lambda \frac{d^2 T_c}{dz^2} = Q_0, \quad -\Lambda \frac{dT_c}{dz}\bigg|_{z=\pm\frac{l}{2}} = \pm h \cdot T_c\big|_{z=\pm\frac{l}{2}}. \tag{7.31}$$

The solution of (7.30) is easy to find. The average temperature T_0 in the center of VBG aperture is the following

$$T_c(z) = \frac{Q_0 l}{2h} + \frac{Q_0 l^2}{8\Lambda}\left(1 - 4z^2/l^2\right) \quad \rightarrow \quad T_0 = \int_{-l/2}^{l/2} T_c(z)dz = \frac{Q_0 l}{2h}\left(1 + \frac{hl}{6\Lambda}\right). \tag{7.32}$$

As we have mentioned before, the radial coordinate *r* is an external parameter, which is only presented as a factor $\rho(r)$ in the power deposition and temperature distributions, has the same parametric dependence on *r*, so the *z*-averaged temperature profile across aperture is equal to $\langle T(r)\rangle_z = T_0 \cdot \rho(r)$.

To summarize, problem of heating of a VBG glass plate by a transmitted and/or reflected laser beam can be efficiently treated by the classical methods of mathematical physics without involving resource-consuming numerical simulations due to the simple geometry of the

boundary conditions. First, the temperature distribution inside grating can be found. Then, for VBG thickness l much less than the laser beam width w_0, the temperature distribution across aperture can be converted into a corresponding thickness expansion so-called "*sag*" across the aperture.

Non-uniform heat transfer problem for a VBG plate with thermally stabilized edges

In this section, analytical and numerical solutions are presented for the problem of the temperature profile in VBG used in the experimental implementation of SBC up to kilo-Watt level. New conditions considered were as follows. The coefficient h [W/(m^{2}K)] of heat removal from the faces $z = \pm l/2$ of a VBG is assumed to be moderate, $h \sim 15$ W/(m^{2}K), in contrast with the previously considered high h for forced cooling of a VBG operating at the hundred kilo-Watt level. As a result, the parameter of depth of the heat profile along z, denoted as δ [m] = Λ/h, turns out to be much larger than the thickness $\Delta z = l$ of the VBG. For the thermal conductivity coefficient of PTR glass $\Lambda \approx 1.05$ W/(m·K) there is $\delta \approx 70$ mm, while $l \approx 4.7$mm for the actual VBG used in current experiments. As a result, the heat flow to the edges at $x = \pm d/2$ and $y = \pm d/2$ may be important for the temperature profile formation. We consider the beams with relatively large diameter $2w_0 = 6$ mm (FWe^{-2}IM), so that the transverse size $d = 21$ mm of the square VBG is about a factor of 3.5 larger than the beam diameter.

The stationary equation of thermal conductivity is the same (7.23). The non-trivial part of the problem is due to the boundary conditions: they are radically different at the input and output faces of the VBG and at the edges of the VBG. We assume that the temperature at the edges is sustained at a fixed level of $T_{\text{edge}} = 55$°C at $x = \pm d/2$ or $y = \pm d/2$. On the other hand, heat transfer

from faces of the VBG moves the temperature towards $T_{\text{room}} = 21°\text{C}$, but only to the extent to which the transfer coefficient allows this:

$$\frac{dT}{dz} = -\frac{h}{\Lambda}(T - T_{\text{room}}) \text{ at } z = \frac{l}{2}, \quad \frac{dT}{dz} = +\frac{h}{\Lambda}(T - T_{\text{room}}) \text{ at } z = -\frac{l}{2}. \tag{7.33}$$

The main technical difficulty of solving the problem is in the different values of T_{edge} and T_{room} for the given of heat deposition $Q(\mathbf{r}) = \alpha[\text{m}^{-1}]\cdot P[\text{W/m}^2]$. To overcome this difficulty, we search for the solution in the form

$$T(\mathbf{r}) = T_1(\mathbf{r}) + T_2(\mathbf{r}). \tag{7.34}$$

Here function $T_1(\mathbf{r})$ satisfies

$$-\Lambda(\nabla\cdot\nabla)T_1(\mathbf{r}) = Q(\mathbf{r}), \quad T_1\big|_{x,y=\pm d/2} = T_{\text{room}}, \quad -\Lambda\frac{dT_1}{dz}\bigg|_{z=\pm l/2} = \pm h(T_1 - T_{\text{room}})\big|_{z=\pm l/2}, \tag{7.35}$$

and

$$-\Lambda(\nabla\cdot\nabla)T_2(\mathbf{r}) = 0, \quad T_2\big|_{x,y=\pm d/2} = T_{\text{edge}}, \quad -\Lambda\frac{dT_2}{dz}\bigg|_{z=\pm l/2} = \pm h(T_2 - T_{\text{room}})\big|_{z=\pm l/2}. \tag{7.36}$$

Eigenfunctions depending on the *x* and *y* coordinates for the problem with fixed value boundary conditions are:

$$g_{n_x}(x), g_{n_y}(y), \quad g_n(x) = \cos(p_n x), \quad p_n = \pi(2n+1)/d, \quad g_n(x = \pm d/2) = 0. \tag{7.37}$$

And the even *z*-dependent functions $f_m(z)$ are the same as used before.

We have found a solution of problem (7.36) in the following form

$$T_2(\mathbf{r}) = T_{\text{room}} + (T_{\text{edge}} - T_{\text{room}})\sum_{m=0}^{M}\eta_m f_m(z)\left(\frac{\cosh(q_m x) + \cosh(q_m y)}{2\cosh(q_m d/2)} + \sum_{n=0}^{N}\gamma_{mn}\left[g_n(x)u_{mn}(y) + g_n(y)u_{mn}(x)\right]\right), \tag{7.38}$$

$$\eta_m = \frac{4\sin(\frac{1}{2}q_m l)}{\sin(q_m l) + q_m l}, \quad \gamma_{mn} = \frac{2(-1)^n}{\pi(2n+1)[1 + \pi^2(2n+1)^2/(q_m d)^2]}, \quad u_{mn}(y) = \frac{\cosh\left(\sqrt{(q_m^2 + p_n^2)}y\right)}{\cosh\left(\frac{1}{2}\sqrt{(q_m^2 + p_n^2)}d\right)}.$$

Numerical results for the temperature profiles of a VBG, averaged in the direction of beam propagation, with thermally fixed edges at $T_{room} = 21°C$, an absorption coefficient $\alpha = \ln 10 \cdot 0.14\ m^{-1}$, and a surface heat removal coefficient $h = 16.4\ W/(m^2K)$ are shown in Figure 22.

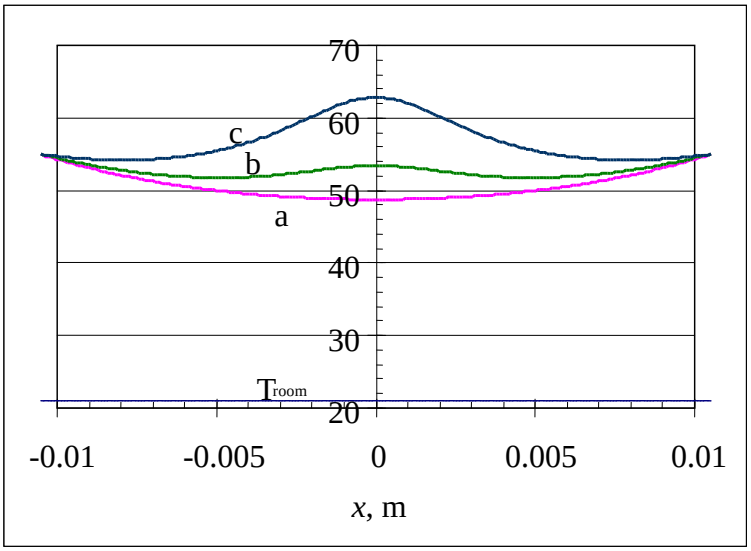

Figure 22. Temperature profiles $\langle T(y=0)\rangle_z$ of a VBG with edges fixed at $T_{edge} = 55°C$: a) no beam; b) reflection of 160 W Gaussian beam; c) transmission of 160 W Gaussian beam.

In this section, we solved a problem, which arises in a real experiment carried out by Prof. L. Glebov's group. Preheating the edges allows one to maintain the alignment of each VBG participating in a spectral beam combining at the same resonant Bragg wavelength. This eliminates the need for angular adjustment of the VBG initially aligned at small operating power.

Deterioration of beam quality under operation by heated VBG

Let us continue the study of a possible realization of a hundred-kilowatt level SBC with the use of large-aperture thin reflective VBGs.

In order to remove deposited heat from a VBG plate, we assume the forced air flow or flow of He gas along its surfaces, which leads to increase of surface heat removal coefficient to reasonably large values, $h \geq 200$ W/(m^2·K).

The foregoing numerical solution of the thermal conductivity equation with a high rate of h for a glass plate, which has a thickness l much smaller than the radius of the heating beam w_0, allowed us to come to following statement. The resulting profile of a temperature change $\delta T(r)$ across the aperture follows the profile of the incident intensity distribution $p(r)$. In this case the one-dimensional approximation of heat transport problem in the z-direction is valid; it gives a simple analytical estimate for $\delta T(r) = T_0 \cdot p(r)$. This temperature change profile for a thin glass plate leads to a linear expansion of the thickness across aperture, $sag(r) = b[\text{m}] \cdot p(r)$, which causes a corresponding phase distortion with the profile $\varphi(r) = \varphi_0 \cdot p(r)$,

$$\varphi_0 = \frac{2\pi}{\lambda_0}(n_0 - 1) \cdot b, \quad b = \beta_T \cdot l \cdot T_0, \quad T_0 = \frac{l}{2h}\left(1 + \frac{hl}{6\Lambda}\right)Q_0. \tag{7.39}$$

Here $\beta_T = 0.85 \cdot 10^{-6}$ K^{-1} is thermal expansion coefficient of glass and $n_0 = 1.49$ is the refractive index of glass.

As an example for the numerical values, $\alpha_{10} = 0.01$ m^{-1}, $w_0 = 3$ cm, $h = 280$ W/(m^2·K), $l = 3$ mm, and $P_{\text{tot}} = 100$ kW, we get the following values in the center of a Gaussian profile: $T_0 = 14.8$ K, $b = 0.378$ μm, $\varphi_0 = 1.09$ radian.

Free space propagation of a beam is characterized by the quality parameter M_x^2, which describes the divergence of the beam in one transverse direction. In the plane of the beam waist the quality parameter is defined as $M_x^2 = 2k\sqrt{\langle x^2\rangle\langle\theta_x^2\rangle}$, where $k = 2\pi/\lambda$ is the wave vector in free space.

The second moments necessary for calculating M_x^2 for a radial beam amplitude profile can be expressed in a cylindrical coordinate system by

$$\langle u^2\rangle = -\frac{1}{Pk^2}\int A^*(\vec{r},z)\frac{\partial^2}{\partial x^2}A(\vec{r},z)d\vec{r}, \quad \langle xu\rangle = -\frac{i}{k}\left(\frac{1}{P}\int A^*(\vec{r},z)x\frac{\partial}{\partial x}A(\vec{r},z)d\vec{r} + \frac{1}{2}\right). \quad (7.40)$$

Now, let us consider the propagation of a Gaussian beam of an initial profile $A_{\text{in}}(r) = A_0 \cdot e^{-r^2/w_0^2}$ in a medium with an intensity dependent self-modulation; for example, through the change of refractive index $n = n_0 + n_2|A|^2$. We are interested in calculating the small increasing parasitic deterioration of M_x^2 from unity. If the propagation path inside the medium Δz is much smaller than the beam divergence Rayleigh length $z_0 = \frac{1}{2}kw_0^2$, then the effect of the medium's nonlinearity is expressed as the phase distortion with a profile proportional to intensity profile

$$A(r) = A_{\text{in}}(r)\cdot\exp\left(i\varphi_0\cdot|A_{\text{in}}(r)|^2/|A_0|^2\right) = A_0 e^{-\frac{r^2}{w_0^2}}\exp\left(i\varphi_0 e^{-2\frac{r^2}{w_0^2}}\right), \quad \varphi_0 = n_2|A_0|^2\frac{2\pi}{\lambda}\Delta z, \quad (7.41)$$

where φ_0 is the maximum phase distortion value at the center of the beam. This phase distortion φ_0 is the main parameter in our problem.

Due to circular symmetry, each of the second moments, $\langle x^2\rangle, \langle xu\rangle, \langle u^2\rangle$, will be equal to half of the corresponding moment calculated along the radial coordinate $r = \sqrt{x^2 + y^2}$; this is the same situation found in classical mechanics with the calculation of the moment of inertia of a thin body of rotation (for example, a disc or circle) along the axis perpendicular to the axis of rotation.

$$\begin{aligned}
\langle x^2\rangle &= \frac{\pi}{P}\int_0^\infty r^2 |A(r)|^2 r dr = \frac{w_0^2}{4}, \quad P = 2\pi\int_0^\infty |A(r)|^2 r dr, \\
\langle xu\rangle &= -\frac{i}{k}\left(\frac{\pi}{P}\int_0^\infty A^*(r) r \frac{dA}{dr} r dr + \frac{1}{2}\right) = -\frac{\varphi_0}{4k}, \\
\langle u^2\rangle &= -\frac{\pi}{k^2 P}\int_0^\infty A^*(r)\frac{d}{dr}\left(r\frac{dA}{dr}\right)dr = \frac{1}{k^2 w_0^2}\left(1 + \frac{4}{9}\varphi_0^2\right) \\
&\rightarrow \quad M_x^2 = 2k\sqrt{\langle x^2\rangle\langle u^2\rangle - \langle xu\rangle^2} = \sqrt{1 + \frac{7}{36}\varphi_0^2}.
\end{aligned} \tag{7.42}$$

As we should expect, the obtained result does not depend on beam size w_0.

In the case of thermal distortion of a VBG glass plate with decimal absorption coefficient α_{10} by a transmitted Gaussian beam of power P_{tot}, the central phase of the distortion profile according to (7.24) and (7.39) will be equal to

$$\varphi_0 = C\cdot\alpha_{10}\cdot P_{tot}, \quad C = \frac{2\pi}{\lambda_0}(n_0 - 1)\cdot\beta_T\cdot l\cdot\frac{l}{2h}\left(1 + \frac{hl}{6K}\right)\cdot 2.3\cdot\frac{2}{\pi w_0^2}. \tag{7.43}$$

This simple analytical expression allows us to analyze the complex problem of beam distortions in a high-power SBC scheme in closed analytical form.

Spectral beam combining with thermally distorted VBGs

High aperture VBGs in PTR glass are promising candidates for future spectral beam combining systems up to hundreds of kilowatts. At 100kW laser power operation, each grating must be actively cooled by gas flow in order to manage the heat load. As a result, the radial profile of the VBG heating follows the profile of the beam intensity, which is usually Gaussian. The thermal expansion of the grating's thickness plate leads to a corresponding Gaussian phase distortion in the transmitted or reflected beam that affects the beam quality.

The analysis of beam distortions by individual VBG under high-power heating has been performed analytically earlier in this chapter. We came to the following qualitative conclusion. The crucial source of the deterioration in performance of the whole system is due to the phase distortion of transmitted beams. Meanwhile, the distortions and diminished diffraction efficiency of reflected beams may be neglected, if the conditions for moderate distortions in the transmitted beams are imposed.

Unfortunately, individual fiber laser cannot deliver all the power in one beam needed for certain applications, e.g. P_{tot} = 100 kW, and SBC is motivated by this problem. Denoting the power of an individual fiber laser as P, one comes to the necessity to combine $N = P_{tot}/P$ individual beams via $N - 1$ elementary VBGs. In process of spectral combining of N laser beams by sequential $N-1$ VBGs, $N >> 1$, the main distortions of combined beams arise due to transmission through thermally distorted VBGs. The latter elements are considered as glass plates with inhomogeneous thickness due to heating caused by material absorption. Before calculating the distortions of serially-combined, mutually incoherent beams due to transmission

through different numbers of VBGs, one must make the following observation. The change of the thickness l of a VBG by $sag(r)$ due to thermal expansion results in slight change of 1) the diffraction efficiency η and 2) the transverse-dependent change of the phase φ of reflected beam, i.e. the distortion.

Taking typical value η = 99%, so $S \approx 3$, and sag at the center $b = 0.378$ μm, we see that the decrease of η is 0.8%, but the deterioration of M_x^2 is considerable, about 10%, to $M_x^2 = 1.115$. Moreover, distortions from reflection affect each individual beam only once (reflection from only one particular VBG), while the distortions from transmission through about $N/2$ individual VBGs are accumulated. We can ignore the thermal deterioration of diffraction efficiency and thermally-induced distortions of the beam in the reflection process, but we must take into account the phase distortions due to transmission of the $N-1$ beams through the sequence of VBGs.

Now, we consider spectral beam combining of $N >> 1$ beams of equal power P_{tot}/N via $N-1$ VBGs, with the scheme depicted on Figure 23.

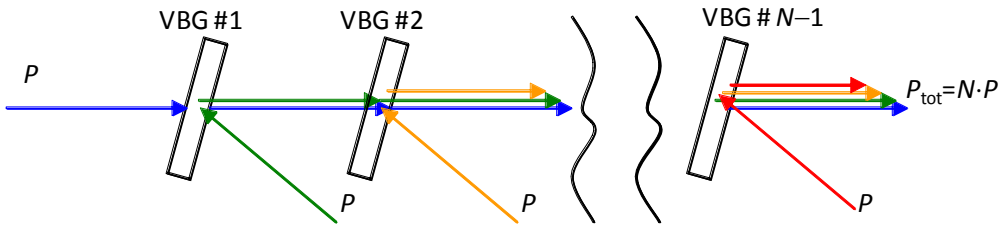

Figure 23. Scheme for spectral combining of N beams with the use of $N-1$ VBGs.

Here P_{tot} is the total power to be produced in the form of combined beam.

We have established, that the distortions due to the process of VBG reflection are much smaller than the distortions due to multiple transmissions of a beam through the remaining VBGs. We will characterize the distorted VBG by the distorting phase φ_{VBG} induced at the center of the aperture. We will assume that this phase is proportional to the total power P_{VBG}, by which each given individual VBG is illuminated. In this assumption we can write that

$$\varphi_{\mathrm{VBG}} = \varphi_0 \frac{P_{\mathrm{VBG}}}{P_{\mathrm{tot}}}, \tag{7.44}$$

were φ_0 is the phase distortion, calculated for the illumination of a VBG by the total power P_{tot}, which is to be produced at the combining output, see the expression for φ_0 in (7.43).

The grating number j transmits the power $P_{\mathrm{VBG}\#j} = P_{\mathrm{tot}} \cdot j/N$, accumulated from all the previous j beams. Then, the VBG number j introduces a phase distortion into each of previous beams

$$\varphi_{\mathrm{VBG}\#j} = \varphi_0 \frac{P_{\mathrm{VBG}}}{P_{\mathrm{tot}}} \frac{P_{\mathrm{tot}}}{N} j = \varphi_0 \frac{1}{P_{\mathrm{tot}}} \frac{P_{\mathrm{tot}}}{N} j = \varphi_0 \frac{j}{N}. \tag{7.45}$$

The next important assumption in our calculations is based on the numerical values of the beam radii in question. We assume that the radius w_0[HWe^{-2}IM] of the beam is w_0 = 30 mm ≡ 0.03 m. Then, the Rayleigh parameter z_0 , beam waist length $z_0 = \Delta z$(HWHIM) of the Gaussian beam, is $z_0 = \pi w_0^2/\lambda \approx 2700$ m at $\lambda = 1.064$ μm. The large value of z_0 relative to the size of the apparatus means that one can completely ignore diffraction of the beams within the combiner. For these conditions, the output phase distortion of beam number m is just the sum of phase distortions of identical shape, accumulated from VBG number m to VBG number $N-1$

$$\varphi_{\mathrm{beam}\#m}^{\mathrm{output}} = \sum_{j=m}^{N-1} \varphi_{\mathrm{VBG}\#j} = \frac{\varphi^{(0)}}{N} \sum_{j=m}^{N-1} j = \frac{\varphi^{(0)}}{N} \left(\frac{N(N-1)}{2} - \frac{m(m-1)}{2} \right). \tag{7.46}$$

The next step is the calculation of the M^2-parameter for the total (combined) beam. Since those N beams are assumed to be incoherent and of equal power P_{tot}/N,

$$M^2_{x,\mathrm{tot}} = \frac{1}{N}\left[\sum_{m=1}^{N-1} M^2_{x,\mathrm{beam}\,\#m} + 1\right]. \tag{7.47}$$

Here we assumed that the last beam number N is subject to reflection only, but not to transmission, and, hence, may be considered as undistorted, so that for the last beam $M_x^2 = 1$.

For small values of φ, which are required for creating a total beam with $M_x^2 \le 1.5$, one can approximate

$$M^2_{x,\mathrm{distortion}} = 1 + \beta\varphi^2. \tag{7.48}$$

We have calculated analytically, that β = 7/72 for a Gaussian beam from (7.42). We also make a very important assumption that the spherical part of distortion has been pre-compensated by an appropriate spherical lens. Then, we come to the expression for

$$M^2_{x,\mathrm{total}} = 1 + \frac{\beta}{N(2N)^2}\left[\varphi^{(0)}\right]^2 \sum_{m=1}^{N-1}\left[N(N-1) - m(m-1)\right]^2. \tag{7.49}$$

It is not difficult to calculate the sum in the equation (7.49) analytically without approximations. We will present here the result for important case in which $N >> 1$:

$$M^2_{x,\mathrm{total}} \approx 1 + \beta\left[\varphi^{(0)}\right]^2 \frac{2}{15} N^2. \tag{7.50}$$

Let us remind that φ_0 is thermal distortion of one beam transmitted through the VBG, which has been (in theory) exposed by the total transmitted power P_{tot} of the combined radiation, see (7.43).

To conclude, the results of those analytic calculations allow for instant re-scaling of all parameters of the system: P_{tot}, necessary number of channels $N = P_{tot}/P_{\mathrm{one\ laser}}$, absorption

coefficient α_{10}, thickness l of individual VBG, beam radius w_0, heat removal coefficient h due to air flow, etc.

Higher tolerance of Super-Gaussian beams to thermal distortions

Previously, the beam quality parameter M_x^2 has been calculated for a self-phase modulated Gaussian beam analytically. We can repeat the same calculation procedure for a super-Gaussian beam profile distorted after propagation through a self-phase modulated medium, $A(r) = A_0 e^{-(r/s_0)^4} \cdot \exp(i\phi_0 e^{-2(r/s_0)^4})$, with maximal phase shift ϕ_0 at the center of beam.

$$\left\langle x^2 \right\rangle = \frac{s_0^2}{2\sqrt{2\pi}}, \quad \left\langle xu \right\rangle = -\frac{\phi_0}{2\sqrt{2}k}, \quad \left\langle u^2 \right\rangle = \frac{4}{\sqrt{2\pi}k^2 s_0^2}\left(1+\frac{4}{9}\phi_0^2\right)$$
$$\rightarrow \quad M_x^2 = \frac{2}{\sqrt{\pi}}\sqrt{1+\left(\frac{4}{9}-\frac{\pi}{8}\right)\phi_0^2}. \tag{7.51}$$

The resulting values of M_x^2 for both Gaussian and super-Gaussian beam profiles depend on the central phases being proportional to the central intensities, which depend on the corresponding beam sizes w_0 and s_0. So, in order to compare sensitivities to self-phase modulation we have to use certain criterion for the beam size ratio. For the 1%-residual power criterion, which means that both beams outside the same radius r_c have the same amount of power $0.01 \cdot P$, the beam size ratio is equal to $s_0/w_0 = 1.337$, which defines the phase ratio $\phi_0/\varphi_0 = \sqrt{2/\pi}\,(w_0/s_0)^2 = 0.446$. In this case, according to (7.42, 7.51), a super-Gaussian beam demonstrates considerably smaller beam quality deterioration than a Gaussian one, despite slightly higher initial $M_x^2 = 2/\sqrt{\pi} = 1.128$.

Corresponding beam profiles of the same power are presented on Figure 24.

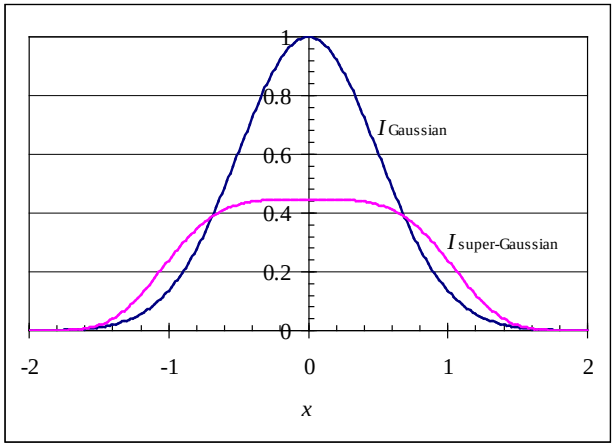

Figure 24. Intensity profiles of Gaussian and super-Gaussian beams with the same power and widths corresponding to the criterion of 0.01 of the residual power outside the circle with the same radius.

Dependences of beam qualities on phase distortion expressed in terms of central phase for a Gaussian beam are presented in Figure 25.

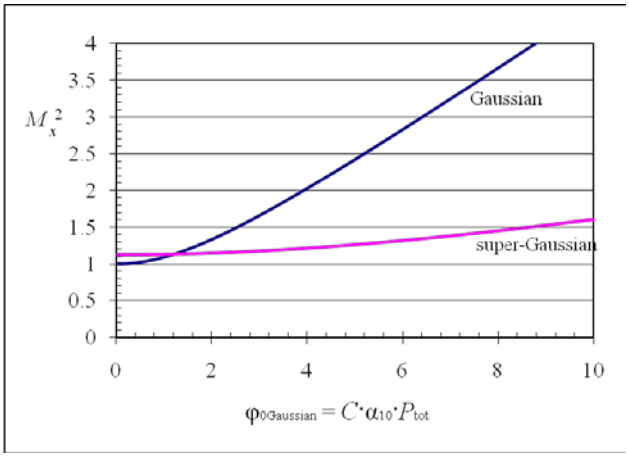

Figure 25. M_x^2 of Gaussian and super-Gaussian beams propagated through a heated glass plate as a function of the absorbed power $C \cdot \alpha_{10} \cdot P_{tot}$.

For example, for the limitation $M_x^2 = 1.5$, a super-Gaussian beam provides more than three times better tolerance to the product of power times the absorption coefficient. Higher-order super-Gaussian beams with significantly higher initial M_x^2, e.g. $\propto \exp[-(r/q_0)^6]$, do not give such an advantage.

We have also calculated analytically the deterioration of M_x^2 of Gaussian and super-Gaussian profiles by higher-order localized radial phase distortion modes. It is important that obtained results cannot be efficiently reproduced by the traditional approach based on polynomial representation of aberrations. This failure is due to the poor convergence of power series representations for Gaussian profiles. These results can be applied to a wide range of problems from nonlinear optics to the analysis of beam propagation through optical elements that are thermally distorted because of material absorption.

CHAPTER EIGHT: CONCLUSION AND SUMMARY OF CONTRIBUTIONS

The present work is devoted to the theoretical study of beam diffraction by high-efficiency volume Bragg gratings (VBGs). Calculations of diffracted and transmitted beam profiles are based on solving coupled wave equations in the slowly varying envelope approximation.

Several original results were obtained. The parameter, called strength of reflection, was proposed for parameterization of the propagation matrix for layered media. It obeys a simple addition law. In the case of the phenomenon of general physical importance, namely of Fresnel reflection, the strength of reflection consists of two separate contributions. One is due to the step of impedance and another is due to the step of the propagation speed. The influence of surface Fresnel reflection on the spectral reflectivity of VBG was also analyzed.

The properties of non-uniform reflective VBGs were numerically modeled. The similarities and differences between variations of the background refractive index and the Bragg period were studied.

A Moiré resonant transmission filter was proposed. Its bandwidth has been found analytically and compared with bandwidths of a regular Fabry-Perot filter and a filter based on uniform VBGs.

Probabilistic amplitude masks were proposed and generated for recording phase plates in photo-thermo refractive glass with additional spatial filtering.

The spectral properties of coherent reflection by multiplexed VBGs were simulated and an analytical expression for propagation matrix was found for the exact Bragg condition.

The solution of the thermal distribution problem for a VBG heated by transmitted beams, reflected beams or both was solved analytically. Formulas for the variation of relative losses inside a Bragg grating with spectral detuning was found analytically. For thin gratings with enforced surface cooling, the approximation that the temperature distribution profile is coincident with the intensity profile of incident beam was formulated. By this approximation, the central distortion phase of the transmitted beam was obtained in terms of beam and grating parameters. The use of super-Gaussian beams for combining was proposed. The deterioration of the beam quality parameters of Gaussian and super-Gaussian beams due to self-phase distortion and higher-order radial-mode phase distortions was found analytically. Approximate analytical formulas for the estimation of the beam quality of a beam combining scheme was derived.

LIST OF REFERENCES

1. S. Mokhov and B. Ya. Zeldovich, "Strength of electromagnetic, acoustic and Schrödinger reflections," Proc. R. Soc. A **464**, 3071−3080 (2008).
2. L. B. Glebov, J. Lumeau, S. Mokhov, V. Smirnov, and B. Ya. Zeldovich, "Reflection of light by composite volume holograms: Fresnel corrections and Fabry-Perot spectral filtering," J. Opt. Soc. Am. A **25**, 751−764 (2008).
3. S. Mokhov and B. Ya. Zeldovich, "Reflection of various types of waves by layered media," Comm. App. Math. and Comp. Sci. **3**, 61−75 (2008).
4. H. Shu, S. Mokhov, B. Ya. Zeldovich, and M. Bass, "The reflection of a laser beam by a deformed highly reflective volume Bragg grating using iteration of the beam propagation method," Appl. Opt. **48**, 22−27 (2009).
5. V. Smirnov, J. Lumeau, S. Mokhov, B. Ya. Zeldovich, and L. B. Glebov, "Ultra-narrow bandwidth Moiré reflecting Bragg gratings recorded in photo-thermo-refractive glass," Opt. Lett. **35**, 592−594 (2010).
6. L. Glebov, J. Lumeau, S. Mokhov, and B. Ya. Zeldovich, "Spectral Transmission of Volume Bragg Gratings: Influence of Uncompensated Fresnel Reflections," in *Frontiers in Optics*, OSA Technical Digest (2006), paper JWD58.
7. S. Mokhov, L. B. Glebov, V. I. Smirnov, and B. Ya. Zeldovich, "Theory of Reflection by Volume Gratings and Boundaries: Polarization and Interference Properties," in *Frontiers in Optics*, OSA Technical Digest (2007), paper FTuS4.

8. S. Mokhov, L. B. Glebov, and B. Ya. Zeldovich, "Porro-Prism Retroreflector Based on Corner Geometry of Volume Bragg Gratings," in *Frontiers in Optics*, OSA Technical Digest (2007), paper FTuV7.

9. S. Mokhov and B. Ya. Zeldovich, "Strength of Electromagnetic Reflection," in *Progress in Electromagnetics Research Symposium*, Cambridge, USA, July 2-6 (2008), paper 3P5.

10. S. V. Mokhov, L. B. Glebov, V. I. Smirnov, and B. Y. Zeldovich, "Propagation of Electromagnetic Waves in Non-Uniform Volume Bragg Gratings," in *Frontiers in Optics*, OSA Technical Digest (2008), paper FMK6.

11. M. Rever, S. Huang, C. Yahus, V. Smirnov, E. Rotari, I. Cohanoshi, S. Mokhov, L. Glebov, and A. Galvanauskas, "Power-Scalable, 200 fs Chirped-Volume-Bragg-Grating Based Fiber-CPA System," in *Advanced Solid-State Photonics*, OSA Technical Digest Series (2009), Denver, CO, February 1-4, paper MF5.

12. S. Mokhov and B. Ya. Zeldovich, "Reflection of Various Types of Waves by Layered Media," talk L41.00012 in *APS March Meeting*, Pittsburgh, PA, March 16-20, 2009.

13. S. Mokhov and B. Ya. Zeldovich, "Strength of electromagnetic, acoustic and Schrodinger reflections," poster T1 77 in *40th Annual Meeting of the APS Division of Atomic, Molecular, and Optical Physics*, Charlottesville, VA, May 19-23, 2009.

14. M. Rever, S. Huang, C. Yahus, V. Smirnov, E. Rotari, I. Cohanoshi, S. Mokhov, L. Glebov, and A. Galvanauskas, "200 fs, 50 W Fiber-CPA System Based on Chirped-Volume-Bragg-Gratings," in *Conference on Lasers and Electro-Optics/International Quantum Electronics Conference*, OSA Technical Digest (CD) (Optical Society of America, 2009), paper CMBB2.

15. L. B. Glebov, J. Lumeau, S. Mokhov, V. Smirnov, and B. Y. Zeldovich, " Moiré reflecting Bragg gratings recorded in photo-thermo-refractive glass," in *CLEO/Europe and EQEC 2009 Conference Digest*, (Optical Society of America, 2009), paper CE4_5.

16. M. Rever, X. Ma, S. Huang, C. Yahus, V. Smirnov, E. Rotari, I. Cohanoshi, S. Mokhov, L. Glebov, and A. Galvanauskas, "Compact High-Power FCPA Enabled by Chirped Volume Bragg Grating and Chirally-Coupled-Core Fiber Technologies," in *CLEO/Europe and EQEC 2009 Conference Digest*, (Optical Society of America, 2009), paper CD7_1.

17. L. B. Glebov, S. V. Mokhov, V. I. Smirnov, and B. Y. Zeldovich, "Analytic Theory of Light Reflection from a Chirped Volume Bragg Grating," in *Frontiers in Optics*, OSA Technical Digest (CD) (Optical Society of America, 2009), paper FWX5.

18. S. Mokhov, L. Glebov, J. Lumeau, V. Smirnov, and B. Zeldovich, "Moiré Filter in Volume Bragg Grating," in *Frontiers in Optics*, OSA Technical Digest (CD) (Optical Society of America, 2009), paper FMF2.

19. M. Rever, S. Huang, C. Yahus, V. Smirnov, E. Rotari, I. Cohanoshi, S. Mokhov, L. Glebov, and A. Galvanauskas, "200W, 350fs fiber CPA system enabled by chirped-volume-Bragg-gratings and chirally-coupled-core fiber technology," paper 7580-33 in *Photonics West*, San Francisco, CA, January 23-28, 2010.

20. S. Mokhov, J. Lumeau, V. Smirnov, B. Zeldovich, and L. Glebov, "High-aperture narrowband filter based on Moiré Principle," paper 7598-28 in *Photonics West*, San Francisco, CA, January 23-28, 2010.

21. S. Mokhov, L. Glebov, J. Lumeau, V. Smirnov, and B. Zeldovich, "Optical Resonant Cavities in Volume Bragg Gratings," talk X29.00006 in *APS March Meeting*, Portland, OR, March 15-19, 2010.

22. S. Mokhov, M. SeGall, D. Ott, V. Rotar, J. Lumeau, B. Zeldovich, L. Glebov, "Direct Recording of Phase Plates in Holographic Material with Using Probabilistic Amplitude Masks," poster JMA11 in *Digital Holography and Three-Dimensional Imaging*, Miami Beach, FL, April 12-14, 2010.

23. M. Rever, G. Chang, V. Smirnov, E. Rotari, I. Cohanoshi, S. Mokhov, L. Glebov, and A. Galvanauskas, "Temporal Reciprocity of Chirped Volume Bragg Grating Pulse Compressors," in *Conference on Lasers and Electro-Optics/International Quantum Electronics Conference*, OSA Technical Digest (CD) (Optical Society of America, 2010), San Jose, CA, May 16-21, talk CThA3.

24. S. Mokhov, J. Lumeau, V. Smirnov, B. Zeldovich, and L. Glebov, "High-Aperture Narrow-Band Moiré Filter in Volume Bragg Grating," poster E1 160 in *41st Annual Meeting of the APS Division of Atomic, Molecular, and Optical Physics*, Houston, TX, May 25-29, 2010.

25. S. Mokhov, A. Jain, C. Spiegelberg, V. Smirnov, O. Andrusyak, G. Venus, B. Zeldovich, and L. Glebov, "Multiplexed Reflective Volume Bragg Grating for Passive Coherent Beam Combining," in *Laser Science*, OSA Technical Digest (CD) (Optical Society of America, 2010), paper LWG2.

26. S. Mokhov, D. Drachenberg, I. Divliansky, G. Venus, B. Zeldovich, and L. Glebov, "Modeling of High-Power Spectral Beam Combining with Thermally Distorted Volume

Bragg Gratings," paper 7915-17 in *Photonics West*, San Francisco, CA, January 22−27, 2011.

27. S. Mokhov, D. Drachenberg, G. Venus, B. Zeldovich, and L. Glebov, "Variation of Losses with Detuning in Bragg Gratings," talk J20.00008 in *APS March Meeting*, Dallas, TX, March 21−25, 2011.
28. M. Born and E. Wolf, *Principles of Optics*, 7th ed., (Cambridge University Press, Cambridge, 1999), pp. 38−49.
29. L. D. Landau and E. M. Lifshitz, *Electrodynamics of continuous media* (Pergamon, Oxford, 1984).
30. H. A. Haus, *Waves and fields in optoelectronics* (Englewood Cliffs, NJ: Prentice-Hall, 1984).
31. L. M. Brekhovskikh, *Waves in layered media* (Academic Press, New York, 1980).
32. P. Yeh, *Optical waves in layered media* (Wiley, New York, 1988).
33. E. Hecht, *Optics*, 4th ed., (Addison Wesley, 2001).
34. V. G. Veselago, "The electrodynamics of substances with simultaneously negative value of ε and μ," Sov. Phys. Usp. **10**, 509–514 (1968).
35. J. B. Pendry, "Positively negative," Nature, **423**, 22−23 (2003).
36. R. A. Shelby, D. R. Smith and S. Schultz, "Experimental verification of a negative index of refraction," Science **292**, 77–79 (2001).
37. C. G. Parazzoli, R. B. Greegor, K. Li, B. E. C. Koltenbah and M. Tanielian, "Experimental Verification and Simulation of Negative Index of Refraction Using Snell's Law," Phys. Rev. Lett. **90**, 107401 (2003).

38. A. A. Houck, J. B. Brock and I. L. Chuang, "Experimental Observations of a Left-Handed Material That Obeys Snell's Law," Phys. Rev. Lett. **90**, 137401 (2003).

39. V. M. Shalaev, W. Cai, U. K. Chettiar, H. -K. Yuan, A. K. Sarychev, V. P. Drachev, and A. V. Kildishev, "Negative index of refraction in optical metamaterials," Opt. Lett. **30**, 3356−3358 (2005).

40. A. K. Sarychev and V. M. Shalaev, *Electrodynamics of Metamaterials* (World Scientific, 2007).

41. G. Dolling, M. Wegener, C. M. Soukoulis, and S. Linden, "Negative-index metamaterial at 780 nm wavelength," Opt. Lett. **32**, 53−55 (2007).

42. H. Kogelnik, "Coupled wave theory for thick hologram gratings," Bell Syst. Tech. J. **48**, 2909−2945 (1969).

43. R. V. Schmidt, D. C. Flanders, C. V. Shank, and R. D. Standley, "Narrow-band grating filters for thin-film optical waveguides," Appl. Phys. Lett., **25**, 651−652 (1974).

44. A. Othonos, "Fiber Bragg gratings," Rev. Sci. Instrum. **68**, 4309−4341 (1997).

45. L. Kazovsky, S. Benedetto, A. Willner, *Optical Fiber Communication Systems* (Artech House, 1996).

46. C. K. Madsen, J. H. Zhao, *Optical Filter Design and Analysis* (Wiley-Interscience, 1999).

47. S. M. Norton, T. Erdogan, and G. M. Morris, "Coupled-mode theory of resonant-grating filters," J. Opt. Soc. Am. A **14**, 629−639 (1997).

48. V. I. Kopp, R. Bose, and A. Z. Genack, "Transmission through chiral twist defects in anisotropic periodic structures," Opt. Lett. **28**, 349−351 (2003).

49. O. M. Efimov, L. B. Glebov, and V. I. Smirnov. "High efficiency volume diffractive elements in photo-thermo-refractive glass." Patent No. US 6,673,497 B2. (6 January, 2004).

50. B. L. Volodin, S. V. Dolgy, E. D. Melnik, E. Downs, J. Shaw, and V. S. Ban, "Wavelength stabilization and spectrum narrowing of high-power multimode laser diodes and arrays by use of volume Bragg gratings," Opt. Lett. **29**, 1891−1893 (2004).

51. T. Chung, A. Rapaport, V. Smirnov, L. B. Glebov, M. C. Richardson, and M. Bass, "Solid-state laser spectral narrowing using a volumetric photothermal refractive Bragg grating cavity mirror," Opt. Lett. **31**, 229−231 (2006).

52. K. -H. Liao, M. -Y. Cheng, E. Flecher, V. I. Smirnov, L. B. Glebov, and A. Galvanauskas, "Large-aperture chirped volume Bragg grating based fiber CPA system," Opt. Express **15**, 4876−4882 (2007).

53. O. Andrusyak, I. Ciapurin, V. Smirnov, G. Venus, and L. Glebov, "Spectral beam combining of fiber lasers with increased channel density," Proc. SPIE Int. Soc. Opt. Eng. **6453**, 64531L (2007).

54. J. R. Leger, "External methods of phase locking and coherent beam addition of diode lasers," in *Surface Emitting Semiconductor Lasers and Arrays*, G. A. Evans and J. M. Hammer, (Academic, 1993), pp. 379–433.

55. T. Y. Fan, "Laser beam combining for high-power, high-radiance sources," IEEE J. Sel. Topics Quantum Electron., **11**, 567−577, (2005).

56. Z. G. Pinsker, *Dynamical Scattering of X-Rays in Ideal Crystals* (Springer, 1978).

57. J. Cowley, *Diffraction Physics*, 3rd ed. (North Holland, 1995).

58. M. G. Moharam and T. K. Gaylord, "Chain-matrix analysis of arbitrary-thickness dielectric reflection gratings," J. Opt. Soc. Am. **72**, 187−190 (1982).

59. P. Sharlandjiev and Ts. Mateeva, "Normal incidence holographic mirrors by the characteristic matrix method. Numerical examples," J. Opt. **16**, 185−189 (1985).

60. J. Lauzon, S. Thibault, J. Martin, and F. Ouellette, "Implementation and characterization of fiber Bragg gratings linearly chirped by a temperature gradient," Opt. Lett. **19**, 2027−2029 (1994).

61. P. C. Hill and B. J. Eggletton, "Strain gradient chirp of fiber Bragg gratings, " Electron. Lett. **30**, 1172−1174 (1994).

62. D. W. Dobbs and B. T. Cunningham, "Optically tunable guided-mode resonance filter," Appl. Opt. **45**, 7286−7293 (2006).

63. T. Komukai and M. Nakazawa, "Fabrication of non-linearly chirped fiber Bragg gratings for higher-order dispersion compensation," Opt. Commun., **154**, 5−8 (1998).

64. K. O. Hill, F. Bilodeau, B. Malo, T. Kitagawa, S. Theriault, D. C. Johnson, J. Albert, and K. Takiguchi, "Chirped in-fiber Bragg gratings for compensation of optical-fiber dispersion," Opt. Lett. **19**, 1314−1316 (1994).

65. V. Mizrahi and J. E. Sipe, “Optical properties of photosensitive fiber phase gratings,” J. Lightwave Technol. **11**, 1513–1517 (1993).

66. E. Popov, M. Nevière, B. Gralak, and G. Tayeb, "Staircase approximation validity for arbitrary-shaped gratings," J. Opt. Soc. Am. A **19**, 33−42 (2002).

67. V. A. Belyakov, *Diffraction Optics of Complex-Structured Periodic Media* (Springer-Verlag, 1992).

68. C. Khoo and S. T. Wu, *Optics and Nonlinear Optics of Liquid Crystals* (World Scientific, 1993).

69. P. G. de Gennes and J. Prost, *The Physics of Liquid Crystals*, 2nd ed. (Clarendon, Oxford, 1993).

70. H. Sarkissian, B. Ya. Zeldovich, and N. Tabiryan, "Longitudinally modulated nematic bandgap structure," J. Opt. Soc. Am. B **23**, 1712−1717 (2006).

71. P. M. Morse and H. Feshbach, *Methods of Theoretical Physics* (McGraw-Hill, 1953).

72. M. G. Moharam and T. K. Gaylord, "Rigorous coupled-wave analysis of planar-grating diffraction," J. Opt. Soc. Am. **71**, 811−818 (1981).

73. R. Alferness and S. K. Case, "Coupling in doubly exposed, thick holographic gratings," J. Opt. Soc. Am. **65**, 730−739 (1975).

74. C. C. Tsai, L. B. Glebov, and B. Ya. Zeldovich, "Adiabatic three-wave volume hologram: large efficiency independent of grating strength and polarization," Opt. Lett. **31**, 718−720 (2006).

75. C. C. Tsai, B. Ya. Zeldovich, L. B. Glebov, and S. Frederick, "Crossed-gratings volume hologram: backward reflection with high angular and spectral selectivity," Opt. Express **14**, 9558−9563 (2006).

76. J. Zhao, P. Yeh, M. Khoshnevisan, and I. McMichael, "Diffraction properties of vector synthetic volume index gratings," J. Opt. Soc. Am. B **17**, 898−903 (2000).

77. J. H. Hong and D. Psaltis, "Dense holographic storage promises fast access," Laser Focus World **32**, 119 (1996).

78. D. Psaltis, J. -J. P. Drolet, E. Chuang, and G. Barbastathis, "Compact, integrated dynamic holographic memory with refreshed holograms," Opt. Lett. **22**, 552−554 (1997).

79. D. Psaltis, Y. Yang, and A. Adibi, "Comparison of Transmission and the 90-Degree Holographic Recording Geometry," Appl. Opt. **42**, 3418−3427 (2003).

80. M. Centurion, Y. Pu, and D. Psaltis, "Holographic capture of femtosecond pulse propagation," J. Appl. Phys. **100**, 063104 (2006).

81. S. Takagi, "A dynamical theory of diffraction for a distorted crystal," J. Phys. Soc. Jpn. **26**, 1239 (1969).

82. K. L. Baker, D. Homoelle, E. Utternback, E. A. Stappaerts, C. W. Siders, and C. P. J. Barty, "Interferometric adaptive optics testbed for laser pointing, wave-front control and phasing," Opt. Express **17**, 16696–16709 (2009).

83. K. Sueda, G. Miyaji, N. Miyanaga, and M. Nakatsuka, "Laguerre-Gaussian beam generated with a multilevel spiral phase plate for high intensity laser pulses," Opt. Express **12**, 3548–3553 (2004).

84. G. A. Swartzlander, Jr., E. L. Ford, R. S. Abdul-Malik, L. M. Close, M. A. Peters, D. M. Palacios, and D. W. Wilson, "Astronomical demonstration of an optical vortex coronagraph," Opt. Express **16**, 10200–10207 (2008).

85. S. M. Popoff, G. Lerosey, R. Carminati, M. Fink, A. C. Boccara, and S. Gigan, "Measuring the Transmission Matrix in Optics: An Approach to the Study and Control of Light Propagation in Disordered Media," PRL **104**, 100601-4 (2010).

86. J. E. Curtis, B. A. Koss, D. G. Grier, "Dynamic holographic optical tweezers," Opt. Commun. **207**, 169–175 (2002).

87. J.-M. Merolla, Y. Mazurenko, J.-P. Goedgebuer, H. Porte, and W. T. Rhodes, "Phase-modulation transmission system for quantum cryptography," Opt. Lett. **24**, 104–106 (1999).

88. S. S. R. Oemrawsingh, J. A. de Jong, X. Ma, A. Aiello, E. R. Eliel, G. W. ’t Hooft, and J. P. Woerdman, "High-dimensional mode analyzers for spatial quantum entanglement," Phys. Rev. A **73**, 032339–7 (2006).

89. G. A. Siviloglou, J. Broky, A. Dogariu, and D. N. Christodoulides, Observation of Accelerating Airy Beams, Phys. Rev. Lett. **99**, 213901-4 (2007).

90. P. Polynkin, M. Kolesik, J. V. Moloney, G. A. Siviloglou, D. N. Christodoulides, "Curved Plasma Channel Generation Using Ultraintense Airy Beams," Science, **324**, 229–232 (2009).

91. I. J. Sola, V. Collados, L. Plaja, C. Mendez, J. San Roman, C. Ruiz, I. Arias, A. Villamarin, J. Atencia, M. Quintanilla and L. Roso, "High power vortex generation with volume phase holograms and non-linear experiments in gases," Applied Physics B **91**, 115–118 (2008).

92. D. Meshulach, D. Yelin, and Y. Silberberg, "Adaptive real-time femtosecond pulse shaping," J. Opt. Soc. Am. B **15**, 1615–1619 (1998).

93. R. M. A. Azzam and N. M. Bashara, *Ellipsometry and Polarized Light* (North-Holland, 1987).

94. R. J. Collier, Ch. B. Burckhardt, and L. H. Lin, *Optical Holography* (Academic, 1971).

95. B. Ya. Zeldovich, A. V. Mamaev, and V. V. Shkunov, *Speckle-Wave Interactions in Application to Holography and Nonlinear Optics* (CRC Press, 1992).

96. L. D. Landau and E. M. Lifshitz, *Fluid Mechanics* (Pergamon, 1987).

97. E. A. Nelin, "Impedance model for quantum-mechanical barrier problems," *Phys. Usp*. **50**, 293−300, 2007.

98. C. C. Tsai and B. Ya. Zeldovich, "Scalar Approximation to Describe Depolarized Light: Equation for Refraction when Impedance is Constant," in Frontiers in Optics, OSA Technical Digest (CD) (Optical Society of America, 2006), paper FThQ3.

99. K. Ennser, M. N. Zervas, and R. I. Laming, "Optimization of linearly chirped grating dispersion compensated system," Opt. Fiber Technol. **3**, 120−122 (1997).

100. O.V. Belai, E.V. Podivilov, D.A. Shapiro, "Group delay in Bragg grating with linear chirp," Opt. Commun. **266**, 512−520 (2006).

101. J. Lumeau, L. B. Glebov, and V. Smirnov, "Tunable narrowband filter based on a combination of Fabry–Perot etalon and volume Bragg grating," Opt. Lett. **31**, 2417–2419 (2006).

102. S. Legoubin, E. Fertein, M. Douay, P. Bernage, P. Niay, F. Bayon, and T. Georges, "Formation of moiré grating in core of germanosilicate fibre by transverse holographic double exposure method," Electron. Lett. **27**, 1945–1947, (1991).

103. R. J. Campbell and R. Kashyap, "Spectral profile and multiplexing of Bragg gratings in photosensitive fiber," Opt. Lett. **16**, 898–900 (1991).

104. L. A. Everall, K. Sugden, J. A. R. Williams, I. Bennion, X. Liu, J. S. Aitchison, S. Thoms, and R. M. De La Rue, "Fabrication of multipassband moiré resonators in fibers by the dual-phase-mask exposure method," Opt. Lett. **22**, 1473–1475 (1997).

105. S. G. Lipson, H. Lipson, and D. S. Tannhauser, *Optical Physics*, 3rd ed., (London: Cambridge U.P., London, 1995).

106. L. B. Glebov, "Volume hologram recording in inorganic glasses," Glass Science and Technology **75** C1, 73-90 (2002).

107. O. M. Efimov, L. B. Glebov, L. N. Glebova, V. I. Smirnov. "Process for production of high efficiency volume diffractive elements in photo-thermo-refractive glass." Patent No. US 6,586,141 B1. July 1, 2003.

108. O. Andrusyak, V. Smirnov, G. Venus, V. Rotar, and L. Glebov, "Spectral Combining and Coherent Coupling of Lasers by Volume Bragg Gratings," IEEE J. Sel. Top. Quantum Electron. **15**, 344–353 (2009).

109. W. Chang, T. Wu, H. G. Winful, and A. Galvanauskas, "Array size scalability of passively coherently phased fiber laser arrays," Opt. Express **18**, 9634-9642 (2010).

110. C. J. Corcoran and F. Durville, "Passive Phasing in a Coherent Laser Array," IEEE J. Sel. Top. Quantum Electron. **15**, 294-300 (2009).

111. J. E. Rothenberg, "Passive coherent phasing of fiber laser arrays," Proc. of SPIE **6873**, 687315-9 (2008).

112. L. Solymar, "Two-dimensional *N*-coupled-wave theory for volume holograms," Opt. Comm. **23**, 199−202 (1977).

113. A. E. Siegman, "Defining, measuring, and optimizing laser beam quality," Proc. SPIE **1868**, 2, (1993).

114. B. Ya. Zeldovich, N. F. Pilipetsky, V. V. Shkunov, Principles of Phase Conjugation, (Springer, 1985); Chap. 3.

115. M. J. Bastiaans, "Wigner distribution function and its application to first-order optics," J. Opt. Soc. Am. **69**, 1710-1716 (1979).

116. J. Serna, R. Martínez-Herrero, and P. M. Mejías, "Parametric characterization of general partially coherent beams propagating through ABCD optical systems," J. Opt. Soc. Am. A **8**, 1094-1098 (1991).

117. A. E. Siegman, *Lasers*, (University Science Books, 1986).

118. H. Bateman, *Higher Transcendental Functions*, vol. II (McGraw-Hill Book Company, 1953).

119. J. H. Lienhard IV and J. H. Lienhard V, *A Heat Transfer Textbook*, 3rd ed., (Phlogiston Press, Cambridge, 2008).